Czech Technical University in Prague

Faculty of Nuclear Sciences and Physical Engineering

Department of Mathematics

Properties and Applications of Geometric Flows

DISSERTATION THESIS

2023

Jiří Minarčík

Bibliographical Entry

Author	Ing. Jiří Minarčík
Title of Dissertation	Properties and Applications of Geometric Flows
Degree of Study	Application of Natural Sciences
Field of Study	Mathematical Engineering
Supervisor	Prof. Dr. Ing. Michal Beneš
Academic Year	2023
Number of Pages	139
Keywords	Geometric flow, space curves, minimal surfaces.

Bibliografický záznam

Autor	Ing. Jiří Minarčík
Název Práce	Properties and Applications of Geometric Flows
Studijní Program	Aplikace přírodních věd
Studijní Obor	Matematické inženýrství
Školitel	Prof. Dr. Ing. Michal Beneš
Akademický Rok	2023
Počet Stran	139
Klíčová Slova	Geometrický tok, prostorové křivky, minimální plochy.

Abstract

English

This thesis focuses on geometric flows of curves in three-dimensional Euclidean space, a subject often overshadowed by the study of higher-dimensional or intrinsic flows. The work presents analytical and topological advancements, particularly in higher codimension curve shortening flow as well as in the introduced minimal surface generating flow and framed curvature flow. Utilizing tools from nondegenerate homotopy and geometric knot theory, the study augments the available methods for understanding the long-term behavior of evolving space curves. These developments have the potential to be applied in various fields, including fluid dynamics, material science, and computer graphics.

Czech

Tato práce se zaměřuje na geometrické toky křivek ve třírozměrném eukleidovském prostoru, téma, které je často zastíněno studiem vyšších dimenzí nebo intrinzických toků. Práce představuje analytické a topologické pokroky, zejména ve zkracování křivek vyšší kodimenze, stejně jako v představeném toku generujícím minimální plochy. S využitím nástrojů z nedegenerované homotopie a geometrické teorie uzlů práce rozšiřuje dostupné metody pro pochopení dlouhodobého chování vyvíjejících se prostorových křivek. Tyto výsledky mohou nalézt uplatnění v různých oblastech, včetně dynamiky tekutin, materiálové vědy a počítačové grafiky.

Acknowledgments

Dedicated to Jaroslav Křenek.

I am profoundly grateful to my parents, Jiří and Pavla, for their unwavering support and the strong foundation they have provided me.

A special note of thanks to my partner, Laura. Her encouragement, thoughtfulness, and resilience were my steady pillars during the times when I was engrossed in this work.

I would like to extend my gratitude to my supervisor, Prof. Michal Beneš. The freedom he granted me to pursue my ideas cultivated a stimulating and friendly academic environment.

Special thanks to Prof. Masato Kimura and Prof. Daniel Ševčovič for their insights that enriched this research. Additional acknowledgment goes to Prof. Renzo Ricca and others who have inspired me, including those I had the fortune to meet at conferences.

I am also indebted to the Penrose team at CMU for their hospitality and to Martin Grill and others from Resistant AI for a flexible and encouraging environment.

The work of was partly supported by the Ministry of Education, Youth, and Sports of the Czech Republic under the OP RDE grant CZ.02.1.01/0.0/0.0/16 019/0000753 "Research Centre for Low-carbon Energy Technologies" and by the Student Grant Agency of the Czech Technical University in Prague grant SGS17/194/OHK4/3T/14 "Application of Advanced Supercomputing Methods for Mathematical Modeling of Natural Processes".

Contents

State of the Art

The study of geometric flows has been an area of rigorous academic inquiry for decades, leading to groundbreaking results like the proof of the Poincaré conjecture. Nonetheless, the majority of this body of work has primarily focused on intrinsic flows, flows in abstract ambient spaces, and higher-dimensional flows of hypersurfaces. While these topics are undoubtedly important, they often leave out the specific challenges and peculiarities of evolving space curves in three-dimensional Euclidean space.

Although the evolution of curves in higher dimensional spaces has seen specialized applications, among others in fluid dynamics through the binormal flow or in computer graphics for modeling elastic rods, the short and long-term behavior of space curves subjected to geometric flows are areas that are not yet fully understood, leaving room for new discoveries.

Goals

The primary aim of this work is to delve into the properties and behaviors of evolving space curves, specifically in three-dimensional Euclidean space. This research looks to fill existing gaps in the literature by addressing challenges tied to the topology and knotted configurations of these curves. Additionally, the work aims to develop new analytical and topological tools tailored to these questions.

Methods

The topic of geometric flows requires knowledge of analytical tools in partial differential equations, geometric measure theory and differential geometry. Furthermore, The challenges related to the definition of Frenet frame demand the use of topological tools from homotopy theory and geometric knot theory. Finally, computational simulations aided by discrete differential geometry and numerical analysis provide empirical support for theoretical findings.

Results

The work offers novel insights into the long-term properties of curve shortening flows in space curves, and presents analysis of new geometric motion laws and their trajectory surfaces. Another contribution is the introduction of a new invariant quantity called the tangent turning signature and the use of nondegenerate homotopy theory for geometric flows.

Ramifications

The findings of this work are anticipated to have ramifications not just in the mathematical understanding of geometric flows but also in applications that extend to data denoising, visualization, and robotics. By deepening the comprehension of how space curves evolve over time, this research stands to offer new avenues for both theoretical and applied sciences.

0 Introduction

This work presents a collection of the author's results related to geometric flows of curves in space. These flows are pivotal for understanding and modelling significant natural phenomena, such as turbulence or the dynamics of dislocation lines. Furthermore, they offer valuable applications in areas like data denoising, visualization, and robotics.

The study of geometric flows is an active research domain with a rich history and important results including the proof of the Poincaré conjecture. Yet, recent research trends have mainly focused on intrinsic flows, flows in abstract ambient spaces, or the higher-dimensional flows of hypersurfaces. The evolution of space curves in three-dimensional Euclidean space is often relegated to specialized contexts, such as fluid dynamics in the binormal flow case or computer graphics for evolving elastic rods.

This leaves many fundamental questions related to the short and long-term behaviour unanswered. Moreover, evolving space curves present challenges posed by the topology of their framing and the potential for knotted configurations. This work aims to address these challenges and provide new analytical and topological tools for answering them.

0.0 Overview

The thesis consolidates and presents key findings drawn from the following research articles:

[MKB19] J. Minarčík, M. Kimura, and M. Beneš. "Comparing motion of curves and hypersurfaces in $\mathbb{R}^m$". In: *Discrete and Continuous Dynamical Systems Series B* 24 (2019), pp. 4815–4826.

[MB20] J. Minarčík and M. Beneš. "Long-term behavior of curve shortening flow in $\mathbb{R}^3$". In: *SIAM Journal on Mathematical Analysis* 52 (2020), pp. 1221–1231.

[MB22a] J. Minarčík and M. Beneš. "Minimal surface generating flow for space curves of non vanishing torsion". In: *Discrete and Continuous Dynamical Systems - Series B* 27 (2022), pp. 6605–6617.

[MB22b] J. Minarčík and M. Beneš. "Nondegenerate Homotopy and Geometric Flows". In: *Homology, Homotopy and Applications* 24 (2022), pp. 255–264.

[MB23] J. Minarčík and M. Beneš. "Trajectory Surfaces of Framed Curvature Flow". *Preprint* 2023.

It is divided into one introductory chapter with an overview of related work, 5 chapters with new results from the articles above, and an appendix with computational experiments. The contents of each chapter are outlined in the following list.

Ch. 0. **Introduction.** This chapter introduces the broader topic of geometric flows with an emphasis on space curve evolution. An extensive list of applications and approaches for modelling geometric flows is provided along with an overview of related work.

Ch. 1. **Higher Codimension Curve Shortening Flow.** Collections of results from articles [MKB19] and [MB20] related to the long-term properties of the curves shortening flow of space curves. Contains the generalized comparison principle, its consequences and results related to evolution of specific families of space curves.

Ch. 2. **Minimal Surface Generating Flow.** In this geometric flow of space curves, introduced in [MB22a], the curve traces out zero mean curvature surface. This chapter covers the properties of general trajectory surfaces, derivation of the minimal surface generating flow and all results from [MB22a], including the terminal time and generated area estimates, analytical example and integral of motion.

Ch. 3. **Nondegenerate Homotopy.** Formulating geometric flows of space curves using quantities derived from the Frenet frame restricts the motion to one connected component of the space of locally convex curves. This chapter addresses this problem by using a new invariant quantity called tangent turning sign, proposed in [MB22b].

Ch. 4. **Framed Curvature Flow.** This chapter introduces the framed curvature flow from [MB23]. It is a generalization of both the curve shortening flow and the vortex filament equation. After establishing local existence and global estimates, we analyze the trajectory surfaces generated by different variations of this flow, specifically those leading to surfaces of constant mean or Gaussian curvature.

Ch. A. **Appendix: Evolution of Filament Networks.** This chapter covers evolving filament networks that optimize energy leading to branching structures with triple junctions. We derive and study the discrete gradient flow for this energy and the branching condition it induces.

Ch. B. **Appendix: Computational Experiments.** The second part of the Appendix contains a collection of selected results from computational experiments related to problems studied in Chapters 1 to 4 and Appendix A.

Apart from introductory sections, the thesis contains only results from author's own work. All restated results from the literature are clearly marked with the appropriate reference.

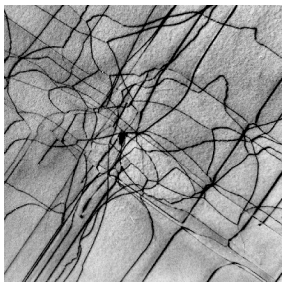

(a) Material dislocation lines. Ex. 9. Image from [KR12].

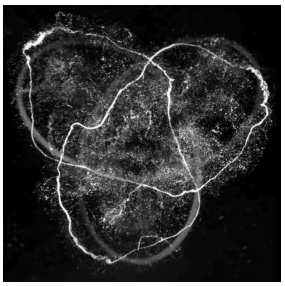

(b) Knotted vortex filament. Ex. 4. Image from [KI13].

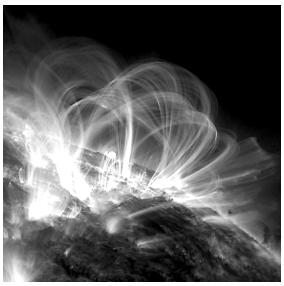

(c) Solar magnetic field lines. Ex. 5. Image from [M A19].

Figure 1: Examples of important natural phenomena at three drastically different scales involving one dimensional filaments that can be modeled as geometric flows of space curves.

0.1 Motivation

Although this work does not address a specific application, it is good to have in mind the possible use-cases of the theory at hand. This section covers a range of possible applications of geometric flows in science, engineering and various domains of mathematics.

0.1.0 Applications in Science

A surprising number of natural and artificial phenomena around us can be described using a one-dimensional filament in three-dimensional Euclidean space moving according to laws formulated as partial differential equations which depend on the state of the environment and the shape of the filament itself. The simplification of complex three-dimensional dynamical systems to a moving space curve enables faster and more scalable numerical simulations and often uncovers new insights and intuitive explanations.

Example List 0.1.1 (Applications in science)**.** *Overview of models based on evolving curves or hypersurfaces that are useful for understanding phenomena in physics, biology and chemistry.*

Ex. 1. **Cell membranes.** The Canham-Helfrich model explains the shape of biological cells by minimizing the energy functional given by

$$CH(\Sigma_t) = \int_{\Sigma_t} \alpha_H (H - H_0) - \alpha_K K \,\mathrm{d}A,$$

where α_H, α_K and H_0 are fixed constants and H, K are the mean and Gauss curvature of the surface Σ_t, respectively. This leads to a modified version of the Willmore flow and its limiting shapes can among others explain the distinctive shape of red blood cells [BLS20].

Ex. 2. **Dynamics of DNA and Proteins:** At the microscopic scale, DNA and proteins exhibit shapes and dynamics that can be represented as evolving curves in $\mathbb{R}^3$. In many

applications, DNA is modeled as an evolving ribbon, especially when simulating effects such as supercoiling [RCV93]. Techniques like the Kirchhoff-Love rod model can be employed for this purpose [ĐGM13]. Another critical aspect is the interaction of topoisomerase with DNA, which is essential for untangling the molecule during meiosis [Sum86].

Ex. 3. **Phase singularites.** Scroll waves in excitable media are spiral-shaped waves that occur in chemical reactions, like the Belousov–Zhabotinsky reaction, or biological systems such as the cardiac tissue where the electrical pulses are modeled using reaction-diffusion equations like the FitzHugh-Nagumo equation. When modeled in three-dimensional space, the phase singularities lie along a space curve that evolves based on geometrical properties such as the twist of the curve [MS16; MS19; Kee88].

Ex. 4. **Magnetic field lines.** The dynamics of solar flares and other astrophysical phenomena can be studied using evolving curves representing magnetic field lines. These models may lead to a better understanding of high-energy events and their impact on Earth [YHW10] and they can also be used for solar corona visualizations [Pad+22].

Ex. 5. **Vortex filaments.** Vortices represent concentrated regions of vorticity in fluid dynamics. Their motion can be modeled by the binormal flow, also known as the vortex filament equation [Veg15], which is the localized induction approximation of the Biot-Savart equation [Ric91]. Vortex filaments in superfluids or Bose-Einstein condensates can be modeled by curvature-driven flow similar to the vortex filament equation [Bar+97]. Unlike the classical vortices that can quickly dissipate, the stability of quantum vortices allows interesting reconnection dynamics [ZR22].

Ex. 6. **Hele-Shaw problem.** Hele-Shaw flows occur when a viscous fluid is squeezed between two parallel plates [Saf86; Hel98]. By treating the fluid boundary as an evolving curve, one can study the fingering pattern formation mechanism [SSY22].

Ex. 7. **Crystal growth.** The process of solidification of materials with crystalline structure can be described as a moving boundary problem in an anisotropic environment [Gur93]. The mathematical formulation of this problem leads to Finsler geometry.

Ex. 8. **Grain boundaries.** The evolution of grain boundaries in grain boundaries of polycrystalline materials affects their mechanical properties and can be modeled as hypersurfaces moving according to the mean curvature flow [Mul56].

Ex. 9. **Dislocation dynamics.** Dislocations in crystals, seen as defects along a curve [Mur87], can be modeled as curvature-driven flow with an external forcing term that can account for interactions with other dislocation loops or other defects [Kol+18].

Ex. 10. **River meandering.** Rivers are dynamic geological structures that can significantly change their shape in timescales of single years. The simplest mathematical model describes the river bed centerline as a planar curve evolving with normal velocity

$$v_N = \sigma \star \kappa, \qquad \sigma(s) = m_1\delta(s) + m_2 H(s) e^{-\alpha s},$$

where m_1, m_2 and α are constants, H is the Heaviside function, δ is the Dirac delta and $\star$ denotes convolution. The model takes into account the upstream curvature of

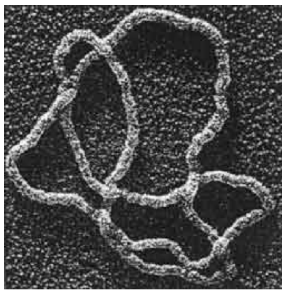

(a) Knotted DNA molecule. Ex. 2. Image from [al85].

(b) Meandering river bed. Ex. 10. Image from [Ima14].

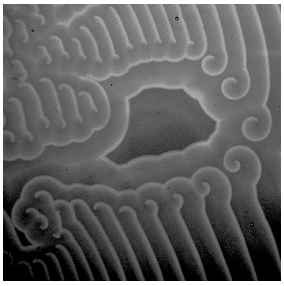

(c) B.–Z. reaction scroll waves. Ex. 3. Image from [WHB09].

Figure 2: Besides physics, modelling of one-dimensional filaments is useful in many domains of science. This figure illustrates examples from biology, geology and chemistry.

the curve to approximate the rate of experienced erosion. This model was suggested in [Fur91] and later studied in e.g. [Fur88; OA08; Par+11; FL13].

Ex. 11. **Wearing process.** One of the first applications of the mean curvature flow was the description of the natural wearing process of stones and other materials that are subjected to various forms of natural wear such as erosion [Fir74].

0.1.1 Applications in Engineering

As three-dimensional digital design advances, both in complexity and prevalence, the relevance of geometric flows in engineering becomes more important. These principles have applications ranging from image processing and architectural design to computer graphics and robotics. By understanding the dynamics of curves and surfaces, engineers have a more rigorous approach to address various challenges in their respective domains.

Example List 0.1.2 (Applications in engineering)**.** *Overview of models based on geometric flows that can be used for solving problems in computer science, civil engineering, robotics, etc.*

Ex. 15. **Image processing.** Although modern image processing techniques usually involve convolutional neural networks or similar architectures, the contour capture via a modified curve shortening flow has been successfully used for segmentation in medical, geological, and other domains [BCM04; Ben+08; Cao03; PM87].

Ex. 16. **Architecture.** In architecture, the design of complex structural forms like bridges, towers, and buildings often involves the movement and optimization of curves in space. Examples of such processes can be found in [Rem+14].

Ex. 17. **Computer graphics.** In computer graphics, modeling objects like ropes, hair, clothes, or smoke involves moving curves or elastic rods in a virtual three-dimensional space. Another technique called Schrödinger's smoke [Che+16] uses binormal flow to model vorticity lines for efficient smoke and dust animations in games and CGI effects.

Ex. 18. **Diagram layout.** Mathematical visualization software like KnotPlot [Sch22] or Penrose [Ye+20] performs automatic layout of geometric primitives like curves by a process that usually involves gradient flows of some curve functional.

Ex. 19. **Network analysis.** Generalized notions of geometric flows have been used in the context of graph learning and network analysis. Recent examples include community detection methods using the Ricci flow [Ni+19] or various uses of the Ollivier-Ricci curvature [CDR22] defined even for hypergraphs.

Ex. 20. **Robotics.** In robotics, for example in the design of multi-jointed manipulators, optimal curves represent the trajectories in the constrained configuration space of the robot. Another interesting example involves the optimisation of medical robot trajectory during colonoscopy [MU14]. Another related example is the optimal origami folding studied in [DO07; FT99].

Ex. 21. **Fire front propagation.** The progression of wildfire fronts can be effectively described as a moving curve whose dynamics depend on the terrain, vegetation, and wind [MKF09]. This helps in forecasting the spread of fires and designing effective firefighting strategies. A related problem with a different solution is the modelling of the smoldering front via the Kuramoto-Sivashinsky model [Kol+21].

Ex. 22. **Data denoising.** In computer graphics and geometry processing, the mean curvature flow can be used for smoothing surfaces, denoising point clouds, or morphing between shapes. Applying the mean curvature flow on point clouds and mesh structures helps in removing noise and imperfections, thus producing smoother and cleaner data representations [Ale+03].

0.1.2 Applications in Mathematics

Besides the applications in science and engineering, various geometric flows have proven to be remarkably useful tools in theoretical fields ranging from geometrical measure theory to differential topology, enabling the proofs of many long-standing problems. We believe that this area is still ripe for new results, particularly in the case of higher codimension motion, which typically receives less attention. For example, open problems from [Gho19] may be within reach, provided that further analysis of framed curvature flow is pursued.

Example List 0.1.3 (Applications in mathematics)**.** *Methods based on geometric flows that have led to important proofs or provided novel insights in various fields of pure mathematics.*

Ex. 23. **Penrose inequality.** The Penrose inequality, a result in the field of general relativity, gives a lower bound for the total mass of a spacetime, given the area of the event horizon of its black holes [HI01]. The proof of this inequality was made possible using the inverse mean curvature flow, demonstrating the profound interconnection between geometric analysis and the physics of black holes.

Ex. 24. **Poincaré conjecture.** Richard Hamilton's work on Ricci flow and later Grigori Perelman's work on the Ricci flow with surgeries [Per02; Per03b] played a central role in the proof of the long-standing Poincaré conjectures in dimension 4.

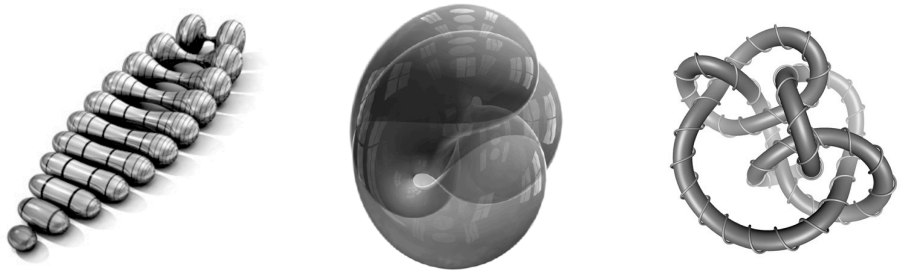

(a) Surface under Ricci flow. Ex. 30. Image from [Sla07].

(b) Sphere eversion model. Ex. 26. Image from [Sul02].

(c) Rendering of knotted tube. Ex. 27. Image from [Sch22].

Figure 3: Rendering of objects obtained by running various geometric flows.

Ex. 25. **Geometrization conjecture.** The Geometrization conjecture, proposed by William Thurston and later proved by Grigori Perelman [Per02; Per03b], provides a comprehensive picture of the possible shapes of three-dimensional spaces. The use of Ricci flow was key to its proof which demonstrates the utility of geometric flows as tools for addressing problems in topology.

Ex. 26. **Sphere eversion.** Sphere eversion is a regular homotopy through immersions of 2-sphere in $\mathbb{R}^3$ from $f\colon S^2 \to \mathbb{R}^3$ to $-f$. In another words, this process turns the initial sphere inside out [Sma58]. There are many proofs and visualizations of this counterintuitive result. Perhaps the most elegant and visually appealing has been achieved by applying the Willmore flow to half-way models such as the Boy's surface.

Ex. 27. **Knot energies.** The evolution of knot embeddings towards the critical points of O'Hara type energies [OHa91] has shown to be a crucial tool in modern knot theory research [Abr+01]. Aiding intuition and adding beautiful visualisations to this topological subject [Sch22].

Ex. 28. **Minimal surface theory:** Minimal surfaces, which are surfaces with zero mean curvature at every point, have been a topic of significant interest due to their beautiful geometric properties and numerous applications in both pure and applied mathematics. One of the primary tools to study and construct minimal surfaces is the mean curvature flow. As minimal surfaces are critical points of this flow, one can use e.g. the Brakke Surface Evolver [Bra92] to investigate and visualize minimal surfaces with prescribed boundary conditions.

Ex. 29. **Willmore conjecture:** The Willmore flow can be used to find surface immersions of minimal bending energy. A famous example is the Clifford torus, which is defined as the product of two circles with different radii in $\mathbb{R}^4$ and then projected to $\mathbb{R}^3$. Thomas Willmore conjectured in 1965 that this shape with Willmore energy of $2\pi^2$ is optimal among all surfaces of genus one. This conjecture remained open for several decades until it was proved by Fernando Coda Marques and André Neves in 2012. Their proof uses min-max theory and the theory of minimal surfaces to confirm the long-standing conjecture [MN14].

Ex. 30. **Ricci flow:** After the excitement about Ricci flow, generated by Perelman's proof, more recent work on Ricci flow led to results such as the Generalized Smale conjecture [BK22] and the Differentiable Sphere Theorem [BS09].

0.2 Geometric Flows

Let us give a brief overview of geometric flows. In simple terms, they are partial differential equations that dictate the time evolution of a manifold given by its properties. One may classify them into two general groups; *intrinsic* and *extrinsic*; based on whether the governing motion law depends on extrinsic properties, i.e. requires the manifold to be immersed in some ambient space. We first describe these two groups in more detail and with specific examples, and then turn to the special case of geometric flows of curves.

0.2.0 Intrinsic Flows

In the context of intrinsic geometric flows, we consider a family of manifolds $(\mathcal{M}, g)$ equipped with a time-dependent Riemannian metric g. The evolution equation of the metric g usually depends on the some notion of curvature.

Definition 0.2.1 (Intrinsic geometric flow)**.** *An intrinsic geometric flow is a one-parameter family of Riemannian metrics $g(t)$ on a smooth manifold $\mathcal{M}$, such that the metric evolves in time according to a given geometric property, like the curvature tensors of the manifold.*

The governing equations for intrinsic flows typically involve the Riemannian curvature tensor R_m, its trace called Ricci curvature $\mathrm{Ric} = \mathrm{tr}R_m$, or the scalar curvature $R = \mathrm{tr}\mathrm{Ric}$.

Example List 0.2.2 (Intrinsic geometric flows)**.** *Specific examples from Definition 0.2.1:*

Ex. 31. **Ricci flow.** The most widely studied intrinsic flow has the form

$$\partial_t g = -2\mathrm{Ric}(g),$$

where Ric is the Ricci curvature tensor, see e.g. [Top06] for general introduction. Ricci flow was introduced by Richard Hamilton [Ham82] and used by Grigori Perelman to prove the Geometrization conjecture and thus the Poincare conjecture in dimension 4 [Per03a]. Although not exactly, it is similar to the heat equation and can be formulated as a gradient flow [Per02]. Even though it can encounter singularities, its existence can be extended by surgeries [Per03b].

Ex. 32. **Yamabe flow.** This flow deforms the Riemannian metric tensor g and tends to a metric of constant scalar curvature R, see [Ye94; Bre05]. It is a gradient flow of the Yamabe functional, which is proportional to the total scalar curvature over $\mathcal{M}$.

Ex. 33. **Calabi flow.** There have been other intrinsic flows, that can be applied to specific types of manifolds with more structure. Notable example is the Calabi flow defined on Kähler manifolds.

As the notion of intrinsic flow is not useful for curves, the rest of this work deals only with extrinsic motion laws. We explore the basic notions in the next section.

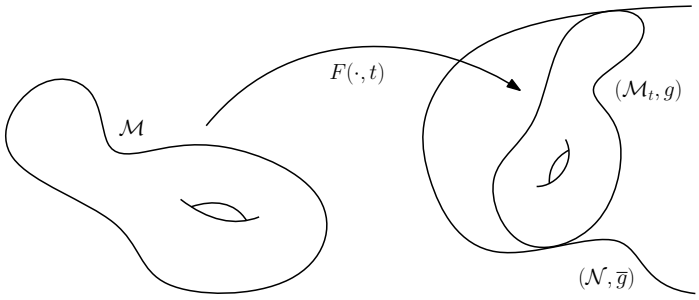

Figure 4: Depiction of objects used in the definition of general extrinsic flows.

0.2.1 Extrinsic Flows

In most scientific applications, we typically study manifolds immersed in specific ambient spaces, such as the Euclidean $\mathbb{R}^3$, the Minkowski spacetime, or the de Sitter space depending on the specific physical context. To this end, we fix the base manifold $\mathcal{M}$ of dimension m and consider a time-dependent family of immersions (see Figure 4)

$$F : \mathcal{M} \times [0, \underline{t}) \to (\mathcal{N}, \overline{g}),$$

where $(\mathcal{N}, \overline{g})$ is the ambient Riemannian manifold of dimension n with metric $\overline{g}$.

The immersion F induces a new metric g on $\mathcal{M}$. In local coordinates of $\mathcal{M}$ with basis $\{x_i\}_{i \leqslant m}$, the metric g is given by the expression

$$g_{ij} = \left\langle \partial_{x_i} F, \partial_{x_j} F \right\rangle.$$

To further simplify the matter for this overview, let us assume that the immersion is a hypersurface of codimension one, i.e. n is one less than m. For a general treatment of higher codimension flow, see the survey [Smo12].

In the codimension one case, we will consider flows in the form

$$\partial_t F(p, t) = V(p, t)\nu(p, t) \tag{1}$$

for $p \in \mathcal{M}$ and $t \in [0, \underline{t})$, where ν is the outward normal vector and the specific expression for the normal velocity V shall be specified in the examples later.

Definition 0.2.3 (Extrinsic flows)**.** *Extrinsic flows describe the evolution of a manifold $\mathcal{M}$ immersed in an ambient space $(\mathcal{N}, \overline{g})$ according to the equation in the form* (1)*, where the normal velocity V depends on geometric properties defined with respect to the ambient space. They often involve the extrinsic curvatures like the mean or Gauss curvature.*

Example List 0.2.4 (Extrinsic flows)**.** *Specific examples from Definition 0.2.3:*

Ex. 34. **Mean curvature flow.** The simplest and most studied flow written as

$$V = -H,$$

where H is the mean curvature of the hypersurface. See e.g. [Hui84].

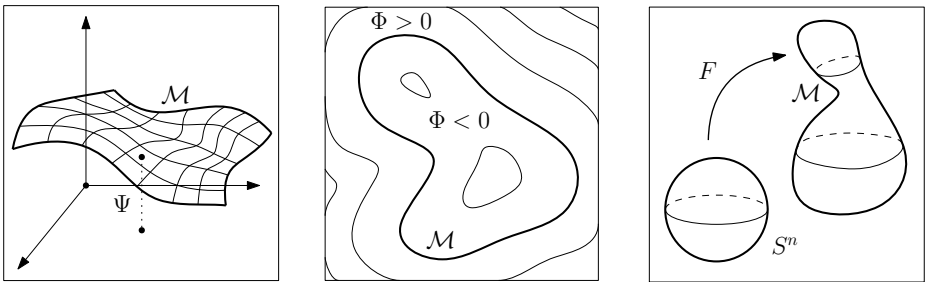

(a) Graph representation. (b) Level set method. (c) Parametric approach.

Figure 5: Types of representations from Example List 0.3.1.

Ex. 35. **Inverse mean curvature flow.** This flow expands, given by

$$V = H^{-1},$$

rather than contracts the initial hypersurface. It led to a new proof for the Riemannian Penrose inequality [HI01] for black holes.

Ex. 36. **Willmore flow.** Gradient flow of the Willmore energy, can be written in the form

$$V = 2\Delta_g H + H^3 - 4HK,$$

where Δ_g is the Laplace-Bertrami operator with respect to the induced metric g, H and K are the mean and Gauss curvatures, respectively. See e.g. [Obe07].

More examples are given in the next section which is focused on one-dimensional objects.

0.3 Curve Flows

This thesis studies the extrinsic flow of curves. This section gives an an overview of this field, covers different approaches, provides specific examples, and introduces the notation.

0.3.0 Representation Approaches

Representing geometric objects, like curves and surfaces, can be accomplished through various mathematical formulations. This section explores commonly used representation methods and discusses their advantages, limitations, and applications.

Example List 0.3.1 (Representations)**.** *Representation approaches and their advantages:*

I. **Parametric approach.** Perhaps the most straightforward representation is one where the base manifold is parametrized by n free variables and the mapping F is given by

$$F(p,t) = \tilde{F}(u_1^\#(p), \dots, u_n^\#(p), t).$$

Note that throughout this work, this function $\tilde{F}$ will usually be denoted by γ. Its advantage lies in simplicity and simple discretization for computational purposes, but it cannot handle topological changes, like merging or splitting [Bän+23].

II. **Graph representation.** Some hypersurfaces can be represented as a collection of points

$$(x^1, \dots, x^{n-1}, \Psi(x^1, \dots, x^{n-1})) \in \mathbb{R}^n,$$

where $x^1, \dots, x^{n-1}$ are first $n-1$ coordinates in some bases of $\mathbb{R}^n$ and Ψ is a functional defined on a domain $\Omega \subset \mathbb{R}^{n-1}$. This approach is quite limited as the functional Ψ must be injective, but after appropriate coordinate transformation, it can sometimes be used for local analysis [DS23].

III. **Level set representation.** The level set method makes use of an auxiliary functional Φ defined on the ambient space $(\mathcal{N}, \overline{g})$. The manifold $(\mathcal{M}_t, g)$ can then be retrieved as the zero level set of Φ, i.e.

$$\mathcal{M}_t = \Phi_t^{-1}(0) = \{x \in \mathcal{N} \colon \Phi(x,t) = 0\},$$

where $\Phi_t = \Phi(\cdot, t)$. This approach handles all topological changes automatically but is numerically more expensive to model as Φ must be defined on potentially large dimensional spaces [Set96; OS88]. It is not easily extensible to the higher codimension case, but this generalisation is possible [Bur+01; AS96].

IV. **Phase field method.** This method is based on the idea of using a smooth function to approximate the characteristic function of the manifold, allowing smooth transitions between phases. It is particularly useful for simulating complex interfacial phenomena. As it is also an implicit model, it shares most of the advantages and disadvantages with the level set method. For details, see e.g. [CH58; Cag86; Ben01; Gar+23].

0.3.1 Parametric Method

Throughout most of this thesis, we use the parametric approach, for its mathematical simplicity and simple numerical implementation. We also aim to take advantage of the fact that, unlike other approaches, it easily generalizes to higher codimension flows.

In this section, we define the necessary notation for the parametric space curves in motion and recall the governing equations for a general geometric flow of curves in $\mathbb{R}^3$.

Let $\{\Gamma_t\}_{t\in[0,\underline{t})}$ denote a family of closed curves in $\mathbb{R}^3$ evolving in time interval $[0, \underline{t})$, where $\underline{t} > 0$ is the terminal time. For given $t \in [0, \underline{t})$, the curve Γ_t is represented by a parametrization $\gamma(\cdot, t) \colon S^1 \to \mathbb{R}^3$, where $S^1 = \mathbb{R}/2\pi\mathbb{Z}$ is the unit circle.

We use the standard notation for the Frenet frame, i.e. T, N, and B denotes the tangent, normal, and binormal vector, respectively. The curvature and the torsion, given by the Frenet-Serret formulae, are denoted by κ and τ, respectively. Finally,

$$g := \|\partial_u \gamma\|$$

is the local rate of parametrization and $\mathrm{d}s = g\,\mathrm{d}u$ is the arclength element.

Definition 0.3.2 (Geometric flow of curves). *The time evolution of* $\{\Gamma_t\}_{t\in[0,\underline{t})}$ *is given by the geometric flow in the form of the following initial-value problem for* $\gamma = \gamma(u,t)$*:*

$$\partial_t \gamma = v_T T + v_N N + v_B B \qquad \text{in } S^1 \times (0,\underline{t}), \tag{2}$$

$$\gamma|_{t=0} = \gamma_0 \qquad \text{in } S^1, \tag{3}$$

where γ_0 *is the parametrization for the initial curve* Γ_0*. Since the motion in the direction of the tangent vector* T *does not affect the shape of the curve, we often assume that* $v_T = 0$*.*

0.3.2 Examples

This subsection provides an extensive overview of geometric flows of curves, both in plane and high-dimensional spaces. It should serve as a useful guide and reference for future readers.

Example List 0.3.3 (Geometric flows of space curves). *Examples from Definition 0.3.2:*

Ex. 37. **Curve shortening flow.** The most famous curve flow and the one that is the easiest to study due to its connection to the heat equation is

$$\partial_t \gamma = \partial_s^2 \gamma = \kappa N.$$

It has been extensively studied in $\mathbb{R}^2$ [GH86; Gra87], and its generalization to higher codimensions is discussed in Chapter 0.4 which also contains further references.

Ex. 38. **Vortex filament equation.** The binormal flow is defined as

$$\partial_t \gamma = \partial_s \gamma \times \partial_s^2 \gamma = \kappa B$$

is in many senses orthogonal to the curve shortening flow. It preserves the local rate of parametrisation g and thus the length has a surprising connection to a nonlinear Schrödinger equation through the so-called Hashimoto transform [Has72] and it arises in fluid dynamics as a model for vortex dynamics via a linear induction approximation of the Biot-Savart equation [Ric91].

Ex. 39. **Elastic flow.** Similarly to the Willmore energy, the elastic energy is the integral of curvature squared over the curve Γ_t. The gradient flow of this energy has the form

$$\partial_t \gamma = (2\kappa\tau^2 - \kappa^3 - 2\partial_s^2\kappa)N - (4\partial_s\kappa\tau + 2\kappa\partial_s\tau)B.$$

Or the equation $\partial_t \gamma = -\kappa^3 N - 2\partial_s^2 \kappa N$ for planar curves. This flow leads to elasticae curves which were studied from the time of Euler [Eul44; LS84].

Ex. 40. **Minimal surface generating flow.** The curve moving according to

$$\partial_t \gamma = \tau^{-\frac{1}{2}} N$$

traces out a zero mean curvature surface. This motion law has been introduced in [MB22a] and is the subject of Chapter 2.

Ex. 41. **Framed curvature flow.** Another flow related to trajectory surfaces is

$$\partial_t \gamma = \kappa \nu_\theta = \kappa \cos\theta \; N + \kappa \sin\theta \; B,$$

where θ is a function defined along the curve and depends on time. This flow is introduced in Chapter 4 of this thesis.

Ex. 42. **Writhe minimising flow.** The following flow of space curves

$$\partial_t \gamma = -\partial_s(\partial_s \gamma \times \partial_s^2 \gamma) = \kappa\tau N - \partial_s \kappa B$$

maximizes the total torsion, or equivalently due to the Călugăreanu theorem, it minimizes the property called writhe of embedded curves.

Ex. 43. **Second-order elastic flow.** Another interesting gradient flow is

$$\partial_t \gamma = (2\partial_s^4 \kappa - \kappa(\partial_s \kappa)^2 + 2\kappa^2 \partial_s^2 \kappa - 2\tau^2 \partial_s^2 \kappa) N + 2(\partial_s \tau \partial_s^2 \kappa + 2\tau \partial_s^3 \kappa) B$$

or again its planar version $\partial_t \gamma = (2\partial_s^4 \kappa - \kappa(\partial_s \kappa)^2 + 2\kappa^2 \partial_s^2 \kappa) N$. In this case, the minimized functional is the integral of $(\partial_s \kappa)^2$ over Γ_t.

Ex. 44. **Knot energy minimisation.** In [OHa91; OHa92], Jun O'Hara studied knot energies that define optimal embeddings of knotted curves [KS97; Abr+01]. The simplest example is the Möbius energy defined as

$$M(\Gamma_t) = \iint\limits_{S^1 \times S^1} \left[\frac{1}{\|\gamma(u,t) - \gamma(v,t)\|^2} - \frac{1}{D(\gamma(u,t), \gamma(v,t))^2} \right] \mathrm{d}u \, \mathrm{d}v,$$

where $D(\gamma(u,t), \gamma(v,t))$ is the shortest arc distance along the curve Γ_t between the two points $\gamma(u,t)$ and $\gamma(v,t)$. Analysis of gradient flows for these energies was conducted in e.g. [Bla18; RS21].

Ex. 45. **Repulsive Flows.** Similarly to the O'Hara-type energies, repulsive flows studied in [Yu+21; YSC21] lead to optimal embeddings of curves or surfaces given their topology. These flows minimize the tangent point energy given by

$$TP(\Gamma_t) = \iint\limits_{S^1 \times S^1} \frac{g(u,t) g(v,t)}{\rho(u,v,t)} \, \mathrm{d}u \, \mathrm{d}v,$$

where $\rho(u,v,t)$ is the radius of the smallest sphere tangent to the curve at $\gamma(u,t)$ and passing through the point $\gamma(v,t)$.

Remark 0.3.4. *This list is not comprehensive, but many other flows studied for specific scientific or engineering applications are derived from the listed motion laws by the addition of external forcing term or can be written as a linear combination of the above laws. For example, in the context of quantum vortices in Bose-Einstein condensate, dictated by the Gross-Pitaevskii equation, the linear induction approximation of the flow has form*

$$\partial_t \gamma = a \partial_s \gamma \times \partial_s^2 \gamma - b \partial_s \gamma \times (\partial_s \gamma \times \partial_s^2 \gamma) = a\kappa B + b\kappa N,$$

where a and b are physical constants. See [ZR22; Bar+97; Fey55].

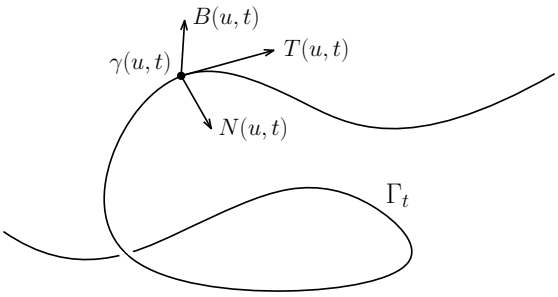

Figure 6: Frenet vectors of curve Γ_t at the point $\gamma(u,t)$.

We also include a short list of alternative but related problem statements.

Example List 0.3.5 (Adjacent curve flow problems)**.** *This list complements Example List 0.3.3 with additional problems that involve the motion of curves but do not fit Definition 0.3.2:*

Ex. 46. **Network flow.** The study of network flow extends the geometric flow of individual curves to a system of interconnected curves or networks. This typically introduces additional complexity, such as the behavior at junctions. One interesting application is in the study of Steiner trees, which aim to connect a set of points with the shortest possible total length. Analysis of network flows has been carried out in [NPP20; NPP19; BW95; Man+18]. The topic is also discussed in Chapter A of this thesis.

Ex. 47. **Anisotropic motion.** Anisotropic motion involves geometric flows where the speed of motion depends not only on curvature but also on the direction of the normal vector. This dependence on direction introduces a Finsler metric into the problem and can lead to the evolution of curves towards certain shapes, known as Wulff shapes, that are determined by the anisotropy [BP96].

Ex. 48. **Exotic ambient spaces.** Another interesting direction is the study of extrinsic flows in non-standard ambient spaces, where even simple flows can lead to unexpected behaviour. For example, one might consider curve shortening flow in the context of Lagrangian mean curvature flow [ELW22], where curves move in a high-dimensional symplectic manifold.

Ex. 49. **Interacting curves.** Interacting curves consider the behavior of multiple curves that influence each other's motion. This interaction can lead to complex dynamics and patterns, such as those studied in [BKŠ22].

0.4 Technical Preliminaries

This purely technical section states useful apparatus utilized across this thesis. It may serve as a useful glossary of evolution equations for curve flows as it covers most of the basic equations for general velocities v_N and v_B. It however ignores the tangential term v_T for simplicity. For alternative equations including non-trivial tangential velocity see e.g. [BKŠ22].

0.4.0 Local Quantities

In the rest of this chapter, we implicitly assume that $\{\Gamma_t\}_{t\in[0,\underline{t})}$ is a family of space curves evolving according to a general geometric flow given by velocities v_N and v_B.

Lemma 0.4.1 (Arc-Length commutator)**.** *The arc-length commutator during the general geometric flow of curves given by*

$$[\partial_t, \partial_s] := \partial_t\partial_s - \partial_s\partial_t = \kappa v_N \partial_s. \tag{4}$$

Equivalently, the local rate of parametrisation evolves as $\partial_t g = -\kappa v_N g$.

Proof. The statement is a special case of Proposition 1 from [BKŠ22]. □

Remark 0.4.2. *Note that some authors express the evolution equations in terms of the normal component of the arc-length derivative ∇_s defined as*

$$\nabla_s\phi = \partial_s\phi - \langle\partial_s\phi, T\rangle T$$

for vector functions $\phi\colon S^1 \to \mathbb{R}^3$. We will avoid this notation and only use ∂_s.

Proposition 0.4.3 (Local quantities)**.** *The evolution equations for the local geometric quantities during the motion given by (2-3) can be retrieved from the general algebraic framework for invariant submanifold flows devised in [Olv08]. According to Example 5.7 from [Olv08], the equations for $v_T = 0$ read*

$$\partial_t g = -g v_N \kappa, \tag{5}$$
$$\partial_t \kappa = \partial_s^2 v_N + \kappa^2 v_N - 2\tau\partial_s v_B - v_B\partial_s\tau - v_N\tau^2, \tag{6}$$
$$\partial_t \tau = 2v_N\kappa\tau + \kappa\partial_s v_B + \partial_s[\tfrac{1}{\kappa}(v_N\partial_s\tau + 2\tau\partial_s v_N + \partial_s^2 v_B - v_B\tau^2)], \tag{7}$$

Proposition 0.4.4 (Frenet frame evolution)**.** *The time evolution of the Frenet frame reads*

$$\partial_t \begin{bmatrix} T \\ N \\ B \end{bmatrix} = \begin{bmatrix} 0 & \partial_s v_N - v_B\tau & v_N\tau + \partial_s v_B \\ -\partial_s v_N + v_B\tau & 0 & \phi \\ -v_N\tau - \partial_s v_B & -\phi & 0 \end{bmatrix} \cdot \begin{bmatrix} T \\ N \\ B \end{bmatrix}, \tag{8}$$

where the last entries are $\phi = \frac{1}{\kappa}(v_N\partial_s\tau + 2\tau\partial_s v_N + \partial_s^2 v_B - v_B\tau^2)$.

0.4.1 Global Quantities

We also include a brief overview of important evolution equations for global geometric quantities. Since the arc-length parametrisation is time-dependent (see Lemma 4.1.1), the path integral does not, in general, commute with the time derivative. Instead, it behaves in the way described in the following lemma.

Lemma 0.4.5. *For any differentiable map $\phi\colon S^1 \times [0,\underline{t}) \to \mathbb{R}^d$ with $d \in \mathbb{N}$ we have*

$$\frac{\mathrm{d}}{\mathrm{d}t}\int_{\Gamma_t} \phi \,\mathrm{d}s = \int_{\Gamma_t} \partial_t\phi - \kappa v_N \phi \,\mathrm{d}s.$$

Proof. Using $\mathrm{d}s = g\,\mathrm{d}u$ we transform the integral into one that commute with ∂_t as

$$\frac{\mathrm{d}}{\mathrm{d}t}\int_{\Gamma_t}\phi\,\mathrm{d}s = \frac{\mathrm{d}}{\mathrm{d}t}\int_{S^1}\phi g\,\mathrm{d}u = \int_{S^1}\partial_t\phi g + \phi\partial_t g\,\mathrm{d}u = \int_{\Gamma_t}\partial_t\phi + \phi\frac{\partial_t g}{g}\,\mathrm{d}s.$$

The statement is then obtained by applying the commutator lemma. □

Based on this lemma, we now state the evolution equation for global quantities of interest.

Proposition 0.4.6 (Evolution of Global Geometric Quantities)**.** *Let $\{\Gamma_t\}_{t\in[0,\underline{t})}$ be a family of curves evolving according to the general geometric flow with velocities v_N and v_B. Then*

$$\begin{aligned}\frac{\mathrm{d}}{\mathrm{d}t}L(\Gamma_t) &= -\int_{\Gamma_t}\kappa v_N\,\mathrm{d}s,\\ \frac{\mathrm{d}}{\mathrm{d}t}\int_{\Gamma_t}\kappa\,\mathrm{d}s &= -\int_{\Gamma_t}\tau\partial_s v_B + \tau^2 v_N\,\mathrm{d}s,\\ \frac{\mathrm{d}}{\mathrm{d}t}\int_{\Gamma_t}\tau\,\mathrm{d}s &= \int_{\Gamma_t}\kappa\tau v_N + \kappa\partial_s v_B\,\mathrm{d}s,\end{aligned}$$

where $L(\Gamma_t)$ denotes the length of the evolving curve Γ_t.

Proof. All formulas follow from Lemma 0.4.5 and use the fact that the curve is closed. □

In later chapters, these equations will lead to important statements about the long-term behaviour of specific geometric flows, like the estimates for the maximal time of existence, classification of singularities, or changes in topological properties like self-linking.

1

High-Codimension Curve Shortening Flow

This Chapter presents results from articles [MKB19] and [MB20] that focus on the long-term behaviour of curve shortening flow in higher dimensional ambient spaces. The theoretical efforts to understand the properties of the original curve shortening problem in $\mathbb{R}^2$ have led to several important results obtained by Hamilton, Gage, and Grayson in [GH86; Gra87]. The well-known Grayson-Gage-Hamilton Theorem states that the curve shortening flow shrinks all simple planar curves to a point, making them asymptotically circular as they approach the singularity and keeping them simple throughout the timespan of the evolution [Whi02]. The motion also preserves the convexity of the curve and makes initially non-convex curves convex in finite time.

Many of these classical results have been generalized for the mean curvature flow of hypersurfaces [Hui84], but they do not hold for the codimension-two problem discussed here. In $\mathbb{R}^3$, the curve shortening flow curves may lead to local singularities before the length vanishes even for embedded curves, and, in general, neither embeddedness nor generalized convexity is preserved in this case.

This problem was first studied by Altschuler and Grayson in [Alt91; AG92], where the short-term existence and uniqueness of the solution were shown. The article [Alt91] also classified all types of singularities that may develop during the motion. Recently, properties of this flow were studied in [MKB19; Kha15; Cor16; He12; MKB19; Lit23] and solitons of the flow were discussed in [Alt+13].

In this chapter, we describe the relationship between moving curves and hypersurfaces via a generalized comparison principle. Convexity of curves and their two-dimensional projections during the flow is discussed in the second part and the third part deals with spherical curves. First, we show that they obey the Avoidance principle and then discuss the behavior of several spherical curves evolving at once.

Let us restate the definition and classical results of curve shortening flow for convenience.

Definition 1.0.1 (Curve shortening flow). *Let $\{\Gamma_t\}_{t\in[0,\underline{t})}$ with $\underline{t} > 0$ be a family of evolving curves. The curve shortening flow is defined as the following initial-value problem:*

$$\partial_t \gamma = \kappa N \qquad \text{on } S^1 \times [0, \underline{t}), \tag{1.1}$$

$$\gamma|_{t=0} = \gamma_0 \qquad \text{in } S^1, \tag{1.2}$$

where $\gamma_0 \in \mathcal{C}^2(S^1; \mathbb{R}^3)$ is the parametrization of the initial curve Γ_0.

Remark 1.0.2. *Although N is undefined for all points on Γ_t where $\kappa = 0$, the right-hand side term $\kappa N = \partial_s^2 \gamma$ in (1.1) remains defined everywhere.*

Let us first state the existence results for curve shortening flow in higher dimensional space that are due to Altshuler.

Theorem 1.0.3 (Short-term existence, Theorem 1.3 in [AG92]). *Let Γ_0 be a closed space curve. Then for some $\varepsilon > 0$, there exists a solution Γ_t to the curve shortening flow (1.1-1.2) with the initial condition Γ_0 on $S^1 \times [0, \varepsilon)$.*

The long term existence is also available for curve shortening in higher dimensional spaces.

Theorem 1.0.4 (Long-term existence, Theorem 1.13 in [AG92]). *Let $\{\Gamma_t\}_{t\in[0,\underline{t})}$ be a solution to the curve shortening flow (1.1-1.2), where $\underline{t} > 0$. If κ is bounded on $S^1 \times [0, \underline{t})$, then there exists an extension of this solution to $S^1 \times [0, \underline{t} + \epsilon)$ for some $\epsilon > 0$.*

Remark 1.0.5. *For local regularity theory consult [Bra78] and [Whi05].*

The fundamental result for curve shortening flow is the Gage-Hamilton-Grayson theorem.

Theorem 1.0.6 (Gage-Hamilton-Grayson theorem [GH86; Gra87]). *Suppose that $\{\Gamma_t\}_{t\in[0,\underline{t})}$ is a family of smooth, embedded, and closed curves in $\mathbb{R}^2$, evolving according to the curve shortening flow (1.1-1.2). Then the following properties hold:*

1. *The length of the curve $L(\Gamma_t)$ is a non-increasing function of t.*
2. *The isoperimetric ratio is a non-decreasing function of t.*

Moreover, under the curve shortening flow, any initial simple closed curve remains embedded for all $t \in [0, \underline{t})$, becomes round as t approaches $\underline{t}$, and vanishes in a round point as t tends to $\underline{t}$.

This theorem however does not generalize to higher codimension. Examples and further discussion of different corner cases will be given throughout this chapter.

There are several tools to analyze long term behaviour and singularities of the curve shortening flow. For example, the entropy formula recently used in [Lit23] to study singularities:

$$\mathcal{E}(\Gamma_t) := \sup_{x_0\in\mathbb{R}^3, t_0>0} \int_{\Gamma_t} \phi_{x_0,t_0}(\gamma(s,t),t)\,\mathrm{d}s.$$

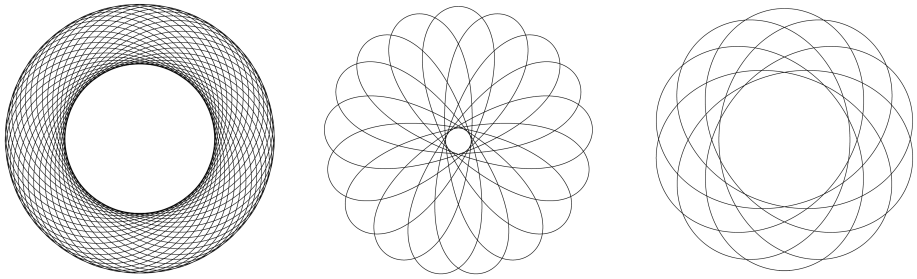

Figure 1.1: Examples of Abresch-Langer shrinkers. Images adapted form [Hal12].

Here ϕ_{x_0,t_0} is the one-dimensional backwards heat kernel centered at (x_0, t_0):

$$\phi_{x_0,t_0}(x,t) = (4\pi t_0)^{-\frac{1}{2}} e^{-\frac{\|x-x_0\|^2}{4t_0}}$$

Due to Huisken's monotonicity result, this entropy is monotone non-increasing under curve shortening flow. The monotonicity formula from [Hui90] states that

$$\frac{\mathrm{d}}{\mathrm{d}t}\int_{\Gamma_t} \phi_{x_0,t_0}\,\mathrm{d}s = -\int_{\Gamma_t}\left|\kappa + \frac{\langle \gamma, N, \rangle}{2(t_0-t)}\right|^2 \phi_{x_0,t_0}\,\mathrm{d}s.$$

Another classical result of Huisken is his comparison principle from [Hui98], which uses

$$R(t) := \sup_{u\neq v} \frac{L(\Gamma_t)}{\pi d_i(u,v,t)} \sin\left[\frac{\pi d_e(u,v,t)}{L(\Gamma_t)}\right],$$

where $d_e(u,v,t) = \|\gamma(u,t) - \gamma(v,t)\|$ is the extrinsic and d_i is the intrinsic distance along the curve. The theorem states that for embedded curves, the value of $R(t)$ is non-increasing. This result can also be used for simpler proof [AB11] of Theorem 1.0.6.

1.0.0 Examples of Solutions

Finding analytical solutions of solutions with given properties gives intuition about the behaviour of a particular problem and provides ideas of feasible theoretical results. In particular, for the curve shortening flow, people studied solutions forming solitons, self-similar solutions [Hal12] or ancient solutions [DHS10] which can be defined in time domain $(-\infty, \underline{t})$. This subsection provides a quick overview of all the known examples.

Example List 1.0.7. *Examples of solutions to the curve shortening flow.*

Ex. 51. **Stationary line.** All straight lines are fixed points due to zero curvature. Lines also represent a limiting shape for the ancient sine curve solution.

Ex. 52. **Shrinking circle.** The simplest non-trivial example is that of shrinking circles $\Gamma_t = \partial B_{\rho(t)}$. Because of the radial symmetry leading to constant curvature, this example leads to an ordinary differential equation for the radius ρ which reads

$$\rho'(t) = -\rho^{-1}(t), \qquad \rho(0) = \rho_0,$$

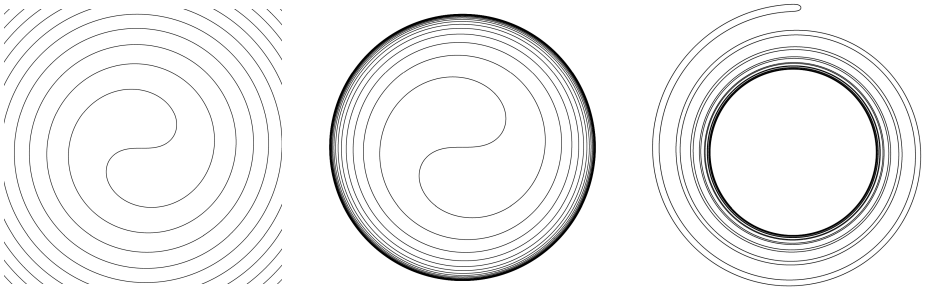

Figure 1.2: Examples of Yin Yang spirals. Images adapted form [Hal12].

where $\rho_0 > 0$ is the initial radius. This equation can be solved analytically as

$$\rho(t) = (\rho_0^2 - 2t)^{\frac{1}{2}},$$

which is defined on $(-\infty, \underline{t})$ with the terminal time $\underline{t} = \frac{1}{2}\rho_0^2$.

Ex. 53. **Helix curve.** Similarly to the shrinking circles example, the helix curve evolution reduces to the following first-order nonlinear ODE for the radius

$$\rho'(t) + (\rho^2(t) + \xi^2)^{-1}\rho(t) = 0,$$

where ξ is a fixed constant from the helix curve paramatrization

$$\gamma(u,t) = (\rho(t)\cos u, \rho(t)\sin u, \xi u)^T.$$

Unlike the circle, this solution approaches the straight line in $\underline{t} = \infty$.

Ex. 54. **Grim reaper.** Another ancient analytical solution is the translating graph

$$\gamma(u,t) = (u, F(u,t))^T, \qquad F(u,t) = -\log\cos u + t$$

for $u \in (-\frac{\pi}{2}, \frac{\pi}{2})$. This example in fact exists for all t in $(-\infty, \infty)$.

Ex. 55. **Paperclip.** Other known analytical examples are given implicitly. The following compact solution, sometimes referred to as the paperclip [Hal12], is given by

$$\Gamma_t = \left\{(x,y)^T \in (-\tfrac{\pi}{2}, \tfrac{\pi}{2}) \times \mathbb{R} \colon \cosh x = e^{-t}\cos y\right\}.$$

This solution is defined for $t \in (-\infty, 0)$ and can be understood as two connected Grim reaper curves that shrink towards a point at $t = 0$.

Ex. 56. **Ancient sine curve.** Another implicitly defined solution similar to the paperclip is the ancient sine curve or hairclip solution [Hal12] defined as

$$\Gamma_t = \left\{(x,y)^T \in \mathbb{R}^2 \colon \sinh x = e^{-t}\cos y\right\}.$$

In this case, the solution exists for $t \in \mathbb{R}$ and is for all times non-compact. It asymptotically approaches a straight line as time approaches infinity.

Ex. 57. **Yin Yang spiral.** Besides the shrinking solitons, there are also many rotating examples or examples that rotate and expand or shrink at the same time [Hal12].

Ex. 58. **Abresch-Langer shrinkers.** This family of planar solutions from [AL86] represent the self-similar limiting shapes for curves with turning numbers larger than 1.

For a comprehensive overview with more examples of solutions in $\mathbb{R}^3$ see [Alt+13]. For other recent developments see [DHS10; Hal12; AY18; Zha+22].

1.0.1 Evolution of Geometric Quantities

This subsection gives an overview of known evolution equations for the curve shortening flow. These technical preliminaries are necessary for most of the results in this chapter.

Lemma 1.0.8. *The evolution equations for the local geometric quantities:*

$$\partial_t g = -g\kappa^2, \tag{1.3}$$
$$\partial_t \kappa = \partial_s^2 \kappa + \kappa^3 - \kappa\tau^2, \tag{1.4}$$
$$\partial_t \tau = 2\kappa^2\tau + \partial_s^2 \tau + \partial_s \left(2\tau \tfrac{\partial_s \kappa}{\kappa}\right). \tag{1.5}$$

Lemma 1.0.9. *The time evolution of the Frenet frame is given by*

$$\partial_t \begin{bmatrix} T \\ N \\ B \end{bmatrix} = \begin{bmatrix} 0 & \partial_s \kappa & \kappa\tau \\ -\partial_s \kappa & 0 & \phi \\ -\kappa\tau & -\phi & 0 \end{bmatrix} \cdot \begin{bmatrix} T \\ N \\ B \end{bmatrix}, \tag{1.6}$$

where bottom right entries are $\phi = \partial_s \tau + 2\tau \frac{\partial_s \kappa}{\kappa}$.

Lemma 1.0.10. *The time evolution of important global quantities is*

$$\begin{aligned} \frac{\mathrm{d}}{\mathrm{d}t} L(\Gamma_t) &= -\int_{\Gamma_t} \kappa^2 \,\mathrm{d}s, \\ \frac{\mathrm{d}}{\mathrm{d}t} \int_{\Gamma_t} \kappa \,\mathrm{d}s &= -\int_{\Gamma_t} \kappa\tau^2 \,\mathrm{d}s, \\ \frac{\mathrm{d}}{\mathrm{d}t} \int_{\Gamma_t} \tau \,\mathrm{d}s &= \int_{\Gamma_t} \kappa^2\tau \,\mathrm{d}s. \end{aligned}$$

The global evolution equations can be used to assess long-term behaviour of the flow.

Proposition 1.0.11. *The length of the curve under the curve shortening flow can be bounded as*

$$L(\Gamma_t) \leqslant (L^2(\Gamma_0) - 8\pi^2 t)^{-\frac{1}{2}} \tag{1.7}$$

Proof. Using Proposition 1.0.10 and the Cauchy-Schwarz inequality yields

$$\frac{\mathrm{d}}{\mathrm{d}t} L(\Gamma_t) = -\int_{\Gamma_t} \kappa^2 \,\mathrm{d}s \leqslant -\frac{1}{L(\Gamma_t)} \left[\int_{\Gamma_t} \kappa \,\mathrm{d}s\right]^2 \leqslant -\frac{4\pi}{L(\Gamma_t)}, \tag{1.8}$$

where the last inequality is due to the Fenchel theorem. □

Note that if Γ_t is knotted for all $t \in [0, \underline{t})$ then the estimate (1.7) can be improved to

$$L(\Gamma_t) \leqslant (L^2(\Gamma_0) - 16\pi^2 t)^{-\frac{1}{2}}.$$

When Γ_t is knotted, one may use the Milnor-Fáry theorem instead of the Fenchel theorem and obtain -8π instead of -4π the right hand side of inequality (1.8).

Corollary 1.0.12. *The maximal time of existence can be bounded as*

$$\underline{t} \leqslant \frac{1}{8\pi^2} L^2(\Gamma_0).$$

The right hand side can be halved when Γ_t remains knotted.

Remark 1.0.13. *In the case of planar curves, one can also consider the evolution of the enclosed area $A(\Gamma_t)$ given by the following, surprisingly simple, formula*

$$A(\Gamma_t) = \frac{1}{2} \int_{\Gamma_t} \langle \gamma, N \rangle \, \mathrm{d}s.$$

Using the Green's Theorem one can show that

$$\frac{\mathrm{d}}{\mathrm{d}t} A(\Gamma_t) = -\int_{\Gamma_t} \kappa \, \mathrm{d}s.$$

For embedded closed curves, the right-hand side is -2π. Thus the area $A(\Gamma_t) = A(\Gamma_0) - 2\pi t$ and vanishes at $\underline{t} = \frac{1}{2\pi} A(\Gamma_0)$. Furthermore, the isoperimetric ratio satisfies

$$\frac{\mathrm{d}}{\mathrm{d}t} \left[\frac{L(\Gamma_t)^2}{A(\Gamma_t)} \right] = -2 \frac{L(\Gamma_t)}{A(\Gamma_t)} \left[\int_{\Gamma_t} \kappa^2 \, \mathrm{d}s - \pi \frac{L(\Gamma_t)}{A(\Gamma_t)} \right].$$

Using this formula and the Bonneson inequality one can show that for an initially convex curve, the isoperimetric ratio approaches 4π as t approaches $\underline{t}$. The isoperimetric inequality implies that the curve must approach a round circle in the limit.

Further maximal time estimates can be achieved by analyzing the curvature.

1.0.2 Curvature estimates

This subsection uses the Weak maximum and minimum principle for scalars from [Topo6] to estimate the evolution of curvature. We begin by restating the classical theorem.

Proposition 1.0.14 (Theorem 3.1.1 from [Topo6])**.** *Let $t \in [0, \underline{t}]$ with $\underline{t} < \infty$. Let $X(t)$ be any smooth real function of time, $F \colon S^1 \times [0, \underline{t}] \to \mathbb{R}$. Suppose $u : S^1 \times [0, \underline{t}] \to \mathbb{R}$ solves*

$$\partial_t u \leqslant \partial_s^2 u + X \partial_s u + F(u, t).$$

Furthermore, let $\alpha \in \mathbb{R}$ and consider $\phi \colon [0, \underline{t}] \to \mathbb{R}$ such that $\phi(0) = \alpha$ and

$$\tfrac{\mathrm{d}\phi}{\mathrm{d}t} = F(\phi(t), t)$$

for all $t \in [0, \underline{t}]$. If $u(\cdot, 0) \leqslant \alpha$, then $u(\cdot, t) \leqslant \phi(t)$ for all $t \in [0, \underline{t}]$.

Remark 1.0.15. *Proposition 1.0.14 also holds if we replace all $\leqslant$ with $\geqslant$. This alternative alternative result is called the weak minimal principle, see Corollary 3.1.2 in [Topo6].*

To point out the differences between the curvature shortening flow in $\mathbb{R}^2$ and $\mathbb{R}^3$, we first state the curvature estimates for the case of planar curves.

Proposition 1.0.16. *Let $\{\Gamma_t\}_{t\in[0,\underline{t})}$ with the terminal time $\underline{t} > 0$ be a family of planar curves evolving according to the curve shortening flow. Furthermore, let us define*

$$\alpha_m := \min_{u\in S^1} \kappa(u,0), \qquad \alpha_M := \max_{u\in S^1} \kappa(u,0). \tag{1.9}$$

Then for all $t \in [0,\underline{t}]$ and all $u \in S^1$ we can bound the curvature from both sides as

$$\alpha_m(1-2\alpha_m^2 t)^{-\frac{1}{2}} \leqslant \kappa(u,t) \leqslant \alpha_M(1-2\alpha_M^2 t)^{-\frac{1}{2}}. \tag{1.10}$$

Proof. For planar curves, the evolution equation for curvature reduces to

$$\partial_t\kappa = \partial_s^2\kappa + \kappa^3.$$

In this case, we may set $X(t) \equiv 0$ and $F(u,t) = u^3$, which leads to

$$\phi(t) := \alpha(1-2\alpha^2 t)^{-\frac{1}{2}},$$

with α being α_m or α_M. The inequality chain (1.10) is then obtained by application of the minimal and maximal principle from Proposition 1.0.14 and Remark 1.0.15. □

The lower estimate of curvature indicates that it must blow up at a finite time. Moreover, the following statement shows how this blow-up time can be upper bounded.

Corollary 1.0.17. *The terminal time $\underline{t}$ of the planar curve shortening flow can be bounded as*

$$\underline{t} \leqslant (2\alpha_m)^{-1},$$

where α_m is the minimum curvature of the initial curve from (1.9).

Proof. The statement follows from the left inequality in (1.10). □

Another, important ramification of inequality (1.9) is the preservation of convexity for planar curves under the curve shortening flow.

Corollary 1.0.18. *Let Γ_t be a planar curve evolving according to curve shortening flow with a convex initial condition, i.e. the signed curvature $\kappa(u,0) \geqslant 0$ for all $u \in S^1$. Then*

$$\kappa(u,t) \geqslant 0$$

for all $u \in S^1$ and $t \in [0,\underline{t})$. Thus, the convexity of the initial curve is preserved.

Proof. The statement follows from the left inequality from (1.10). Initially, non-negative curvature will only increase in time. □

Remark 1.0.19. *Another important inequality involving the curvature is the Hamilton-Harnack inequality from [Ham95]. Their theorem states that assuming Γ_t is convex then*

$$\frac{\partial_t \kappa}{\kappa} - \frac{(\partial_s \kappa)^2}{\kappa^2} + \frac{1}{2t} \leqslant 0.$$

This result is useful for uniqueness proofs for translating solitons [Ham95].

The application of the maximum principle to the three-dimensional case is not as powerful.

Proposition 1.0.20. *Let $\{\Gamma_t\}_{t\in[0,\underline{t})}$ with the terminal time $\underline{t} > 0$ be a family of space curves evolving according to the curve shortening flow. Furthermore, let us define*

$$\alpha_M := \max_{S^1} \kappa(\cdot, 0).$$

Then for all $t \in [0, \underline{t}]$ and all $u \in S^1$ we can upper bound the curvature as

$$\kappa \leqslant \alpha_M (1 - 2\alpha_M^2 t)^{-\frac{1}{2}}.$$

Proof. As the additional term $-\kappa\tau^2$ in (todo) is always non-positive, we may upper bound expression for the curvature derivative $\partial_t \kappa$ to get the following inequality

$$\partial_t \kappa = \partial_s^2 \kappa + \kappa^3 - \kappa\tau^2 \leqslant \partial_s^2 \kappa + \kappa^3,$$

which allows us to use Proposition 1.0.14 as in the proof of Proposition 1.0.16. □

Remark 1.0.21. *For estimates of curvature derivatives see e.g. Theorem 1.25 in [Has16].*

As we have not established the curvature lower bound as in Proposition 1.0.16. This result does not lead to a straightforward estimate of terminal time. To achieve this, we explore new version of the comparison principle in the next Section.

1.1 Generalized Comparison Principle

As suggested in the previous sections, the long term behaviour of the curve shortening flow in higher codimension is not as straightforward as the planar case. Also, some of the tooling used for planar analysis do not generalize to space curves. One such tool is the avoidance or comparison principle, see Theorem 1.0.6. As the notion of inside and outside loses meaning for curves in space, the classical formulation of this result is not applicable.

This section describes results from [MKB19], which expand the comparison principle to higher codimension by bounding the space curve by moving hypersurface. This leads to alternative proof for some of the known results for spherical curves but also allows us to obtain new knowledge about the long term behavior, among others by obtaining a new upper bound for the maximal time of existence.

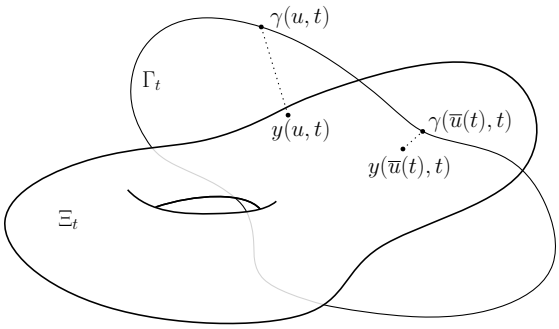

Figure 1.3: Diagram depicting $y(u,t)$ and $\bar{u}(t)$.

1.1.0 Moving Hypersurfaces

For the purposes of this section, we introduce the notion of moving hypersurface in the notation from Chapter 5 of [Kimo8]. Consider a family of closed oriented $\mathcal{C}^2$-class hypersurfaces in m-dimensional Euclidean space $\mathbb{R}^m$, denoted by $\{\Xi_t\}_{t\in[0,t_\Xi)}$ with $t_\Xi > 0$.

Since Ξ_t is oriented and closed manifold at each time t, there are two disjoint open sets $\Omega_t^\pm$ such that $\Omega_t^+ \cup \Omega_t^- = \mathbb{R}^m \backslash \Xi_t$. The sign convention of $\Omega_t^\pm$ determines the direction of the unit normal vector denoted by ν. For every time $t \in [0, t_\Xi)$ and point $y \in \Xi_t$, we set $\nu(y,t)$ to point outward of Ω_t^+.

Let ∇_{Ξ_t} denote the surface gradient on Ξ_t and W denote the Weingarten map given by

$$W(y,t) = -(\nabla_{\Xi_t}\nu_1, \ldots, \nabla_{\Xi_t}\nu_m)(y,t).$$

We further define the principal curvatures $\kappa_1, \ldots, \kappa_{m-1}$ which are the eigenvalues of the Weingarten map W with $\langle e_i, \nu\rangle = 0$, i.e. $We_i = \kappa_i e_i$ for $i = 1, \ldots, m-1$ and $W\nu = 0$. Note that $\{e_1, \ldots, e_{m-1}, \nu\}$ becomes an orthonormal basis of $\mathbb{R}^m$ (see Chapter 2 in [Kimo8] for further details).

Remark 1.1.1. *By changing the orientation of Ξ_t, i.e. swapping Ω_t^+ and Ω_t^-, we not only affect the direction of the normal vector ν but also the sign of the principal curvatures $\kappa_1, \ldots, \kappa_m$. For example, if we consider $\Xi_t = \partial B$ and $\Omega_t^- = B$, where $B \in \mathbb{R}^m$ is a unit ball, the normal vector ν is pointing towards the center of B and all principal curvature are equal to* 1.

Following the notation in Chapter 5 from [Kimo8], we say that $\{\Xi_t\}_{t\in[0,\underline{t})}$ is a $\mathcal{C}^{2,1}$-class if $\nu \in \mathcal{C}^1(\mathcal{M}; \mathbb{R}^m)$, where we formally define $\mathcal{M}$ as the set

$$\mathcal{M} := \bigcup_{t\in[0,\underline{t})} \Xi_t \times \{t\} \subset \mathbb{R}^m \times \mathbb{R}.$$

Finally, the time evolution of $\{\Xi_t\}_{t\in[0,t_\Xi)}$ is given by its normal velocity functional

$$V(x,t) = \left\langle z'(t), \nu(x,t)\right\rangle,$$

where z is a differentiable function of time t with initial condition $z(0) = x$ and such that $z(t') \in \Xi_{t'}$ for all t' from some neighborhood of t.

1.1.1 Signed Distance Function

We analyse the relationship between the evolving curve Γ_t and the moving hypersurface Ξ_t by means of the signed-distance function ϕ. For point $x \in \mathbb{R}^m$ and time t, we define ϕ as

$$\phi(x,t) := \begin{cases} \text{dist}(x, \Xi_t) & \text{for } x \in \Omega_t^+ \\ 0 & \text{for } x \in \Xi_t \\ -\text{dist}(x, \Xi_t) & \text{for } x \in \Omega_t^- \end{cases}.$$

For readers' convenience, we introduce the following notation depicted in Figure 1.3:

$$y(u,t) = \operatorname*{argmin}_{z \in \Xi_t} \|\gamma(u,t) - z\|, \tag{1.11}$$

$$\bar{u}(t) = \operatorname*{argmin}_{u \in S^1} \|\gamma(u,t) - y(u,t)\|. \tag{1.12}$$

With the help of this notation, we recall the properties of signed distance functions and summarize them in the following lemma. For more details, see Chapter 3 in [Kimo8].

Lemma 1.1.2. *When Ξ_t is sufficiently smooth, there exists $\varepsilon_0 > 0$ such that when*

$$\text{dist}(\gamma(u,t), \Xi_t) < \varepsilon_0$$

for some parameter $u \in S^1$ and time $t \in [0, \underline{t})$, then the helper function $y(u,t)$ is unique and the derivatives of the signed distance function ϕ can be expressed as

$$\nabla\phi(\gamma(u,t),t) = -\nu(y(u,t),t), \tag{1.13}$$

$$\Delta_s\phi(\gamma(u,t),t) = \sum_{i=1}^{m-1} \frac{\kappa_i(y(u,t),t)}{1 + \phi(\gamma(u,t),t)\kappa_i(y(u,t),t)}, \tag{1.14}$$

$$H\phi(\gamma(u,t),t) = (\mathbb{I} + \phi(\gamma(u,t))W(y(u,t),t))^{-1}W(y(u,t),t), \tag{1.15}$$

$$\partial_t\phi(\gamma(u,t),t) = v(y(u,t),t). \tag{1.16}$$

where $H\phi$ is the Hessian of ϕ and $\mathbb{I}$ is the m by m identity matrix.

Proof. Proofs of all formulas as well as other details concerning signed distance functions of hypersurfaces can be retrieved from Chapter 3 of [Kimo8]. □

1.1.2 Comparison Theorem

Before stating the generalized comparison theorem, we define an auxiliary function ρ, describing the minimal distance between the curve Γ_t and the hypersurface Ξ_t, as

$$\rho(t) := \min_{u \in S^1} \text{dist}(\gamma(u,t), \Xi_t). \tag{1.17}$$

In simpler terms, this function can be rewritten as

$$\rho(t) = \text{dist}(\gamma(\bar{u}(t),t), \Xi_t) = \|\gamma(\bar{u}(t),t) - y(\bar{u}(t),t)\|.$$

We can now state the main result of this Section.

Proposition 1.1.3 (Main theorem from [MKB19]). *Let $\{\Gamma_t\}_{t\in[0,t_\Gamma)}$ with $t_\Gamma > 0$ be a family of space curves moving according to the curve shortening flow equation (1.1-1.2) and let $\{\Xi_t\}_{t\in[0,t_\Xi)}$ with $t_\Xi > 0$ be a $\mathcal{C}^{2,1}$-class moving hypersurface with V satisfying*

$$V(y,t) \geqslant \max_{1\leqslant i<m} \kappa_i(y,t) \tag{1.18}$$

for all $t \in [0,t_\Xi)$ and all $y \in \Xi_t$. Assume that the initial curve Γ_0 lies inside Ω_0^+ and the parametrisation γ_0 is from $\mathcal{C}^2(S^1;\mathbb{R}^m)$. Furthermore assume that there is $\varepsilon_0 > 0$ such that, for all $u \in S^1$ and $t \in [0,t_\Xi)$ for which

$$0 < \operatorname{dist}(\gamma(u,t),\Xi_t) < \varepsilon_0$$

there exist $y(u,t)$ and $\bar{u}(t)$ and equations (1.13-1.16) are satisfied. Finally, assume that both the normal velocity V of Ξ_t and the curvature K of Γ_t are uniformly bounded. Then

$$\rho(t) \geqslant \min\{\varepsilon_0, \rho(0)\}. \tag{1.19}$$

for all t between 0 and $\min\{t_\Gamma, t_\Xi\}$.

Proof. Let us abbreviate $\bar{\gamma}(t) := \gamma(\bar{u}(t),t)$ and $\bar{y}(t) := y(\bar{u}(t),t)$ and for $\varepsilon > 0$ denote

$$I_\varepsilon := \{t \in [0,\min\{t_\Gamma,t_\Xi\}) \,:\, \operatorname{dist}(\bar{\gamma}(t),\Xi_t) < \varepsilon\}.$$

Lemma 1.1.2 implies the existence of $\varepsilon_0 > 0$ such that the formulae (1.13-1.16) hold on the subset I_{ε_0}. As $\phi(\gamma(\cdot,t),t)$ attains its minimum at $\bar{u}(t)$ and is $\mathcal{C}^2$-class, its first derivative is

$$0 = \tfrac{\mathrm{d}}{\mathrm{d}u}\left[\phi(\gamma(u,t),t)\right]|_{u=\bar{u}(t)} = \left\langle \nabla\phi(\bar{\gamma}(t),t), \partial_u\gamma(\bar{u}(t),t)\right\rangle \tag{1.20}$$

and the second derivative satisfies the following inequality

$$\begin{aligned} 0 &\leqslant \tfrac{\mathrm{d}^2}{\mathrm{d}u^2}\left[\phi(\gamma(u,t),t)\right]|_{u=\bar{u}(t)} = \tfrac{\mathrm{d}}{\mathrm{d}u}\left\langle \nabla\phi(\gamma(u,t),t), \partial_u\gamma(u,t)\right\rangle|_{u=\bar{u}(t)} \\ &= \left\langle H\phi(\bar{\gamma}(t),t)\partial_u\gamma(\bar{u}(t),t), \partial_u\gamma(\bar{u}(t),t)\right\rangle + \left\langle \nabla\phi(\bar{\gamma}(t),t), \partial_u^2\gamma(\bar{u}(t),t)\right\rangle, \end{aligned} \tag{1.21}$$

where $\partial_u\gamma(u,t) = \|\partial_u\gamma(u,t)\|T(u,t)$ and

$$\partial_u^2\gamma(u,t) = \|\partial_u\gamma(u,t)\|^{-1}\partial_u\|\partial_u\gamma(u,t)\|\partial_u\gamma(u,t) + \|\partial_u\gamma(u,t)\|^2K(u,t)N(u,t).$$

From (1.13) and (1.20), it follows that $\langle T(\bar{u}(t),t), \nu(y(t),t)\rangle = 0$. Moreover,

$$\left\langle \nabla\phi(\bar{\gamma}(t),t), \partial_u^2\gamma(\bar{u}(t),t)\right\rangle = -\|\partial_u\gamma(\bar{u}(t),t)\|^2\left\langle \nu(\bar{y}(t),t), (KN)(\bar{u}(t),t)\right\rangle. \tag{1.22}$$

Combining the above formulate (1.22) to (1.21) yields

$$\left\langle H\phi(\bar{\gamma}(t),t)T(\bar{u}(t),t), T(\bar{u}(t),t)\right\rangle \geqslant \left\langle \nu(\bar{y}(t),t), (KN)(\bar{u}(t),t)\right\rangle. \tag{1.23}$$

In the following, we show that ρ from (1.17) is Lipschitz continuous in I_{ε_0}. From the definition of the closest point parameter $\bar{u}(t)$, we obtain the following inequality

$$\begin{aligned} \rho(t_2) - \rho(t_1) &= \phi(\gamma(\bar{u}(t_2),t_2),t_2) - \phi(\gamma(\bar{u}(t_1),t_1),t_1) \\ &\leqslant \phi(\gamma(\bar{u}(t_1),t_2),t_2) - \phi(\gamma(\bar{u}(t_1),t_1),t_1). \end{aligned}$$

The derivative $\frac{\mathrm{d}}{\mathrm{d}t}\phi(\gamma(u,t),t)$ can be upper bounded as

$$\begin{aligned}\left|\tfrac{\mathrm{d}}{\mathrm{d}t}\phi(\gamma(u,t),t)\right| &= \left|\langle\nabla\phi(\gamma(u,t),t),\partial_t\gamma(u,t)\rangle + \partial_t\phi(\gamma(u,t),t)\right| \\ &\leqslant \left|\langle\nabla\phi(\gamma(u,t),t),K(u,t)N(u,t)\rangle\right| + |v(y(u,t),t)|.\end{aligned}$$

Furthermore, the properties of $\phi(\gamma(u,t),t)$ imply an existence of a positive constant $C>0$ such that for a fixed parameter value $u\in S^1$ and for all times t from the interval I_{ε_0} we get

$$\left|\tfrac{\mathrm{d}}{\mathrm{d}t}\phi(\gamma(u,t),t)\right| \leqslant \sup_{t\in[0,\min\{t_\Gamma,t_\Xi\})}\left[\max_{u\in S^1}|K(u,t)| + \max_{y\in\Xi_t}|v(y,t)|\right] =: C,$$

which implies that $|\rho(t_2)-\rho(t_1)|\leqslant C|t_2-t_1|$. We now use the Rademacher theorem (see e.q. [EG92]), which ensures the existence of a subset $\mathcal{N}\subset I_{\varepsilon_0}$ with zero one-dimensional Lebesgue measure $\mu(\mathcal{N})=0$ such that for all $t\in I_{\varepsilon_0}\backslash\mathcal{N} =: \tilde{I}_{\varepsilon_0}$ we can write

$$\rho'(t) = \lim_{h\to 0^+}\frac{\rho(t+h)-\rho(t)}{h} = \lim_{h\to 0^+}\frac{\rho(t)-\rho(t-h)}{h} \leqslant C.$$

For time t from the new interval $\tilde{I}_{\varepsilon_0}$ and for small value $h>0$ we get

$$\rho(t+h)-\rho(t) \leqslant \phi(\gamma(\bar{u}(t),t+h),t+h) - \phi(\gamma(\bar{u}(t),t),t), \tag{1.24}$$
$$\rho(t)-\rho(t-h) \geqslant \phi(\gamma(\bar{u}(t),t),t) - \phi(\gamma(\bar{u}(t),t-h),t-h). \tag{1.25}$$

In the limit as h approaches 0 from above, the above inequalities (1.25) and (1.24) lead to

$$\rho'(t) \leqslant \tfrac{\mathrm{d}}{\mathrm{d}t}\phi(\gamma(u,t),t)|_{u=\bar{u}(t)}, \tag{1.26}$$
$$\rho'(t) \geqslant \tfrac{\mathrm{d}}{\mathrm{d}t}\phi(\gamma(u,t),t)|_{u=\bar{u}(t)}. \tag{1.27}$$

Thus we arrive at a formula for $\rho'(t)$ that can be further rewritten as

$$\begin{aligned}\rho'(t) &= \tfrac{\mathrm{d}}{\mathrm{d}t}\phi(\gamma(u,t),t)|_{u=\bar{u}(t)} \\ &= \langle\nabla\phi(\bar{\gamma}(t),t),\partial_t\gamma(\bar{u}(t),t)\rangle + \partial_t\phi(\bar{\gamma}(t),t) \\ &= -\langle\nu(\bar{y}(t),t),(KN)(\bar{u}(t),t)\rangle + v(\bar{y}(t),t).\end{aligned}$$

Using (1.23) and the assumption (1.18), we can lower bound $\psi'(t)$ by

$$\rho'(t) \geqslant \max_{1\leqslant i<m}\kappa_i(\bar{y}(t),t) - \langle H\phi(\bar{\gamma}(t),t)T(\bar{u}(t),t),T(\bar{u}(t),t)\rangle. \tag{1.28}$$

The second term in (1.28) can be rewritten as the following sum

$$\begin{aligned}\langle H\phi(\bar{\gamma}(t),t)T(\bar{u}(t),t),T(\bar{u}(t),t)\rangle &= \left\langle\frac{W(\bar{y}(t),t)T(\bar{u}(t),t)}{I+\phi(\bar{\gamma}(t),t)W(\bar{y}(t),t)},T(\bar{u}(t),t)\right\rangle \\ &= \sum_{i=1}^{m-1}\frac{\kappa_i(\bar{y}(t),t)\langle T(\bar{u}(t),t),e_i(\bar{y}(t),t)\rangle^2}{1+\phi(\bar{\gamma}(t),t)\kappa_i(\bar{y}(t),t)},\end{aligned}$$

where part of the summand can be upper bounded from non-negativity of $\phi(\bar{\gamma}(t),t)$ as

$$\frac{\kappa_i(\bar{y}(t),t)}{1+\phi(\bar{\gamma}(t),t)\kappa_i(\bar{y}(t),t)} \leqslant \kappa_i(\bar{y}(t),t) \leqslant \max_{1\leqslant j<m}\kappa_j(\bar{y}(t),t).$$

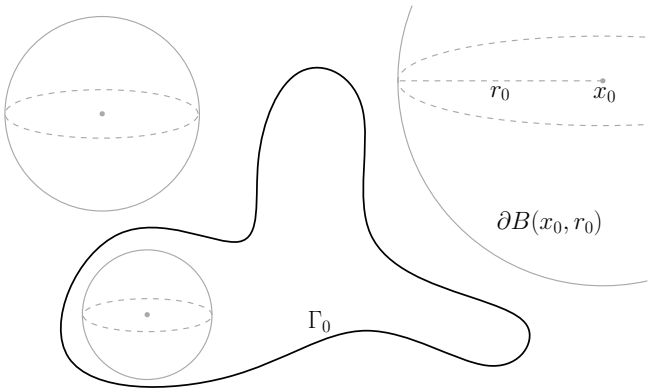

Figure 1.4: According to Corollary 1.1.4, the initial curve Γ_0 surrounded by disjoint spheres will remain disjoint with all of them as they simultaneously shrink according to the curvature shortening flow and the mean curvature flow, respectively.

As $\{e_1, \dots, e_{m-1}, \nu\}$ forms an orthonormal basis, we get

$$\rho'(t) \geqslant \left[1 - \sum_{i=1}^{m-1} \langle T(\bar{u}(t), t), e_i(\bar{y}(t), t)\rangle^2\right] \max_{1 \leqslant i < m} \kappa_i(\bar{y}(t), t) = 0.$$

For convenience, define a positive constant

$$c_0 := \min\{\varepsilon_0, \rho(0)\},$$

where $\rho(0)$ is positive from the assumption $\Gamma_0 \subset \Omega_0^+$. For contradiction, assume there is $t_1 \in (0, \min\{t_\Gamma, t_\Xi\})$ such that $\rho(t_1) \in (0, c_0)$ and $\rho(t_1) \leqslant \rho(t)$ for $t \in [0, t_1]$. Since the function ρ is continuous on $[0, \min\{t_\Gamma, t_\Xi\})$, there exists $t_0 \in [0, t_1)$ such that

$$\rho(t_1) < \rho(t_0) \quad \text{and} \quad \rho(t) < \varepsilon_0 \text{ for } t \in [t_0, t_1]. \tag{1.29}$$

Since $\rho' \geqslant 0$ almost everywhere on $[t_0, t_1]$, its integral must be non-negative and thus

$$\rho(t_1) - \rho(t_0) = \int_{t_0}^{t_1} \rho'(t)\mathrm{d}t \geqslant 0.$$

As this contradicts equation (1.29), we conclude that $\rho(t) \leqslant c_0$. This proves the original statement (1.19). □

1.1.3 Ramifications

By choosing different moving hypersurfaces Ξ_t to bound the motion of space curves from inside or outside, one can use Theorem 1.1.3 to uncover the following insights about the long term behaviour of space curves during the curve shortening flow, see Figure 1.4.

Corollary 1.1.4 (Corollary 1 from [MKB19]). *Let Γ_t satisfy (1.1-1.2) with the initial condition Γ_0 satisfying $\Gamma_0 \cap \partial B(x_0, r_0) = \varnothing$ for some $x_0 \in \mathbb{R}^m$ and $r_0 > 0$. Then*

$$\Gamma(t) \cap \partial B\left(x_0, \sqrt{r_0^2 - 2t}\right) = \varnothing.$$

for all t between 0 and $\underline{t}$. Furthermore, if $\Gamma_0 \subset B(x_0, r_0)$, the maximal time of existence $\underline{t}$ is upper bounded by $\frac{1}{2}r_0^2$.

Proof. Consider the following family of moving hypersurfaces

$$\Xi_t := \partial B\left(x_0, \sqrt{r_0^2 - 2t}\right)$$

with the orientation defined by position of Γ_0 in such a way that $\Gamma_0 \subset \Omega_0^+$. The hypersurface Ξ_t evolves with normal velocity

$$v = \max_{1 \leqslant i \leqslant m} \kappa_i = \pm(r_0^2 - 2t)^{-\frac{1}{2}},$$

with the sign determined by the orientation of Ξ_t. The statement trivially follows from Theorem 1.1.3. □

Theorem 1.1.3 gives us an alternative proof of the fact that spherical curves remain spherical under the curve shortening flow. The original proof can be found in [He12] and several ramifications of this result have been described in [Cor16; Kha15].

Corollary 1.1.5 (Corollary 2 from [MKB19]). *Let Γ_t satisfy (1.1-1.2) with the initial curve Γ_0 which lies in a sphere $\Gamma_0 \subset \partial B(x_0, r_0)$ with center $x_0 \in \mathbb{R}^m$ and radius $r_0 > 0$. Then*

$$\Gamma_t \subset \partial B\left(x_0, \sqrt{r_0^2 - 2t}\right)$$

for all t between 0 and the terminal time $\underline{t}$.

Proof. Using Corollary 1.1.4 we can bound Γ_t between two concentric spheres

$$\Gamma_t \subset B\left(x_0, \sqrt{r_0^2 + \varepsilon - 2t}\right) \setminus \bar{B}\left(x_0, \sqrt{r_0^2 - \varepsilon - 2t}\right),$$

where $0 < \varepsilon < r_0^2$ and the time t lies between 0 and $\min\left\{\underline{t}, \frac{1}{2}(r_0^2 - \varepsilon)\right\}$. Letting ε approach 0 from above proves the statement. □

Furthermore, we show how Theorem 1.1.3 can be used with non-spherical surfaces Ξ_t. In this case, we assume the surface is a boundary of a convex set, see Figure 1.5, but one can also prove other variations of the following statement.

Corollary 1.1.6 (Corollary 3 from [MKB19]). *Let Γ_t satisfy (1.1-1.2) with the initial curve $\Gamma_0 \subset \Omega$, where $\Omega \subset \mathbb{R}^n$ is a bounded convex domain with a C^2-class boundary $\partial\Omega$. Then*

$$\forall t \in [0, \underline{t}) : \ \Gamma_t \subset \Omega.$$

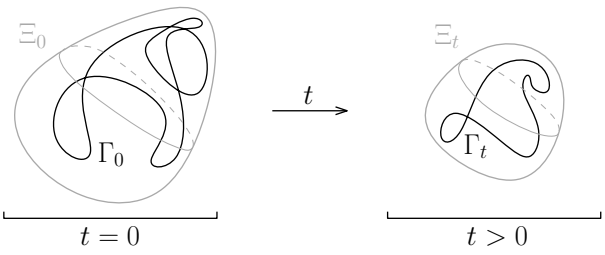

Figure 1.5: Corollary 1.1.6 states that Γ_t stays inside of the convex hull of the initial curve Γ_0.

Proof. As Ω is convex, we can choose a trivial static hypersurface $\Xi_t := \partial\Omega$ with the normal velocity $v \equiv 0$. In this case, all principal curvatures of $\partial\Omega$ are non-positive and thus the assumption (1.18) from Theorem 1.1.3 is trivially satisfied. □

Finally we apply Theorem 1.1.3 to curves bounded by a shrinking cylinder.

Corollary 1.1.7 (Cylindrical Estimate)**.** *Let the family of compact space curves Γ_t satisfy the curve shortening flow (1.1-1.2) with the initial curve Γ_0 which lies inside a cylinder*

$$C_{p,v,\rho_0} := \{x \in \mathbb{R}^3 \colon \|x - p\|^2 - \langle x - p, v\rangle^2 \leqslant \rho_0^2\},$$

where $p, v \in \mathbb{R}^3$ are both constants and v is a unit vector. Then Γ_t will remain inside the cylinder $C_{p,v,\rho(t)}$, where the radius shrinks in time as $\rho(t) = (\rho_0^2 - 2t)^{\frac{1}{2}}$.

Proof. The moving hypersurface $\Xi_t = \partial C_{p,v,\rho(t)}$ has principle curvatures $\kappa_1 = \rho(t)^{-1}$ and $\kappa_2 = 0$. We can thus apply the same argument as in Corollary 1.1.4 and prove the statement using Theorem 1.1.3. □

Remark 1.1.8. *Using Corollary 1.1.7, one can further bound the maximal time of existence for curves inside a cylinder in the same way we did with spheres in Corollary 1.1.4. It is important to note that Corollary 1.1.7 does not work for non-compact curves. For instance, the Grim reaper solution from Ex. 54. or the shrinking helix curve from Ex. 53. exist forever and do not stay inside any cylinder that vanishes in finite time.*

We end this subsection with another upper bound for the maximal time of existence $\underline{t}$ that requires the following definition.

Definition 1.1.9 (Curve diameter)**.** *The diameter of space curve Γ is defined as*

$$\operatorname{diam}(\Gamma) = 2\inf\{\rho \colon \exists x \in \mathbb{R}^3, \Gamma \subset B_\rho(x)\}, \tag{1.30}$$

where $B_\rho(x)$ is a ball of radius ρ centered at the point x.

Finally we state a terminal time estimate obtained from the generalized comparison principle.

Corollary 1.1.10. *Let $\{\Gamma_t\}_{t\in[0,\underline{t})}$ satisfy (1.1-1.2) with the initial curve Γ_0. Then we get*

$$\underline{t} \leqslant \tfrac{1}{8}\operatorname{diam}^2(\Gamma_0)$$

Proof. The result is directly implied by Corollary 1.1.4. □

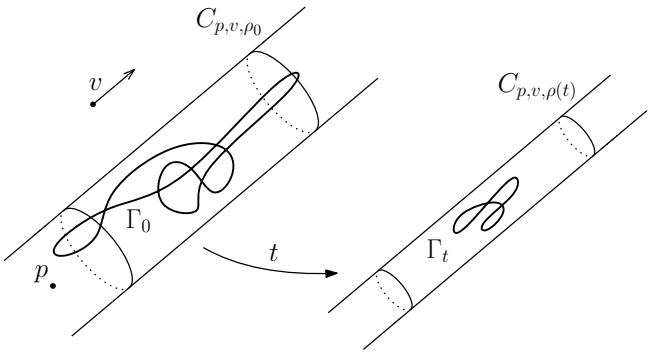

Figure 1.6: Diagram depicting cylindrical estimate from Corollary 1.1.7.

1.2 Convexity Conditions

The curve shortening flow in $\mathbb{R}^2$ preserves convexity as we demonstrated in Corollary 1.0.18. The same is true for the mean curvature flow in higher dimensional spaces. However, with increasing codimension, the situation becomes more complex.

1.2.0 Convex Space Curves

Results from this section can be found in [MB20], where the following definition of convexity is proposed. Although global convexity is not commonly defined for space curves, we define this notion using Minkowski functional.

Definition 1.2.1 (Definition 3.1 from [MB20]). *For a convex set $K \subset \mathbb{R}^n$ and point $y \in \mathbb{R}^n$, let $\mathscr{M}_K^y : \mathbb{R}^n \to \mathbb{R}^+$ denote the Minkowski functional prescribed by*

$$\mathscr{M}_K^y(x) := \inf\left\{\lambda \in \mathbb{R}^+ : \tfrac{1}{\lambda}(x-y) \in K\right\}.$$

for all $x \in \mathbb{R}^n$. We say that a closed curve Γ is convex if there exist $y \in \mathbb{R}^n$ such that

$$\mathscr{M}^y_{\mathrm{C}(\Gamma)}\Big|_\Gamma \equiv 1,$$

where $\mathrm{C}(\Gamma)$ is the convex hull of the curve Γ, i.e. the smallest convex superset of Γ.

The convexity defined above is in general not preserved during the curve shortening flow.

Proposition 1.2.2. *The curve shortening flow in $\mathbb{R}^3$ does not preserve convexity.*

Proof. We prove this statement by direct construction of counterexample (see Example 3.2 from [MB20]). Consider the initial curve Γ_0 given by the following parametrization

$$\gamma_0(u) := \begin{bmatrix} \cos(\alpha u^3 + \beta u) \\ \sin(\alpha u^3 + \beta u) \\ \sin u - \frac{1}{2}\sin(2u) \end{bmatrix}, \qquad \alpha := \frac{\pi+2}{2(1-\pi^2)}, \qquad \beta := \frac{\pi^3+2}{2(\pi^2-1)}, \tag{1.31}$$

for all $u \in S^1$. One can show that this curve is convex according to Definition 1.2.1, but it will lose its convexity while evolving according to the curve shortening flow. Since the curvature of Γ_0 at the point $u = 0$ is greater than its curvature at $u = \omega$ and $u = -\omega$, where

$$\omega := (\pi^3 + 2)^{\frac{1}{2}}(\pi + 2)^{-\frac{1}{2}},$$

$\gamma(0, t)$ departs from the line segment $\mathrm{C}(\{\gamma(-\omega, t), \gamma(\omega, t)\})$ which lies on the boundary of $\mathrm{C}(\Gamma_t)$. Thus Γ_t will stop being convex immediately after $t = 0$. □

We now know that the convexity proposed in Definition 1.2.1 is not preserved. But we will later present a result stating that the convexity of their orthogonal projections is preserved. To achieve that, we need to prepare several lemmas.

1.2.1 Star-shaped Curves

The following two lemmas are used in the proof of Proposition 1.2.6. Lemma 1.2.4 uses the notion of star-shaped curves, which are boundaries of star-shaped sets. We call a closed curve Γ_t star-shaped if it bounds a star-shaped region. Let us present a simple sufficient condition.

Lemma 1.2.3 (Star-Shaped Curve)**.** *Consider a closed planar curve Γ_t such that there is $x \in \mathbb{R}^2$ such that $\gamma(u, t) - x$ and $T(u, t)$ are linearly dependent for all $u \in S^1$. Then Γ_t is star-shaped.*

We will use the fact that small variations of convex curve will still be star-shaped. The following lemma formalizes this idea.

Lemma 1.2.4. *Let $\{\Gamma_t\}_{t\in[0,\underline{t})}$ be a family of closed planar curves such that Γ_0 is convex with a $\mathcal{C}^1$-class parametrization. Then there exists $t_0 > 0$ such that Γ_t is star-shaped for all $t \in [0, t_0)$.*

Proof. For a fixed vector x for the interior of the initial curve Γ_0, let us define

$$\varphi(u, t) := \|\gamma(u, t) - x\| - |\langle \gamma(u, t) - x, T(u, t)\rangle|.$$

for all $(u, t) \in S^1 \times [0, \underline{t})$. Note that this functional is continuous from the assumptions and, furthermore, φ is non-negative due to the Cauchy-Schwarz inequality. Since the initial curve is convex, $\varphi > 0$ in $t = 0$, it is also star-shaped with respect to any point inside. Thus there is $t_0 \in [0, \underline{t})$ such that x is in the interior of Γ_t and

$$\varphi(u, t) > \tfrac{1}{2} \inf_{S^1} \varphi(\cdot, 0)$$

for all $u \in S^1$ and $t \in [0, t_0)$, because φ is continuous. Thus the curve Γ_t is star-shaped with respect to the point x for all $t \in [0, t_0)$. □

1.2.2 Orthogonal Projection

Note that Lemma 1.2.4 imposes regularity assumption on the parametrization γ but it does not require the curve to follow the curve shortening equation (1.1-1.2). One more technical lemma is required before we prove the preservation of projection convexity. This lemma shows the relationship between the original and projected normal vectors.

Lemma 1.2.5. *Let $\mathcal{P} \in \mathcal{L}(\mathbb{R}^3)$ be an orthogonal projection of rank 2, i.e.* $\operatorname{dimRan}\mathcal{P} = 2$. *For a space curve Γ, denote the projected curve $\mathcal{P}\Gamma$ and its curvature κ_P. Let $u \in S^1$ denote any fixed parameter such that the projected curve satisfies $\|\partial_u \mathcal{P}\gamma(u)\| > 0$ and $\kappa_{\mathcal{P}}(u) > 0$. Then*

$$\langle \mathcal{P}N(u), N_{\mathcal{P}}(u)\rangle > 0,$$

where $N(u)$ is the principal normal vector of Γ at the point $\gamma(u)$ and $N_{\mathcal{P}}(u)$ denotes the normal vector of the projected planar curve $\mathcal{P}\Gamma$ at point $\mathcal{P}\gamma(u)$.

Proof. Note that the positivity of $\kappa_P(u) > 0$ also implies the positivity of $\kappa(u) > 0$ and that both N and $N_{\mathcal{P}}$ are well defined at u. We thus can express

$$\langle \mathcal{P}N, N_{\mathcal{P}}\rangle = \left\langle \frac{1}{\kappa}\partial_s^2 \mathcal{P}\gamma, \frac{1}{\kappa_{\mathcal{P}}\|\partial_s \mathcal{P}\gamma\|^2}\partial_s^2 \mathcal{P}\gamma - \frac{\partial_s\|\partial_s \mathcal{P}\gamma\|}{\kappa_{\mathcal{P}}\|\partial_s \mathcal{P}\gamma\|^3}\partial_s \mathcal{P}\gamma \right\rangle,$$

where we omitted writing the parameter u for better readability. Using the Cauchy-Schwarz inequality, we immediately obtain the non-negativity condition $\langle \mathcal{P}N, N_{\mathcal{P}}\rangle \geqslant 0$, because

$$\kappa\kappa_{\mathcal{P}}\|\partial_s \mathcal{P}\gamma\|^4 \langle \mathcal{P}N, N_{\mathcal{P}}\rangle = \|\partial_s^2 \mathcal{P}\gamma\|^2\|\partial_s \mathcal{P}\gamma\|^2 - \langle \partial_s \mathcal{P}\gamma, \partial_s^2 \mathcal{P}\gamma\rangle^2 \geqslant 0.$$

The equality $\langle \mathcal{P}N, N_{\mathcal{P}}\rangle = 0$ would occur only if there was $\alpha \geqslant 0$ such that $\partial_s^2 \mathcal{P}\gamma = \alpha\partial_s \mathcal{P}\gamma$. This implies that $\partial_u^2 \mathcal{P}\gamma = \beta\partial_u \mathcal{P}\gamma$ with $\beta = \alpha g + \frac{1}{2}\partial_u g^2$. Moreover,

$$\kappa_{\mathcal{P}} N_{\mathcal{P}} = \|\partial_u \mathcal{P}\gamma\|^{-2}\partial_u^2 \mathcal{P}\gamma - \|\partial_u \mathcal{P}\gamma\|^{-3}\partial_u\|\partial_u \mathcal{P}\gamma\|\partial_u \mathcal{P}\gamma.$$

Altogether, this leads to the following formula for the curvature $\kappa_{\mathcal{P}}$ of the projected curve:

$$\kappa_{\mathcal{P}} = \beta\|\partial_u \mathcal{P}\gamma\|^{-2} - \|\partial_u \mathcal{P}\gamma\|^{-4}\left\langle \partial_u \mathcal{P}\gamma, \partial_u^2 \mathcal{P}\gamma\right\rangle = 0,$$

which contradicts the assumption $\kappa_{\mathcal{P}} > 0$ and thus the inequality is strict. □

1.2.3 Convex Projection

From the counterexample given in Proposition 1.2.2, we know that the curve shortening flow in higher codimension does not preserve convexity introduced in Definition 1.2.1. The following proposition states that the convexity of their orthogonal projections is preserved.

Proposition 1.2.6 (Proposition 3.5 from [MB20])**.** *Let $\mathcal{P} \in \mathcal{L}(\mathbb{R}^3)$ be an orthogonal projection of rank 2 and let Γ_0 be a space curve with a convex projection $\mathcal{P}\Gamma_0$. Assume that the parametrization $\mathcal{P}\gamma(\cdot, t)$ of the projected curve $\mathcal{P}\Gamma_t$ is regular for all $t \in [0, \underline{t})$. If Γ_t evolves according to the curve shortening flow from Γ_0, then $\mathcal{P}\Gamma_t$ remains convex for all $t \in [0, \underline{t})$.*

Proof. For a contradiction, assume that $\mathcal{P}\Gamma_t$ loses its convexity during the evolution. We will formalize the proof using a functional $\psi\colon S^1 \times [0, \underline{t}) \to \mathbb{R}_0^+$ defined as

$$\psi(u, t) := \operatorname{dist}\left(\mathcal{P}\gamma(u, t),\ \ \partial\mathrm{C}(\mathcal{P}\Gamma_t)\right).$$

and another helper induced function of time $\Psi\colon [0, \underline{t}) \to \mathbb{R}_0^+$ given by

$$\Psi(t) := \max_{u \in S^1} \psi(u, t). \tag{1.32}$$

The proof is structured in the following way. It is divided into proofs of four individual steps labeled (A), (B), (C), and (D). The combination of statements leads to the contradiction.

(A) $\psi(\cdot, t)$ is continuous on S^1 for each time t in $[0, \underline{t})$.

Since $\gamma(\cdot, t)$ is a continuous function, we know that for every $t \in [0, \underline{t})$, $u \in S^1$ and $\varepsilon > 0$ there exists a positive constant $\delta > 0$ such that $|v - u| < \delta$ implies $\|\gamma(v, t) - \gamma(u, t)\| < \varepsilon$ for all $v \in S^1$. We can estimate the value of ψ at v by the following expression

$$\psi(v, t) = \inf_{Y \in \mathcal{G}} \|\mathcal{P}\gamma(v, t) - Y\| \leqslant \|\mathcal{P}\gamma(v, t) - \mathcal{P}\gamma(u, t)\| + \inf_{Y \in \mathcal{G}} \|\mathcal{P}\gamma(u, t) - Y\|,$$

where we denote $\mathcal{G} := \partial \mathrm{C}(\mathcal{P}\Gamma_t)$ for convenience. From the continuity we have

$$\psi(v, t) \leqslant \|\gamma(v, t) - \gamma(u, t)\| + \psi(u, t) < \varepsilon + \psi(u, t).$$

By the same argument, we get $\psi(u, t) < \varepsilon + \psi(v, t)$ and thus $|\psi(v, t) - \psi(u, t)| < \varepsilon$ when $|v - u| < \delta$. This implies the continuity of $\psi(\cdot, t)$ on S^1. Note that the continuity also confirms that Ψ given by in Equation (1.32) is defined properly, because the maximum is indeed attained. This function will be relevant because it vanishes iff $\mathcal{P}\Gamma_t$ is convex.

(B) The function ϕ is continuous on the whole domain $[0, \underline{t})$.

We aim to show that for all $t \in [0, \underline{t})$, $u \in S^1$ and $\varepsilon > 0$, there exists $\delta > 0$ such that for all $t' \in [0, \underline{t})$ and all $v \in S^1$, $|v - u| < \delta$ implies $|\psi(u, t') - \psi(u, t)| < \varepsilon$. Since $\mathcal{G}$ is compact, it contains $\tilde{Y}$ such that we can express $\psi(u, t)$ i the following form:

$$\psi(u, t) = \inf_{Y \in \mathcal{G}} \|\mathcal{P}\gamma(u, t) - Y\| = \|\mathcal{P}\gamma(u, t) - \tilde{Y}\|. \tag{1.33}$$

For t' close enough to t, the set $\mathcal{G}$ is close to $\mathcal{G}' := \partial \mathrm{C}(\mathcal{P}\Gamma_{t'})$ in terms of the Hausdorff distance. This means that there is $\tilde{Y}' \in \partial\mathcal{G}'$ such that $\|\tilde{Y}' - \tilde{Y}\|$ can be arbitrarily small if t' and t are close enough. Then we can rewrite $\psi(u, t')$ in the following form

$$\psi(u, t') = \inf_{Y \in \mathcal{G}'} \|\mathcal{P}\gamma(u, t') - Y\| \leqslant \|\mathcal{P}\gamma(u, t') - \tilde{Y}'\|$$

and further bound the expression by $\psi(u, t)$ and the positive constant ϵ as

$$\begin{aligned}\psi(u, t') &\leqslant \|\mathcal{P}\gamma(u, t') - \mathcal{P}\gamma(u, t)\| + \|\mathcal{P}\gamma(u, t) - \tilde{Y}\| + \|\tilde{Y} - \tilde{Y}'\| \\ &= \|\gamma(u, t') - \gamma(u, t)\| + \|\tilde{Y} - \tilde{Y}'\| + \psi(u, t) < \varepsilon + \psi(u, t).\end{aligned}$$

Similarly $\psi(u, t) < \varepsilon + \psi(u, t')$. Therefore $|\psi(u, t') - \psi(u, t)| < \varepsilon$ when $|t' - t| < \delta$.

We now move to the function Ψ and define the time when Γ looses its convexity as

$$t_0 := \inf\{t \in (0, \underline{t}) : \ \Psi(t) > 0\}. \tag{1.34}$$

Note that the set $\{t \in (0, \underline{t}) : \ \Psi(t) > 0\}$ is nonempty by the assumption.

(C) The function Ψ vanishes at the time t_0.

Assume that $\Psi(t_0) > 0$. Since Ψ is continuous on $[0, \underline{t})$, there is $\varepsilon > 0$ such that

$$\Psi(t) > \tfrac{1}{2}\Psi(t_0) > 0$$

for all $t \in (t_0 - \varepsilon, t_0)$, which contradicts the definition of t_0 from (1.34).

(D) There is t_1 in $(t_0, \underline{t})$ such that $\Psi(t)$ is non-increasing on (t_0, t_1).

Since the projected curve $\mathcal{P}\Gamma_t$ is regular and $\mathcal{P}$ is a linear operator, the regularity of the parametrization $\mathcal{P}\gamma$ is at least $\mathcal{C}^1$. This allows us to use Lemma 1.2.4 and assume the existence of $t_1 \in (t_0, \underline{t})$ such that $\mathcal{P}\Gamma_t$ is star-shaped for all $t \in (t_0, t_1)$.

For a fixed time $t \in (t_0, t_1)$, the function $\psi(\cdot, t)$ reaches its maximum at the point denoted by $u_2 \in S^1$. Let $u_1, u_3 \in S^1$ such that $u_2 \in [u_1, u_3]$ and

$$\mathcal{P}\gamma(u, t) \in \partial \mathrm{C}(\mathcal{P}\Gamma_t) \text{ for } u \in \{u_1, u_3\},$$
$$\mathcal{P}\gamma(u, t) \notin \partial \mathrm{C}(\mathcal{P}\Gamma_t) \text{ for } u \in (u_1, u_3).$$

Consider orthogonal basis $\{e_1, e_2\}$ of $\operatorname{Ran}\mathcal{P}$ such that the e_1 is parallel to $\mathcal{P}\gamma(u_3, t) - \mathcal{P}\gamma(u_1, t)$ and $\mathcal{P}\gamma(u_2, t) - \mathcal{P}\gamma(u_1, t)$ has points in the positive direction of e_2. Since $\mathcal{P}\Gamma_t$ is star-shaped, no small kinks can develop along the curve and we can express $\Psi(t)$ as the difference between the e_2 coordinate of $\mathcal{P}\gamma(u_2, t)$ and $\mathcal{P}\gamma(u_1, t)$.

If $\kappa_{\mathcal{P}}(u_2, t) > 0$, Lemma 1.2.5 and the motion law (1.1) imply that the e_2 coordinate of $\mathcal{P}\gamma(u_2, t)$ is non-increasing in time. Similarly, when $\kappa_{\mathcal{P}}(u_1, t) > 0$ and/or $\kappa_{\mathcal{P}}(u_3, t) > 0$, the e_2 coordinate of $\mathcal{P}\gamma(u_1, t)$ and/or $\mathcal{P}\gamma(u_3, t)$ is non-decreasing, respectively. When $\kappa_{\mathcal{P}} = 0$ at u_1, u_2 or u_3, the e_2 coordinate of the corresponding point remains constant as the motion takes place only in the e_1 direction.

In all scenarios, the distance between $\mathcal{P}\gamma(u_2, t)$ and $\partial \mathrm{C}(\mathcal{P}\Gamma_t)$ cannot increase and thus $\Psi(t)$ cannot increase either. This proves the last statement (D).

Putting together the previous statements (B), (C) and (D) yields the following inequality

$$0 \leqslant \Psi(t) \leqslant \Psi(t_0) = 0$$

for all t in (t_0, t_1), which implies that $\Psi(t) = 0$ for all t in (t_0, t_1). This contradicts the definition of t_0 in (1.34). Thus the convexity of $\mathcal{P}\Gamma_t$ must be preserved for all $t \in [0, \underline{t})$. □

1.3 Spherical Curves

The space curve Γ is called spherical if there exists a point $x \in \mathbb{R}^3$ and a positive constant ρ such that $\|x - y\| = \rho$ for all $y \in \Gamma$. Their behaviour during the curve shortening flow has been studied in [He12; MKB19] and some consequences were discussed in [Kha15]. This section describes our results related to spherical curves from [MKB19].

1.3.0 Spherical Invariance

Before further analysis, one must establish the invariance of sphericity during the flow. It has been shown in e.g. [He12] and an alternative proof is also in Corollary 1.1.5. Among the ways to show this property, the most straightforward and enlightening proof is the following.

Lemma 1.3.1. *The curve shortening flow in $\mathbb{R}^3$ preserves spherical curves.*

Proof. Let $x \in \mathbb{R}^3$ be the center of sphere $\partial B(x, \rho_0)$ on which the curve Γ_0 lies. Then

$$\begin{aligned}\partial_t \|\gamma - x\|^2 &= 2\langle \gamma - x, \partial_t \gamma \rangle = 2\langle \gamma - x, \partial_s^2 \gamma \rangle \\ &= 2\partial_s \langle \gamma - x, \partial_s \gamma \rangle - 2\|\partial_s \gamma\|^2 = 2\partial_s \langle \gamma - x, T \rangle - 2.\end{aligned}$$

If Γ_t is spherical and centered around the point x, then $\|\gamma - x\|$ does not depend on s and

$$0 = \partial_s \|\gamma - x\|^2 = 2\langle \gamma - x, T \rangle.$$

Thus, provided that the initial curve lies in $\partial B(x, \rho_0)$, the time derivative $\partial_t \|\gamma - x\|$ does not depend on $u \in S^1$ either and the sphericity is preserved. □

Remark 1.3.2. *The proof of Lemma 1.3.1 gives us for free the evolution of the spherical radius*

$$\rho(t) = (\rho_0^2 - 2t)^{\frac{1}{2}},$$

because $\rho'(t) = -\rho^{-1}(t)$. This can also be deduced from the analytical solution of the great circle of the shrinking sphere, which follows the same equation.

1.3.1 Heat Equation Lemma

We aim to show that spherical curves share similar long term characteristics with curves evolving in plane. Specifically, we will generalize the avoidance principle and present its ramifications. We will do so by generalizing the classical proof from [GH86], but several technical obstacles must be resolved first.

Following the proof from [GH86], let us define the functional $\phi \colon T^2 \times [0, \underline{t}) \to \mathbb{R}^+$ as

$$\phi(u_1, u_2, t) := \|\gamma(u_2, t) - \gamma(u_1, t)\|^2, \tag{1.35}$$

where $T^2 = S^1 \times S^1$ is the 2-torus.

Lemma 1.3.3. *Let Γ be a spherical space curve. Consider the functional ϕ from (1.35), but without the time dependency. If $\phi = \phi(u_1, u_2)$ has a local minimum at $(u_1, u_2) \in T^2$ and $u_1 \neq u_2$, then the tangent vectors $T(u_1)$ and $T(u_2)$ are collinear.*

Proof. The functional ϕ has an extremum at (u_1, u_2) and thus its gradient vanishes:

$$\nabla \phi(u_1, u_2) = 2 \begin{bmatrix} \langle \gamma(u_1) - \gamma(u_2), \|\partial_u \gamma(u_1)\| T(u_1) \rangle \\ \langle \gamma(u_2) - \gamma(u_1), \|\partial_u \gamma(u_2)\| T(u_2) \rangle \end{bmatrix} = \begin{bmatrix} 0 \\ 0 \end{bmatrix}.$$

Since we only consider regular curves the parametrisation rate $\partial_u \gamma$ is positive everywhere and the vanishing gradient implies the following orthogonality conditions:

$$\langle T(u_1), \gamma(u_2) - \gamma(u_1) \rangle = \langle T(u_2), \gamma(u_2) - \gamma(u_1) \rangle = 0.$$

Moreover, with x denoting the center of the sphere, $\gamma(u_1)-x$ and $\gamma(u_2)-x$ are orthogonal to the tangent plane of the sphere at the point $\gamma(u_1)$ and $\gamma(u_2)$, respectively. Thus $T(u_1)$ and $T(u_2)$ are orthogonal to $\gamma(u_1)-x$ and $\gamma(u_2)-x$, respectively. Together, we have

$$\begin{aligned} T(u_1) &\in \operatorname{span}(\gamma(u_2)-\gamma(u_1))^\perp \cap \operatorname{span}(\gamma(u_1)-x)^\perp, \\ T(u_2) &\in \operatorname{span}(\gamma(u_1)-\gamma(u_2))^\perp \cap \operatorname{span}(\gamma(u_2)-x)^\perp, \end{aligned}$$

where $\operatorname{span}\Omega$ and $\Omega^\perp$ denote the linear span and the orthogonal complement of the set Ω, respectively. From the linearity of the inner product, we have

$$T(u_1), T(u_2) \in \operatorname{span}(\gamma(u_1)-x)^\perp \cap \operatorname{span}(\gamma(u_2)-x)^\perp. \tag{1.36}$$

Since $u_1 \neq u_2$, the intersection of $\operatorname{span}(\gamma(u_1)-x)^\perp$ and $\operatorname{span}(\gamma(u_2)-x)^\perp$ from (1.36) is a one-dimensional affine space, which proves the original statement. □

Remark 1.3.4. *The statement of Lemma 1.3.3 is specific to spherical curves in $\mathbb{R}^3$ and does not generalize to spherical curves in higher dimensional spaces. As a counterexample in dimension 4, consider the following curve with the parametrization*

$$\gamma(u) := \begin{bmatrix} \sin(\cos u) \\ \cos(\cos u)\sin(\sin(2u)) \\ \cos(\cos u)\cos(\sin(2u))\cos(\frac{1}{2}\sin u) \\ \cos(\cos u)\cos(\sin(2u))\sin(\frac{1}{2}\sin u). \end{bmatrix},$$

One can verify that this curve lies not a unit 3-sphere and yet the functional ϕ achieves its local minimum at the point $(u_1,u_2) = \left(\frac{\pi}{2}, \frac{3\pi}{2}\right)$ but $\langle T(u_1), T(u_2)\rangle = 0$.

Another lemma we will need is a straightforward generalisation of result from [GH86] to our codimension two setting and works even for non-spherical curves.

Lemma 1.3.5 (Generalization of Lemma 3.2.2 from [GH86])**.** *The functional ϕ defined in* (1.35) *satisfies a strictly parabolic partial differential equation related to the heat equation:*

$$\partial_t \phi - \Delta_s \phi = -4, \tag{1.37}$$

where the arc-length Laplace operator Δ_s is formally defined as $\Delta_s = \partial_{s_1}^2 + \partial_{s_2}^2$.

Proof. Using $\partial_t \gamma = \kappa N$ and the chain rule leads to the time derivative

$$\partial_t \phi(u_1,u_2,t) = 2\langle \gamma(u_1,t)-\gamma(u_2,t), \kappa(u_1,t)N(u_1,t) - \kappa(u_2,t)N(u_2,t)\rangle.$$

Moreover, using the Frenet-Serret formulae yields

$$\begin{aligned} \partial_{s_1}^2 \phi(u_1,u_2,t) &= 2 + 2\langle \gamma(u_1,t)-\gamma(u_2,t), \kappa(u_1,t)N(u_1,t)\rangle, \\ \partial_{s_2}^2 \phi(u_1,u_2,t) &= 2 - 2\langle \gamma(u_1,t)-\gamma(u_2,t), \kappa(u_2,t)N(u_2,t)\rangle. \end{aligned}$$

Subtracting $\partial_t \phi - \Delta_s \phi$ indeed leads to a constant -4. □

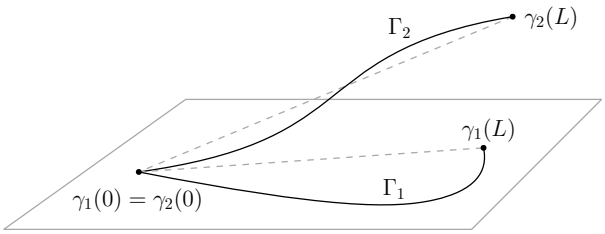

Figure 1.7: Visualization of the Schur Comparison Theorem.

1.3.2 Generalised Schur Comparison

The following Lemma ensures the absence of small kinks in a curve with bounded curvature. The original result for planar curves is due to Schur [Sch21] and a generalized version was introduced by Schmidt [Sch25]. The following formulation of Schur Theorem is from [Lóp11]. The visual interpretation of the result is depicted in Figure 1.7.

Lemma 1.3.6 (Generalized Schur Comparison Theorem)**.** *Let Γ_1 and Γ_2 be both arc-length parametrized open space curves with the same length $L > 0$. Assume that Γ_1 is planar and*

$$\Gamma_1 \cup \partial \mathrm{C}(\Gamma_1) \subset \partial \mathrm{C}(\Gamma_1 \cup \partial \mathrm{C}(\Gamma_1)).$$

Let κ_1 and κ_2 denote curvatures of Γ_1 and Γ_2, respectively. And assume that $\kappa_1(s) \geqslant \kappa_2(s)$ for all $s \in [0, L]$. Then we have $\|\gamma_1(0) - \gamma_1(L)\| \leqslant \|\gamma_2(0) - \gamma_2(L)\|$.

The generalized Schur Comparison Theorem, stated in Lemma 1.3.6, allows us to adapt Corollary 3.2.4 from [GH86] for our higher codimension setting.

Lemma 1.3.7 (Generalization of Corollary 3.2.4 from [GH86])**.** *Let Γ_t be uniformly bounded curvature κ by a constant $C > 0$. Then the functional ϕ from (1.35) satisfies*

$$\phi(u_1, u_2, t) \geqslant \frac{4}{C^2} \left[\sin\left(\frac{2}{C} \int_{u_1}^{u_2} \|\partial_u \gamma(u, t)\| \, \mathrm{d}u \right) \right]^2,$$

for all $u_1, u_2 \in S^1$ and all $t \in [0, \underline{t})$.

Proof. Setting Γ_1 to a circular arc with radius C^{-1} in Lemma 1.3.6 yields the inequality. □

1.3.3 Spherical Avoidance Principle

With Lemma 1.3.3, 1.3.5, 1.3.6 and 1.3.7, we are ready to proof the avoidance principle for spherical curves. It states that embedded spherical curves with bounded curvature cannot intersect themselves during the curve shortening flow in $\mathbb{R}^3$. The idea of the proof and its steps are based on the planar version of this result from [GH86].

Proposition 1.3.8 (Proposition 4.6 from [MB20])**.** *Let $\{\Gamma_t\}_{t \in [0, \underline{t})}$ be a family of space curves evolving according to the curve shortening flow from an initial curve Γ_0, which is an embedded, spherical curve. Assume that the curvature κ can be uniformly bounded by a positive constant C for all $u \in S^1$ and $t \in [0, \underline{t})$. Then Γ_t will remain embedded for all $t \in (0, \underline{t})$.*

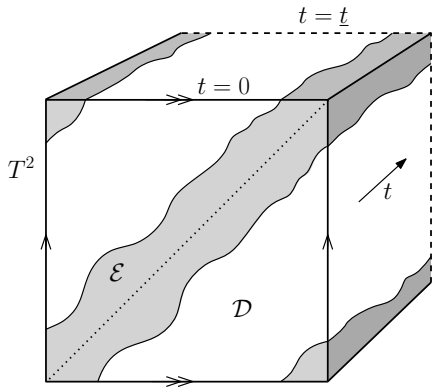

Figure 1.8: Decomposition of $T^2 \times [0, \underline{t})$ into $\mathcal{E}$ and $\mathcal{D}$. Linear arrows and double arrows indicate the fundamental polygon of each slice in time.

Proof. Let us first split the domain $T^2 \times [0, \underline{t})$ of the ϕ from (1.35) into two disjoint parts

$$\mathcal{E} := \left\{ (u_1, u_2, t) \in T^2 \times [0, \underline{t}) : \int_{u_1}^{u_2} \|\partial_u \gamma(u, t)\| \, \mathrm{d}u < \frac{\pi}{C} \right\} \tag{1.38}$$

end the remainder $\mathcal{D} = \left(T^2 \times [0, \underline{t})\right) \setminus \mathcal{E}$. Note that from this construction,

$$\phi(u_1, u_2, t) = 0$$

implies $u_1 = u_2$ for all $(u_1, u_2, t) \in \mathcal{E}$ due to Lemma 1.3.7. Thus, to prove Γ_t will remain embedded, it suffices to show that $\phi(u_1, u_2, t) > 0$ everywhere on $\mathcal{D}$. Furthermore, all points (u_1, u_2, t) on the boundary $\partial\mathcal{E}$ satisfy

$$\int_{u_1}^{u_2} \|\partial_u \gamma(u, t)\| \, \mathrm{d}u = \frac{\pi}{C}$$

from the construction. Together with Lemma 1.3.7, we can lower bound ϕ on $\partial\mathcal{E}$ by a constant $\frac{4}{C^2}$. Because Γ_0 is embedded and closed, there exists $m_1 \in \left(0, \frac{4}{C^2}\right)$ such that

$$\inf_{\partial\mathcal{D}} \phi(u_1, u_2, t) \geqslant \min \left\{ \inf_{\partial\mathcal{D} \setminus \partial\mathcal{E}} \phi(u_1, u_2, t), \frac{4}{C^2} \right\} > m_1.$$

We extend the definition of ϕ from (1.35) for $\varepsilon > 0$ and (u_1, u_2, t) from $T^2 \times [0, \underline{t})$ to

$$\phi_\varepsilon(u_1, u_2, t) := \phi(u_1, u_2, t) + \varepsilon t. \tag{1.39}$$

For contradiction, assume there exists $m_2 \in (0, m_1)$ and $(u_1^o, u_2^o, t^o) \in \mathcal{D}$ such that

$$\phi_\varepsilon(u_1^o, u_2^o, t^o) = m_2,$$

and without loss of generality let t^o be the smallest possible. Since ϕ_ε attains its local minimum at (u_1^o, u_2^o, t^o), we can use Lemma 1.3.3 to conclude that

$$|\partial_{s_1} \partial_{s_2} \phi_\varepsilon(u_1^o, u_2^o, t^o)| = 2|\langle T(u_1^o, t^o), T(u_2^o, t^o) \rangle| = 2\|T(u_1^o, t^o)\| \|T(u_2^o, t^o)\| = 2.$$

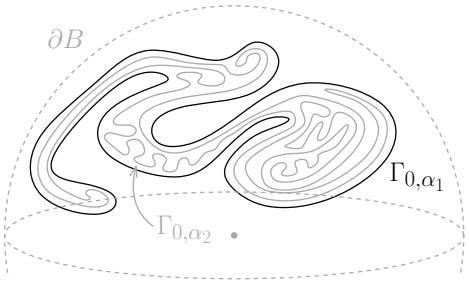

Figure 1.9: Two disjoint and mutually spherical curves Γ_{0,α_1} and Γ_{0,α_2} will remain embedded and mutually spherical while shrinking without touching.

Since t^o is the smallest possible, the derivative $\partial_t \phi_\varepsilon(u_1^o, u_2^o, t^o)$ is non-positive and

$$\det \begin{bmatrix} \partial_{s_1}^2 \phi_\varepsilon(u_1^o, u_2^o, t^o) & \partial_{s_1}\partial_{s_2}\phi_\varepsilon(u_1^o, u_2^o, t^o) \\ \partial_{s_2}\partial_{s_1}\phi_\varepsilon(u_1^o, u_2^o, t^o) & \partial_{s_2}^2 \phi_\varepsilon(u_1^o, u_2^o, t^o) \end{bmatrix} \geqslant 0. \tag{1.40}$$

With the Young inequality and inequality (1.40) we can bound the arc-length Laplacian as

$$\begin{aligned} \Delta_s \phi_\varepsilon(u_1^o, u_2^o, t^o) &= \partial_{s_1}^2 \phi_\varepsilon(u_1^o, u_2^o, t^o) + \partial_{s_2}^2 \phi_\varepsilon(u_1^o, u_2^o, t^o) \\ &\geqslant 2(\partial_{s_1}^2 \phi_\varepsilon(u_1^o, u_2^o, t^o)\ \partial_{s_2}^2 \phi_\varepsilon(u_1^o, u_2^o, t^o))^{\frac{1}{2}} \\ &\geqslant 2|\partial_{s_1}\partial_{s_2}\phi_\varepsilon(u_1^o, u_2^o, t^o)| = 4. \end{aligned}$$

Together with Lemma 1.3.5 and the definition of ϕ_ε in (1.39) we obtain the inequality

$$\begin{aligned} 0 \geqslant \partial_t \phi_\varepsilon(u_1^o, u_2^o, t^o) &= \partial_t \phi(u_1^o, u_2^o, t^o) + \varepsilon = \Delta_s \phi(u_1^o, u_2^o, t^o) - 4 + \varepsilon \\ &= \Delta_s \phi_\varepsilon(u_1^o, u_2^o, t^o) - 4 + \varepsilon \geqslant \varepsilon, \end{aligned}$$

which contradicts the initial assumption $\varepsilon > 0$ and thus proves the statement. □

1.3.4 Mutually Spherical Curves

Similarly to its planar counterpart, the spherical avoidance principle can be extended to multiple independent curves subjected to the same motion law. In our case, however, the curves must initially lie on either a disjoint sphere or on the same one. To capture this behaviour, we introduce the notion of mutually spherical curves.

Definition 1.3.9 (Definition 4.7 from [MB20]). *Let $\mathcal{A}$ be a finite set of indexes. The family of space curves $\{\Gamma_\alpha\}_{\alpha\in\mathcal{A}}$ is mutually spherical if and only if there is $x \in \mathbb{R}^3$ such that for each $\alpha \in \mathcal{A}$ there is $r > 0$ for which $\|y - x\| = r$ for all points $y \in \Gamma_\alpha$.*

Corollary 1.3.10 (Corollary 4 from [MB20]). *Let $\mathcal{A}$ denote some finite set of indices and $\{\Gamma_{t,\alpha}\}_{t\in[0,\underline{t}),\alpha\in\mathcal{A}}$ be a family of curves all evolving according to the curve shortening flow from a family of initial curves $\{\Gamma_\alpha\}_{\alpha\in\mathcal{A}}$ that are mutually spherical and disjoint. Furthermore, assume that the curvatures of the evolving families of curves can be uniformly bounded. Then the curves $\Gamma_{t,\alpha}$ will remain disjoint for all $t \in (0, \underline{t})$.*

Remark 1.3.11. *The avoidance principle also works when the curves are on different spheres which bound balls that are all disjoint. Since they will remain on these shrinking spheres, they can never intersect either.*

The example of how the spherical avoidance principle affects several mutually spherical curves under the curve shortening flow is depicted in Figure 1.9.

1.4 Conclusions

The long-term behavior of curve shortening flow in higher codimensional spaces diverges significantly from the well-understood planar case. While classical results such as the Grayson-Gage-Hamilton Theorem describe the behavior in $\mathbb{R}^2$, higher dimensions introduce complexities, including formation of different singularities and lack of preservation of convexity.

This chapter covers two author's publications on this topic. The first contribution [MKB19] introduces a generalized comparison principle for bounding space curves with respect to moving hypersurfaces. The second article [MB20] analyzes convexity preservation and proves the Avoidance principle for spherical curves.

The study of higher codimension flows is an active field with recent developments and open problems. The analysis of these problems often requires more complex apparatus from different fields like topology as the normal vector can be non-unique or undefined. To tackle these issues we investigated the theory of nondegenerate homotopies in article [MB22b] which is covered in Chapter 3.

2

Minimal Surface Generating Flow

This chapter covers results from author's article [MB22a]. In particular, it introduces two concepts that play a significant role in the context of this thesis and author's work.

First is the notion of trajectory surface, which is generated by the evolving curve. It can be used as a tool for studying the long term behaviour of any geometric flow of curves. In this chapter, we define these surfaces and describe their geometric properties.

The second main contribution of the chapter is the minimal surface geometric flow, which was first introduced and studied in [MB22a]. This flow generates surfaces of zero mean curvature bounded by the initial curve and thus can be used for their analysis.

2.0 Introduction

Minimal surfaces are not just mathematically intriguing but also useful in various applied fields. Originally conceptualized to model soap films stretched across wireframes, minimal surfaces have been studied in the context of cell membranes [LL14], crystal structures in zeolites [AHB85; And+88; Scr76], and even in general relativity as representations of black hole apparent horizons [HI01].

The aesthetic qualities of minimal surfaces also influence architecture and art, as seen in Munich's Olympiastadion. More recently, periodic minimal surfaces have been explored for new composite material development [AAR16], and soap film dynamics with moving boundaries have been investigated [Gol+10; Gol+14]. In knot theory, surfaces constrained by a fixed boundary are related to the concept of Seifert surfaces and the genus knot invariant [WC06].

Minimal surfaces with a given boundary can be computed and analysed using multiple different existing approaches. The level set method focuses on solving the mean curvature flow,

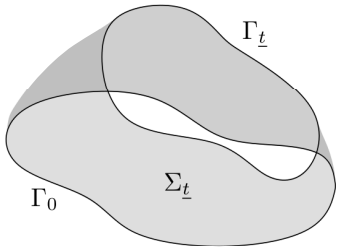

Figure 2.1: General trajectory surface geometry.

ultimately converging to a surface with zero mean curvature [Cho93; Dzi90]. Another approach numerically approximates the Weierstrass-Enneper representation formulas [Ter90]. Alternative methods include the stretched grid technique and the discrete differential geometry approach, as elaborated in [BHS06; PP93; SW19].

2.0.0 Trajectory Surface

The main driving concept behind articles [MB22a] and [MB23] is the notion of the trajectory surface for an evolving curve. It is the set of points swept out by the evolving curve and can be seen as a surface parametrized by the curves parameter $u \in S^1$ and the time coordinate $t \in [0, \underline{t})$. We formalize this notion in the following definition.

Definition 2.0.1 (Definition 2.1 from [MB22a]). *Let $\{\Gamma_t\}_{t\in[0,\underline{t})}$ be a family of space curve in $\mathbb{R}^3$ that evolve according to a given geometric flow with velocities v_N and v_B and the initial condition Γ_0. We define the trajectory surface $\Sigma_{\underline{t}}$ formally as*

$$\Sigma_{\underline{t}} := \bigcup_{t\in[0,\underline{t})} \Gamma_t.$$

One can also view the trajectory surface $\Sigma_{\underline{t}}$ as a parametric surface given by the map $\gamma(u, t)$, where the time t is treated just as another parameter parameter in the same way as u.

These surfaces may not be embedded even if all of the individual curves are. Note that $\Sigma_{\underline{t}}$ is not related to moving surfaces described in Section 1.1.

Remark 2.0.2. *After their introduction in [MB22a], trajectory surfaces were further analyzed in [ZZW22], which includes a description of properties of u-curves, i.e. open curves given by the parametrization $\gamma(\cdot, u)$ with a fixed parameter $u \in S^1$ defined on the time domain $[0, \underline{t})$.*

2.0.1 Surface Geometry

To analyze the generated trajectory surfaces, we describe their geometry in terms of the geometry of the evolving curve and the velocity vector of the given motion law. We first compute the fundamental forms and then provide formulas for the Gauss and mean curvatures.

Lemma 2.0.3. *The first fundamental form I of the trajectory surface $\Sigma_{\underline{t}}$ can be represented as a diagonal matrix $\mathrm{I} \equiv \mathrm{diag}(g^2, v^2)$, where $v^2 := v_N^2 + v_B^2$ is the magnitude of velocity.*

Proof. The first fundamental form can be expressed in terms of the parametrisation of Γ_t as

$$\mathrm{I} \equiv \begin{bmatrix} \mathcal{E} & \mathcal{F} \\ \mathcal{F} & \mathcal{G} \end{bmatrix} = \begin{bmatrix} \|\partial_u \gamma\|^2 & \langle \partial_u \gamma, \partial_t \gamma \rangle \\ \langle \partial_t \gamma, \partial_u \gamma \rangle & \|\partial_t \gamma\|^2 \end{bmatrix}.$$

Using the equations (5-8), we obtain the elements of the matrix representation of I:

$$\mathcal{E} = g^2, \qquad \mathcal{F} = 0, \qquad \mathcal{G} = v_N^2 + v_B^2. \tag{2.1}$$

The first fundamental form is thus indeed diagonal with entries g^2 and v^2. □

The second fundamental form, presented in the next lemma, is more involved but computed in the same way as the first fundamental form.

Lemma 2.0.4. *Elements of the second fundamental form* II *of the trajectory surface* $\Sigma_{\underline{t}}$ *read*

$$\mathcal{L} = -\frac{g^2 \kappa v_B}{v}, \qquad \mathcal{M} = g\left[\frac{v_N \partial_s v_B - v_B \partial_s v_N}{v} + \tau v\right],$$
$$\mathcal{N} = \frac{v_N \partial_t v_B - v_B \partial_t v_N}{v} + \frac{v}{\kappa}(v_N \partial_s \tau + 2\tau \partial_s v_N + \partial_s^2 v_B - v_B \tau^2),$$

where $\mathcal{L}$ *and* $\mathcal{N}$ *are the diagonal entries,* $\mathcal{M}$ *lies on the antidiagonal and* $v := (v_N^2 + v_B^2)^{\frac{1}{2}}$.

Proof. As in Lemma 2.0.3 we can express the second fundamental form in terms of γ:

$$\mathrm{II} \equiv \begin{bmatrix} \mathcal{L} & \mathcal{M} \\ \mathcal{M} & \mathcal{N} \end{bmatrix} = \begin{bmatrix} \langle \partial_u^2 \gamma, n \rangle & \langle \partial_u \partial_t \gamma, n \rangle \\ \langle \partial_t \partial_u \gamma, n \rangle & \langle \partial_t^2 \gamma, n \rangle \end{bmatrix},$$

where the unit normal vector n of the trajectory surface $\Sigma_{\underline{t}}$ can be expressed as

$$n = \|\partial_u \gamma \times \partial_t \gamma\|^{-1} \partial_u \gamma \times \partial_t \gamma = (v_N^2 + v_B^2)^{-\frac{1}{2}}(v_N B - v_B N).$$

Straightforward algebraic manipulation and equations (5-8) yield the statement. □

With the equations for both fundamental forms from the previous lemmas, we are ready to write down the formulas for the Gauss curvature K and mean curvature H.

Lemma 2.0.5. *We can write* K *and* H *in terms of the functions* v_N, v_B, κ *and* τ *as*

$$\begin{aligned} K =& \kappa v_B \frac{v_B \partial_t v_N - v_N \partial_t v_B}{v^4} - v_B \frac{v_N \partial_s \tau + 2\tau \partial_s v_N + \partial_s^2 v_B - v_B \tau^2}{v^3} \\ & - \frac{(v_N \partial_s v_B - v_B \partial_s v_N)^2}{v^4} - 2\tau \frac{v_N \partial_s v_B - v_B \partial_s v_N}{v^2} - \tau^2, \\ H =& -\frac{\kappa v_B}{v} + \frac{v_N \partial_t v_B - v_B \partial_t v_N}{v^3} + \frac{v_N \partial_s \tau + 2\tau \partial_s v_N + \partial_s^2 v_B - v_B \tau^2}{\kappa v}. \end{aligned}$$

Proof. The Gauss curvature K and the mean curvature H of $\Sigma_{\underline{t}}$ are then computed as

$$K = \frac{\det \mathrm{II}}{\det \mathrm{I}} = \frac{\mathcal{L}\mathcal{N} - \mathcal{M}^2}{\mathcal{E}\mathcal{G} - \mathcal{F}^2}, \qquad H = \mathrm{Tr}(\mathrm{II}(\mathrm{I})^{-1}) = \frac{\mathcal{L}}{\mathcal{E}} + \frac{\mathcal{N}}{\mathcal{G}}.$$

The formulas above are then obtained by straightforward algebraic manipulation. □

2.0.2 Motion Law

Assume $v_B = 0$ and the curve is moving only in the direction of the principal normal vector N. The expression for the mean curvature H significantly simplifies to

$$H = (|v_N|\kappa)^{-1}(v_N \partial_s \tau + 2\tau \partial_s v_N). \tag{2.2}$$

It is worth noting that in the case of $v_B = 0$, the Gaussian curvature $K = -\tau^2$ does not depend on the normal velocity term v_N. Moreover, K is always non-positive and the surface $\Sigma_{\underline{t}}$ is developable (meaning $K = 0$) if and only if the curve Γ_t is evolving in a plane.

Furthermore, when $v_B = 0$ we can rewrite the mean curvature as

$$H = \frac{v_N \tau}{|v_N|\kappa}\left[\frac{\partial_s \tau}{\tau} + 2\frac{\partial_s v_N}{v_N}\right] = \frac{v_N \tau}{|v_N|\kappa}\partial_s\left(\log|\tau| + 2\log|v_N|\right).$$

This means that we can ensure that H is zero everywhere only when we set $v_N = F\tau^{-\frac{1}{2}}$ with $F = F(t)$ being any function constant with respect to the parameter u. We choose the $F \equiv 1$ for simplicity and introduce the new motion law in the next definition.

Definition 2.0.6 (Definition 3.1 from [MB22a]). *Let Γ_0 be a closed space curve with positive curvature and torsion. We say that a family of curves $\{\Gamma_t\}_{t\in[0,\underline{t})}$ is evolving according to the minimal surface generating flow if its parametrization γ satisfies the initial value problem:*

$$\partial_t \gamma = \tau^{-\frac{1}{2}} N \qquad \text{in } S^1 \times (0, \underline{t}), \tag{2.3}$$

$$\gamma|_{t=0} = \gamma_0 \qquad \text{in } S^1, \tag{2.4}$$

where γ_0 is parametrization of the initial curve Γ_0 and τ is the torsion of the curve.

2.1 Technical Preliminaries

In this section, we first adapt the necessary evolution equations of geometric quantities from their general form to the minimal surface generating flow and then prepare other useful lemmas by applying the Gauss-Bonnet formula to the generated trajectory surface.

2.1.0 Evolution Equations

For the convenience of the reader, we list the evolution equations for geometric quantities derived from Proposition 0.4.3 and adjusted to the specific geometric flow from Definition 2.0.6.

Lemma 2.1.1 (Evolution equations). *The local geometric quantities g, κ and τ satisfy*

$$\partial_t g = -g\kappa\tau^{-\frac{1}{2}}, \tag{2.5}$$

$$\partial_t \kappa = \partial_s^2(\tau^{-\frac{1}{2}}) + \tau^{-\frac{1}{2}}(\kappa^2 - \tau^2), \tag{2.6}$$

$$\partial_t \tau = 2\kappa\tau^{\frac{1}{2}}. \tag{2.7}$$

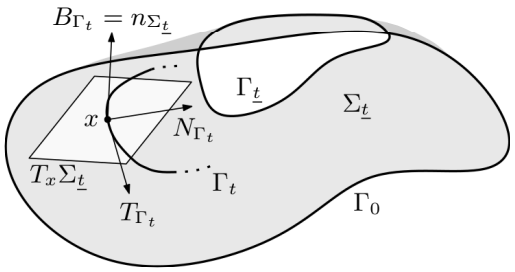

Figure 2.2: Trajectory surface geometry for the minimal surface generating flow.

The evolution equations for the Frenet frame can be written in the following compact form

$$\partial_t \begin{bmatrix} T \\ N \\ B \end{bmatrix} = \begin{bmatrix} 0 & \partial_s(\tau^{-\frac{1}{2}}) & \tau^{\frac{1}{2}} \\ -\partial_s(\tau^{-\frac{1}{2}}) & 0 & 0 \\ -\tau^{\frac{1}{2}} & 0 & 0 \end{bmatrix} \cdot \begin{bmatrix} T \\ N \\ B \end{bmatrix}. \tag{2.8}$$

The first immediate application of Lemma 2.1.1 is an important result for the existence of the solution. Because the normal velocity $v_N = \tau^{-\frac{1}{2}}$ is ill-defined when τ is zero, we need to ensure its positivity throughout the flow. We achieve this in the following proposition.

Proposition 2.1.2 (Proposition 1 from [MB22a]). *Let Γ_0 be a space curve with non-vanishing curvature and positive torsion. Then the torsion $\tau(\cdot, t)$ remains positive everywhere for all $t \in [0, \underline{t})$. Moreover, the function $\tau(u, t)$ is strictly increasing in time for any fixed $u \in S^1$.*

Proof. From (2.7) from Lemma 2.1.1 we get surprisingly simple evolution formula

$$\partial_t \tau^{\frac{1}{2}} = \tfrac{1}{2}\tau^{-\frac{1}{2}}\partial_t \tau = \tfrac{1}{2}\tau^{-\frac{1}{2}}(2\tau^{\frac{1}{2}}\kappa + \partial_s[\tfrac{1}{\kappa}(\tau^{-\frac{1}{2}}\partial_s\tau + 2\tau\partial_s(\tau^{-\frac{1}{2}}))]) = \kappa. \tag{2.9}$$

Since the curvature κ is positive by the assumptions, we can use (2.9) to estimate

$$\tau(u, t_1) = \left[\tau(u, t_0)^{\frac{1}{2}} + \int_{t_0}^{t_1} \kappa(u, t)\,\mathrm{d}t\right]^2 > \tau(u, t_0)$$

for all $u \in S^1$ and all $t_0, t_1 \in [0, \underline{t})$ such that $t_0 < t_1$. Thus τ strictly increases. □

2.1.1 Gauss-Bonnet Theorem

The Gauss-Bonnet theorem relates the global geometry of a surface to its topological property, namely its Euler characteristic. General results that connect topology and geometry in a non-trivial way, like the Milnor-Fáry theorem or the Călugăreanu theorem, are often very useful and the same is true for this formula. Let us first restate the Gauss-Bonnet theorem.

Theorem 2.1.3 (Gauss-Bonnet theorem, see e.g. [Car76]). *Let $\mathcal{M}$ be a compact Riemannian manifold of dimension 2 and Euler characteristic $\chi(\mathcal{M})$. Then*

$$\int_{\mathcal{M}} K\,\mathrm{d}A + \int_{\partial\mathcal{M}} \kappa_g\,\mathrm{d}s = 2\pi\chi(\mathcal{M}), \tag{2.10}$$

where K is the Gauss curvature of $\mathcal{M}$ and κ_g is the geodesic curvature of the boundary $\partial\mathcal{M}$.

Let us also recall, e.g. from [Hato2], that the Euler characteristic of a surface $\mathcal{M}$ is given by

$$\chi(\mathcal{M}) = b_0(\mathcal{M}) - b_1(\mathcal{M}) + b_2(\mathcal{M}), \tag{2.11}$$

where $b_i(\mathcal{M})$ denotes the i-th Betti number, i.e. the rank of the corresponding homology group $H_i(\mathcal{M})$. We will use this formula to compute the Euler characteristic of the trajectory surface in the following result which applies the Gauss-Bonnet theorem to our setting.

2.1.2 Total Curvature

The total curvature is an extremely useful quantity as is can be used in various estimates due to the theorems of Fenchel and Milor-Fáry. In our case, this integral also appears in the Gauss-Bonnet formula stated in the previous subsection. This fact is used in the following lemma.

Lemma 2.1.4 (Lemma 3.3 from [MB22a]). *The total curvature for the curve evolving according to the minimal surface generating flow in the time interval* $[0, \underline{t})$ *satisfies*

$$\int_{\Gamma_{\underline{t}}} \kappa \,\mathrm{d}s - \int_{\Gamma_0} \kappa \,\mathrm{d}s = -\int_0^{\underline{t}} \int_{\Gamma_t} \tau^{\frac{3}{2}} \,\mathrm{d}s \,\mathrm{d}t. \tag{2.12}$$

Proof. Applying the Gauss-Bonnet theorem (stated in Theorem 2.1.3) to $\Sigma_{\underline{t}}$ yields

$$\int_{\Sigma_{\underline{t}}} K \,\mathrm{d}A + \int_{\partial\Sigma_{\underline{t}}} \kappa_g \,\mathrm{d}s = 2\pi\chi(\Sigma_{\underline{t}}), \tag{2.13}$$

where the boundary $\partial\Sigma_{\underline{t}} = \Gamma_0 \cup \Gamma_{\underline{t}}$ consist of two curves, the initial Γ_0 curve and terminal one $\Gamma_{\underline{t}}$. Next, we will expand all terms of Equation (2.13) starting with the first integral

$$\int_{\Sigma_{\underline{t}}} K \,\mathrm{d}A = \iint_{\mathcal{T}\times S^1} K\tau^{-\frac{1}{2}} g \,\mathrm{d}u \wedge \mathrm{d}t = -\int_0^{\underline{t}} \int_{\Gamma_t} \tau^{\frac{3}{2}} \,\mathrm{d}s \,\mathrm{d}t,$$

where $\mathcal{T}$ denotes the time interval $[0, \underline{t})$ and the area element $\mathrm{d}A$ was computed as

$$\mathrm{d}A = (\mathcal{E}\mathcal{G} - \mathcal{F}^2)^{\frac{1}{2}} \,\mathrm{d}u \wedge \mathrm{d}t = g\tau^{-\frac{1}{2}} \,\mathrm{d}u \wedge \mathrm{d}t,$$

where $\mathcal{E}, \mathcal{G}$ and $\mathcal{F}$ are elements of the first fundamental form defined in (2.1). For the second integral in (2.13), we use the fact that $n = B$ on $\partial\Sigma_{\underline{t}}$ which consists of two parts

$$\partial\Sigma_{\underline{t}} = \Gamma_0 \cup \Gamma_{\underline{t}}$$

and the geodesic curvature satisfies $\kappa_g = \kappa$ on Γ_0 and $\kappa_g = -\kappa$ on $\Gamma_{\underline{t}}$. Thus we have

$$\int_{\partial\Sigma_{\underline{t}}} \kappa_g \,\mathrm{d}s = \int_{\Gamma_0} \kappa \,\mathrm{d}s - \int_{\Gamma_{\underline{t}}} \kappa \,\mathrm{d}s.$$

Finally, since the surface $\Sigma_{\underline{t}}$ is homeomorphic to a cylinder its homology groups are

$$H_0(\Sigma_{\underline{t}}) \cong \mathbb{Z}, \quad H_1(\Sigma_{\underline{t}}) \cong \mathbb{Z}, \quad H_2(\Sigma_{\underline{t}}) \equiv 0.$$

This means that $b_0(\Sigma_{\underline{t}}) = b_1(\Sigma_{\underline{t}}) = 1$ and all higher Betti numbers are zero. Thus

$$\chi(\Sigma_{\underline{t}}) = b_0(\Sigma_{\underline{t}}) - b_1(\Sigma_{\underline{t}}) + b_2(\Sigma_{\underline{t}}) = 0.$$

Substituting all three terms from above into the original equation (2.13) yields (2.12). □

Remark 2.1.5. *Equation (2.12) can also be confirmed by a straightforward differentiation*

$$\frac{\mathrm{d}}{\mathrm{d}t}\int_{\Gamma_t}\kappa\,\mathrm{d}s=\int_{S^1}\kappa\partial_t g+\partial_t\kappa g\,\mathrm{d}u=\int_{\Gamma_t}\partial_s^2(\tau^{-\frac{1}{2}})-\tau^{\frac{3}{2}}\,\mathrm{d}s=-\int_{\Gamma_t}\tau^{\frac{3}{2}}\,\mathrm{d}s,$$

where the middle integral of $\partial_s^2(\tau^{-\frac{1}{2}})$ is zero because the curve Γ_t is closed.

The formula (2.12) will be used in several important estimates later, but it also has a straightforward implication for curves shrinking to a point.

Proposition 2.1.6. *Let $\{\Gamma_t\}_{t\in\mathcal{T}}$ be a family of space curves evolving according to the minimal surface generating flow. Assume that the curve Γ_t shrinks to a point at the terminal time $\underline{t}$. This assumption means that the length $L(\Gamma_t)$ asymptotically vanishes as t approaches $\underline{t}$. Then the total curvature of the initial curve Γ_0 must be strictly larger than 4π.*

Proof. In this case, the final surface $\Sigma_{\underline{t}}$ including the limiting point toward which the curve shrinks is homeomorphic to a disk instead of a cylinder. The Euler characteristic is then equal to 1, not 0 as before, and the Gauss-Bonnet theorem implies

$$-\int_0^{\underline{t}}\int_{\Gamma_t}\tau^{\frac{3}{2}}\,\mathrm{d}s\,\mathrm{d}t+\int_{\Gamma_0}\kappa\,\mathrm{d}s-\lim_{t\to\underline{t}}\int_{\Gamma_t}\kappa\,\mathrm{d}s=2\pi.$$

After applying the Fenchel theorem and simple algebraic manipulation, we get an inequality

$$\int_{\Gamma_0}\kappa\,\mathrm{d}s\geqslant 4\pi+\int_0^{\underline{t}}\int_{\Gamma_t}\tau^{\frac{3}{2}}\,\mathrm{d}s\,\mathrm{d}t.$$

Since the integral is strictly positive, the total curvature must be larger than 4π. □

2.2 Basic Properties

Let us explore several basic properties of the minimal surface generating flow introduced in Definition 2.0.6. We first show a trivial analytical solution in Subsection 2.2.0, then present a preserved geometric quantity in Subsection 2.2.2 and bound the evolving curve in the convex hull of the initial condition using the Maximum principle in Subsection 2.2.1.

2.2.0 Analytical Solution

Analytical solutions to partial differential equations are often useful for gaining insight into the behaviour of general solutions and can help as sanity checks for computational experiments. In the case of the minimal surface generating flow, we only have one analytical solution, for the highly symmetric case of the helix curve that traces out the helicoid surface.

Example 2.2.1 (Example 2 from [MB22a])**.** *In this example, we show that the helix curve generates helicoid as its trajectory surface. Thanks to the symmetries of the helix and zero binormal velocity term, the solution has to be in the following form:*

$$\gamma(u,t):=[\rho(t)\cos u,\rho(t)\sin u,\xi u]^T,$$
$$\gamma_0(u):=[\rho_0\cos u,\rho_0\sin u,\xi u]^T,$$

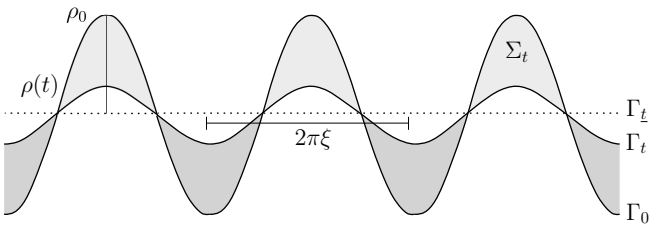

Figure 2.3: Diagram of the helix analytical solution from Example 2.2.1.

where both ρ_0 and ξ are positive constants. As the torsion can be retrieved from ρ and ξ as

$$\tau(\cdot, t) \equiv \xi(\rho(t)^2 + \xi^2)^{-1}$$

and the normal vector points toward the central line, this setup reduces to an equation

$$\dot{\rho}(t) = -(\xi^{-1}\rho(t)^2 + \xi)^{\frac{1}{2}}.$$

This ordinary differential equation has a unique solution in the following implicit form

$$t = \underline{t} - \tfrac{1}{2}\xi^{\frac{3}{2}} \log\left[\xi^{-1}\rho(t) + \zeta(t)\right] - \tfrac{1}{2}\xi^{\frac{1}{2}}\rho(t)\zeta(t),$$

where the terminal time $\underline{t}$ is determined by the initial condition ρ_0 and ζ is given by

$$\zeta(t)^2 := 1 + \left(\xi^{-1}\rho(t)\right)^2.$$

Thus the radius ρ of the helix monotonically strictly decreases and asymptotically approaches zero as the helix approaches a straight line as the time t tends to the finite $\underline{t}$.

One should note that this example is an open curve. No analytical solution of a closed curve evolving by the minimal surface generating flow is currently known.

2.2.1 Integral of Motion

Integrals of motion are useful for analysis of the long term behaviour as well as for the verification of numerical schemes. In the case of the minimal surface generating flow, we have the following curious preserved interval.

Corollary 2.2.2 (Corollary 1 from [MB22a])**.** *Let Γ_t evolve according to the minimal surface generating flow. Then the integral of $\tau^{\frac{1}{2}}$ along the curve Γ_t does not change during the flow.*

Proof. Differentiation of the integral using the formulae (2.5-2.8) leads to

$$\frac{\mathrm{d}}{\mathrm{d}t}\int_{\Gamma_t} \tau^{\frac{1}{2}}\,\mathrm{d}s = \frac{\mathrm{d}}{\mathrm{d}t}\int_{S^1} \tau^{\frac{1}{2}} g\,\mathrm{d}u = \int_{S^1} \partial_t(\tau^{\frac{1}{2}})g + \tau^{\frac{1}{2}}\partial_t g\,\mathrm{d}u. \tag{2.14}$$

After algebraic manipulation, all terms in the integral (2.14) cancel out. □

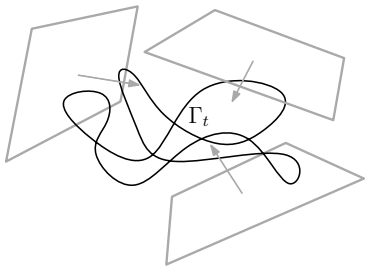

(a) Restriction of Γ_t inside of half-planes.

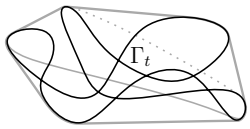

(b) Restriction within the convex hull.

Figure 2.4: Stages of restriction of Γ_t from Lemma 2.2.4 to Proposition 2.2.5.

As all other flows with positive velocity term in the principal normal direction, the minimal surface generating flow reduces the length of the curve in time.

Proposition 2.2.3 (Proposition 2 from [MB22a]). *The length $L(\Gamma_t)$ of a curve Γ_t under the minimal surface generating flow monotonically strictly decreases in time.*

Proof. Straightforward differentiation and the application of formulae (2.5-2.8) yields

$$\frac{\mathrm{d}}{\mathrm{d}t}L(\Gamma_t) = \int_{S^1} \partial_t g \,\mathrm{d}u = -\int_{\Gamma_t} \kappa\tau^{-\frac{1}{2}} \,\mathrm{d}s.$$

The integrand in the last term is always non-negative and, furthermore, it must be positive on a part of the curve with a non-trivial one-dimensional measure. □

We later show the length for closed curves must decrease to zero if the flow exists forever.

2.2.2 Maximum Principle

In this subsection, we use a maximum principle-like argument to bound the parametric function γ inside a convex hull of its initial range. We prove this fact for the minimal surface generating flow, but the following arguments are applicable to any geometric motion law with no binormal velocity and non-negative principle normal velocity component.

Lemma 2.2.4 (Improved Lemma 3.2 from [MB22a]). *Let $\mathcal{B}$ denote an orthonormal basis of $\mathbb{R}^3$. For an evolving family of closed curves Γ_t and all basis vectors $b \in \mathcal{B}$, we define*

$$\underline{m}_b(t) := \min_{u\in S^1}\langle b, \gamma(u,t)\rangle \quad \textit{and} \quad \overline{m}_b(t) := \max_{u\in S^1}\langle b, \gamma(u,t)\rangle.$$

If Γ_t is evolving according to the minimal surface generating flow, it must satisfy

$$\underline{m}_b(0) \leqslant \langle b, \gamma(u,t)\rangle \leqslant \overline{m}_b(0)$$

for all basis vectors $b \in \mathcal{B}$ and all times t in $[0, \underline{t})$. Thus Γ_t must remain within a minimal cuboid containing Γ_0 which is axis-aligned with respect to the basis vectors from $\mathcal{B}$.

Proof. Since S^1 is compact and $\gamma(\cdot,t)$ is continuous, the function $\phi_{b,t} := \langle b, \gamma(\cdot,t)\rangle$ attains its minimum and maximum for fixed $b \in \mathcal{B}$ and $t \in [0,\underline{t})$ at some points $\underline{u}_b(t) \in S^1$ and $\overline{u}_b(t) \in S^1$, respectively. The function $\phi_{b,t}$ must then satisfy

$$\begin{aligned}\partial_u \phi_{b,t}(\underline{u}_b(t)) = 0 = \partial_u \phi_{b,t}(\overline{u}_b(t)),\\ \partial_u^2 \phi_{b,t}(\underline{u}_b(t)) \geqslant 0 \geqslant \partial_u^2 \phi_{b,t}(\overline{u}_b(t)).\end{aligned}$$

Furthermore, the same inequalities at points $\underline{u}_b(t)$ and $\overline{u}_b(t)$ hold for the $\partial_t \phi_{b,t}$ because

$$\partial_t \langle b,\gamma\rangle = \langle b, \partial_t \gamma\rangle = \tau^{-\frac{1}{2}} \langle b, \partial_t N\rangle = (\kappa \tau^{\frac{1}{2}} g^3)^{-1} [g\langle b, \partial_u^2 \gamma\rangle - \partial_u g \langle b, \partial_u \gamma\rangle].$$

Thus the function $\underline{m}_b(t)$ is increasing and $\overline{m}_b(t)$ is decreasing, or in another words

$$\underline{m}_b(0) \leqslant \underline{m}_b(t) \leqslant \overline{m}_b(t) \leqslant \overline{m}_b(0)$$

for all times $t \in [0,\underline{t})$ and all basis vectors $b \in \mathcal{B}$, which proves the statement. □

Proposition 2.2.5 (Proposition 3 from [MB22a]). *Let $\{\Gamma_t\}_{t\in[0,\underline{t})}$ be a family of closed curves evolving according to the minimal surface generating flow (2.3-2.4) with the initial condition Γ_0. Then Γ_t remains inside the convex hull of the initial curve Γ_0 for all times t in $[0,\underline{t})$.*

Proof. Applying Lemma 2.2.4 with respect to all orthonormal bases $\mathcal{B}$ from the Stiefel manifold $V_3(\mathbb{R}^3)$ restricts the curve Γ_t within the intersection of all minimal cuboids containing the initial curve Γ_0, i.e. with the convex hull of Γ_0. □

2.3 Long Term Behaviour

This section covers long term properties from [MB22a] of the the minimal surface generating flow. In particular, we show that the length vanishes at $\underline{t} = \infty$ in Subsection 2.3.0 and provide global area and terminal estimates in Subsections 2.3.1 and 2.3.3, respectively.

2.3.0 Length Limit

The minimal surface generating flow shrinks the curve as we shown in Proposition 2.2.3. However, this claim can be made even stronger. Using Lemma 2.1.4, we can show that the length must shrink to zero provided the flow exists long enough.

Proposition 2.3.1 (Proposition 4 from [MB22a]). *Let the initial curve Γ_0 satisfy*

$$\inf_{\Gamma_0} \tau = \inf_{u\in S^1} \tau(u,0) > 0.$$

Let Γ_t evolve according to the minimal surface generating flow and assume that the flow exists forever, i.e. $\underline{t} = \infty$. Then Γ_t shrinks to a point as its length vanishes in the limit.

Proof. Proposition 2.1.2 and the assumptions for the initial curve Γ_0 allow us to estimate

$$\int_0^{\underline{t}} \int_{\Gamma_t} \tau^{\frac{3}{2}} \,\mathrm{d}s\,\mathrm{d}t \geqslant \int_0^{\underline{t}} \inf_{\Gamma_t} \tau^{\frac{3}{2}} \int_{\Gamma_t} \mathrm{d}s\,\mathrm{d}t \geqslant \inf_{\Gamma_0} \tau^{\frac{3}{2}} \int_0^{\underline{t}} \int_{\Gamma_t} \mathrm{d}s\,\mathrm{d}t.$$

Reversing the order of the inequality and applying equation (2.12) and the Fenchel theorem gives the following estimate of the length integrated through time

$$\int_0^{\underline{t}} L(\Gamma_t)\,\mathrm{d}t = \int_0^{\underline{t}} \int_{\Gamma_t} \mathrm{d}s\,\mathrm{d}t \leqslant \frac{1}{\inf_{\Gamma_0} \tau^{\frac{3}{2}}} \left(\int_{\Gamma_0} \kappa\,\mathrm{d}s - 2\pi \right). \tag{2.15}$$

The upper bound is finite and does not depend on time. Furthermore, the length is always non-negative. If $\underline{t} = \infty$, this forces the integrand $L(\Gamma_t)$ to approach zero as $t \to \underline{t}$. □

2.3.1 Area Estimate

The formula for the total curvature obtained from the Gauss-Bonnet theorem ca be used for global area estimate of the trajectory surface swept by the evolving curve.

Proposition 2.3.2 (Proposition 5 from [MB22a]). *Let $A(\Sigma_{\underline{t}})$ denote the area of $\Sigma_{\underline{t}}$, i.e.*

$$A(\Sigma_{\underline{t}}) := \int_{\Sigma_{\underline{t}}} \mathrm{d}A.$$

Assume that Γ_t evolves according to the minimal surface generating flow (2.3-2.4) from the initial condition Γ_0 which satisfies $\tau > 0$ for all points. Then the area can be bounded as

$$A(\Sigma_{\underline{t}}) \leqslant \frac{1}{\inf_{\Gamma_0} \tau^2} \left(\int_{\Gamma_0} \kappa\,\mathrm{d}s - 2\pi \right). \tag{2.16}$$

Proof. Using the formula for the area element $\mathrm{d}A = \tau^{-\frac{1}{2}} g\,\mathrm{d}u \wedge \mathrm{d}t$ we get

$$A(\Sigma_{\underline{t}}) = \iint_{\mathcal{T}\times S^1} \tau^{-\frac{1}{2}} g\,\mathrm{d}u \wedge \mathrm{d}t = \int_0^{\underline{t}} \int_{\Gamma_t} \tau^{-\frac{1}{2}}\,\mathrm{d}s\,\mathrm{d}t \leqslant \frac{1}{\inf_{\Gamma_0} \tau^2} \left(\int_{\Gamma_0} \kappa\,\mathrm{d}s - 2\pi \right),$$

where the inequality follows from Proposition 2.1.2 and inequality (2.15). □

The estimate (2.16) can be further improved for knotted curves. Provided that the curve Γ_t represents an embedding of a non-trivial knot for all t, one can replace 2π in the right-hand-side of the inequality (2.16) by 4π using the theorem of Milnor-Fáry instead of Fenchel.

2.3.2 Averaged Curvature

To further investigate the existence of the solution and the formation of singularities during the flow, we shall understand the long term behavior of curvature and torsion. However, the analysis of these evolution equations is complicated by the second order term $\partial_s^2(\tau^{-\frac{1}{2}})$ in

$$\partial_t \kappa = \partial_s^2(\tau^{-\frac{1}{2}}) + \tau^{-\frac{1}{2}}(\kappa^2 - \tau^2),$$

We avoid this problem by the following trick. Instead of analysing the curvature itself, we integrate the equations (2.5-2.8) along the curve. This removes the term $\partial_s^2(\tau^{-\frac{1}{2}})$ as the curves are closed and allows us to study the evolution of the averaged curvature $\langle\kappa\rangle$ given by

$$\langle\kappa(\cdot,t)\rangle := \fint_{\Gamma_t} \kappa(s,t)\,\mathrm{d}s := \frac{1}{L(\Gamma_t)}\int_{\Gamma_t}\kappa(s,t)\,\mathrm{d}s, \tag{2.17}$$

where $L(\Gamma_t)$ is the length of Γ_t. Since the curvature κ is non-negative, the averaged curvature $\langle\kappa\rangle$ cannot vanish when Γ_t is a closed curve. Thus tracking whether and when the averaged curvature approaches zero can give us a bound for maximum time of existence for the flow.

2.3.3 Terminal Time

Using the averaged curvature $\langle\kappa\rangle$ defined in (2.17), we can bound the terminal time for a certain subclass of initial curves Γ_0 with non-vanishing curvature and torsion.

Proposition 2.3.3 (Proposition 6 from [MB22a]). *Let Γ_0 be a closed curve such that*

$$\tau_0 := \inf_{\Gamma_0}\tau > 0 \qquad \textit{and} \qquad \langle\kappa(\cdot,0)\rangle < \tau_0.$$

Then the minimal surface generating flow (2.3-2.4) cannot exist beyond the terminal time

$$\underline{t} \leqslant \frac{1}{2}\tau_0^{-\frac{1}{2}}\log\left[1+\frac{2\langle\kappa(\cdot,0)\rangle}{\tau_0-\langle\kappa(\cdot,0)\rangle}\right]. \tag{2.18}$$

Proof. The evolution of the averaged curvature can be computed using (2.5-2.8) and reads

$$\frac{\mathrm{d}}{\mathrm{d}t}\langle\kappa(\cdot,t)\rangle = -\fint_{\Gamma_t}\tau^{\frac{3}{2}}\,\mathrm{d}s + \langle\kappa(\cdot,t)\rangle\fint_{\Gamma_t}\kappa\tau^{-\frac{1}{2}}\,\mathrm{d}s. \tag{2.19}$$

Let us denote the right-hand side of (2.19) by $\xi(\langle\kappa(\cdot,t)\rangle,t)$. Using the torsion assumption, the equation (2.17) and Proposition 2.1.2 we can bound this expression as

$$\xi(\langle\kappa(\cdot,t)\rangle,t) \leqslant -\inf_{\Gamma_t}\tau^{\frac{3}{2}} + \langle\kappa(\cdot,t)\rangle^2\sup_{\Gamma_t}\tau^{-\frac{1}{2}} \leqslant \tau_0^{-\frac{1}{2}}\left[\langle\kappa(\cdot,t)\rangle^2-\tau_0^2\right]. \tag{2.20}$$

Note that the right-hand-side of (2.20) is only a function of the averaged curvature. We can thus denote it by $\zeta(\langle\kappa(\cdot,t)\rangle)$ and use it to define an associated initial value problem

$$\dot{x}(t) = \zeta(x(t)), \qquad x(0) = \langle\kappa(\cdot,0)\rangle.$$

This ordinary differential equation can be solved analytically and the solution is given by

$$x(t) = -\tau_0\frac{\langle\kappa(\cdot,0)\rangle\cosh(\sqrt{\tau_0}t)-\tau_0\sinh(\sqrt{\tau_0}t)}{\langle\kappa(\cdot,0)\rangle\sinh(\sqrt{\tau_0}t)-\tau_0\cosh(\sqrt{\tau_0}t)}.$$

The positive function $x(t)$ monotonically decreases until it reaches zero at the terminal time

$$\bar{t} = -\frac{1}{2}\tau_0^{-\frac{1}{2}}\log\left[\frac{\tau_0-\langle\kappa(\cdot,0)\rangle}{\tau_0+\langle\kappa(\cdot,0)\rangle}\right].$$

The difference between $\langle\kappa(\cdot,t)\rangle$ and $x(t)$ which we denote by $y(t)$ satisfies the inequality

$$\dot{y}(t) = \xi(t) - \zeta(x(t)) \leqslant \zeta(\langle\kappa(\cdot,t)\rangle) - \zeta(x(t)) = \frac{\langle\kappa(\cdot,t)\rangle + x(t)}{\sqrt{\tau_0}} y(t).$$

Finally, from the Grönwall lemma and the zero initial condition $y(0) = 0$, we obtain

$$\langle\kappa(\cdot,t)\rangle = y(t) + x(t) \leqslant y(0) \exp\left[\int_0^t \frac{\langle\kappa(\cdot,r)\rangle + x(r)}{\sqrt{\tau_0}}\,\mathrm{d}r\right] + x(t) = x(t).$$

Since $x(t)$ is a supersolution of the averaged curvature $\langle\kappa(\cdot,t)\rangle$, we obtain $\underline{t} \leqslant \bar{t}$. □

Remark 2.3.4. *The maximum time of existence estimate from Proposition 2.3.3 says that the flow cannot exist forever for initial curves that satisfy the assumptions. The Proposition 2.3.1 thus cannot be applied to this subclass of initial curves.*

The main advantage of the minimal surface generating flow is its simplicity, however, it also has many drawbacks. The issues that are related to frame topology are further analyzed in Chapter 3 and the improved version of this flow is proposed in Chapter 4.

2.4 Conclusion

The chapter covers the article [MB22a] which introduces the minimal surface generating flow and develops methods required for analysis of surfaces traced out by general geometric flows. The study of trajectory surfaces is a tool for studying the long-term behavior of geometric flows and in this chapter, we showed how these surfaces can also be used for the study of specific types of surfaces.

The main results of the analysis for this specific flow include the monotonicity of torsion, the evolution of total curvature and other global quantities including an integral of motion, the use of Maximum principle for constraining the flow in space, and various global estimates including the upper bound for the generated area and terminal time.

However, the analysis uncovered issues related to the frame topology, which are further addressed in the article [MB22b] covered in Chapter 3. Moreover, a modified approach based on curve frame evolution has been developed in preprint [MB23] contained in Chapter 4.

3

Nondegenerate Homotopy

This chapter covers results obtained in [MB22b]. In contrast to the other chapters of this thesis, which focus on the analysis of specific geometric motion laws, this chapter aims to address general topological problems encountered in a broad range of curve flows in space.

Although all closed curves are homeomorphic to S^1, the topology of their framing and of their complement in three-dimensional spaces is considerably more complex. This serves as the foundation for knot theory—a vibrant field of study with wide-ranging applications beyond pure mathematics [Sos04]. While this chapter does not directly employ specific results from knot theory, it is informed by one of the field's key insights: the remarkable utility and efficacy of various topological invariants [Ada04].

To address topological complexities associated with geometric flows, we introduce a novel topological invariant. While plane curves benefit from well-established invariants such as the turning number, no precise analog exists for space curves. To bridge this gap, we put forth the concept of the tangent turning signature.

Additionally, recent work has suggested generalized winding numbers for incomplete data sets [JKS13]. For a comprehensive contemporary treatment of winding numbers for curves embedded on surfaces, see [FGC23].

3.0 Problem Formulation

Utilizing local geometric quantities from the Frenet frame to describe geometric flows is both intuitive and useful. However, because the construction of the Frenet frame requires positive curvature, this approach effectively limits the motion to locally convex space curves. This chapter aims to expand on and apply concepts from regular and nondegenerate homotopy

theory to better understand these restrictions. For more comprehensive details, see [MB22b].

First, we establish the link between a series of geometric evolution equations and findings from nondegenerate homotopy theory. Then, we introduce a new invariant metric called the tangent turning sign to help distinguish between different nondegenerate homotopy classes of space curves. By doing this, we can anticipate the variety of possible trajectories for evolving curves based on their starting geometric layout.

3.0.0 Vanishing Curvature

Let us restate the definition for the geometric flow of space curves with general velocity terms.

Definition 3.0.1 (Restated Definition 0.3.2)**.** *We define the general geometric flow of the family of space curves $\{\Gamma_t\}_{t\in[0,\underline{t})}$ as the following initial-value problem for the parametrization γ:*

$$\partial_t\gamma = v_T T + v_N N + v_B B \qquad \text{in } S^1 \times (0,\underline{t}), \tag{3.1}$$

$$\gamma|_{t=0} = \gamma_0 \qquad \text{in } S^1, \tag{3.2}$$

where γ_0 is the parametrization for the initial curve Γ_0 and $\underline{t}$ is the terminal time.

The problem with Definition 0.3.2 restated above is the explicit dependence on the Frenet frame vectors N and B, which are undefined when the curvature vanishes. There are cases this issue can be avoided by the trick described in the following remark.

Remark 3.0.2. *Let us consider a geometric flow described by v_T, v_N, and v_B which do not explicitly involve the torsion τ. Let us further assume that for any curve we have*

$$\lim_{u\to u_0}(v_N^2 + v_B^2) = 0. \tag{3.3}$$

for all points $u_0 \in S^1$ where the curvature κ vanishes. In this case, one can modify (3.1) to

$$\partial_t\gamma = \begin{cases} v_T T + v_N N + v_B B, & \kappa > 0, \\ v_T T, & \kappa = 0. \end{cases}$$

Notably, one can apply this modification to the curve shortening flow and the vortex filament equation, described by $\partial_t\gamma = \kappa N$ and $\partial_t\gamma = \kappa B$, respectively. However, there are many cases, where this is not possible. We shall discuss such scenarios in the next subsection.

3.0.1 Frenet Frame Dependent Flows

This subsection introduces the notion of Frenet frame dependent geometric flow and defines a notation for curve spaces with different regularity classes and their quotient spaces induced by different types of homotopies, like regular and nondegenerate homotopy.

Definition 3.0.3 (Definition 2.2 from [MB22b])**.** *Geometric flow with velocities v_T, v_N and v_B from Definition 0.3.2 is called Frenet frame dependent flow if it does not satisfy (3.3)*

To streamline the writing in upcoming sections, we introduce a concise notation for curves with non-vanishing derivatives of various orders.

Definition 3.0.4. *Let k be a positive integer and $\mathcal{M}$ be a Riemannian manifold. We denote $\mathcal{R}^k(\mathcal{M})$, the space of all closed $\mathcal{C}^k$-class curves with paramatrization $\gamma\colon S^1 \to \mathcal{M}$ satisfying*

$$\|\partial_u^i \gamma(u)\| > 0$$

for all parameters $u \in S^1$ and all positive integers i up to the value of k.

Example 3.0.5. *In this thesis, we only discuss the spaces $\mathcal{R}^k(\mathcal{M})$ from Definition 3.0.4 for small values of the parameter k and Euclidean $\mathcal{M}$. Let us examine these spaces more closely:*

1. *$\mathcal{R}^1(\mathcal{M})$ are all regular curves immersed in the ambient space $\mathcal{M}$.*
2. *$\mathcal{R}^2(\mathcal{M})$ are all locally convex curves in $\mathcal{M}$, e.i. curves of non-vanishing curvature. Note that for $\mathcal{M} = \mathbb{R}^2$, all embedded curves from $\mathcal{R}^2(\mathbb{R}^2)$ are convex.*
3. *$\mathcal{R}^3(\mathbb{R}^3)$ are curves with non-vanishing torsion, either positive or negative everywhere.*

For the convenience of the reader, we present the following trivial, but useful, statement.

Observation 3.0.6. *Let Γ be a closed, $\mathcal{C}^2$-class space curve. Then the curve Γ is locally convex from the space $\mathcal{R}^2(\mathbb{R}^3)$ if and only if its tangent indicatrix belongs to $\mathcal{R}^1(S^2)$.*

Proof. Follows immediately from the first Frenet-Serret equation $\partial_s T = \kappa N$. □

The main focus of this chapter is the space $\mathcal{R}^2(\mathbb{R}^3)$ of locally convex curves. Let us explore the specific type of homotopy, called nondegenerate homotopy, that is crucial for these curves.

Definition 3.0.7. *A regular homotopy h_t between two locally convex curves from $\mathcal{R}^2(\mathbb{R}^3)$ is called nondegenerate homotopy if and only if each intermediate curve Γ_t generated by the homotopy h_t belongs to the same space $\mathcal{R}^2(\mathbb{R}^3)$. The equivalence between two curves from $\mathcal{R}^2(\mathbb{R}^3)$, induced by the nondegenerate homotopy is denoted by $\sim$, the associated quotient map by $q_\sim$ and the associated quotions space by $\mathcal{R}^1(\mathcal{M})/\sim$.*

To avoid confusion, we denote the equivalence relation induced by regular homotopies as $\approx$, the associated quotient map by $q_\approx$ and the associated quotions space by $\mathcal{R}^1(\mathcal{M})/\approx$.

3.1 Tangent Turning Signature

This section contains the definition and analysis of an invariant called tangent turning signature [MB22b]. Its values categorize locally convex curves into distinct equivalence classes.

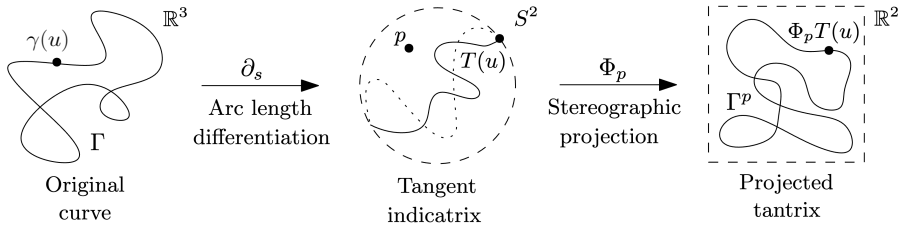

Figure 3.1: Construction of Γ^p from Definition 3.1.1. Adapted from [MB22b].

3.1.0 Topological Preliminaries

In this section, we describe and use the notion of nondegenerate homotopy in the context of Frenet frame-dependent geometric flows. The motivation comes from the fact that during these flows, the curve $\Gamma_t \in \mathcal{R}^2(\mathbb{R}^3)$ at any time t and its initial condition Γ_0 belong to the same equivalence class in $\mathcal{R}^2(\mathbb{R}^3)/\sim$.

Let us thus examine the topology of $\mathcal{R}^2(\mathbb{R}^3)/\sim$. In [Fel68], Feldman addressed the cardinality of this quotient space by studying the Frenet frame of a locally convex curve as a mapping

$$\mathcal{F} : S^1 \to SO(3),$$

and, using properties related to the fundamental group of $SO(3)$, specifically that

$$\pi_1(SO(3)) \cong \mathbb{Z}_2,$$

Feldman demonstrated that $\mathcal{R}^2(\mathbb{R}^3)/\sim$ is comprised of two equivalence classes.

Although Feldman's findings clarify the cardinality of equivalence classes, the methodology for classifying a specific curve within $\mathcal{R}^2(\mathbb{R}^3)$ remains unaddressed. This chapter introduces a new topological invariant aimed at facilitating such classifications and elucidating the structure of $\mathcal{R}^2(\mathbb{R}^3)/\sim$. Further elaboration on this invariant follows.

3.1.1 Well-definedness

This subsection introduces the notion of tangent turning signature and proves that the definition is proper. We later prove that this signature is invariant with respect to nondegenerate homotopy and thus preserved during any Frenet frame dependent geometric flow.

Definition 3.1.1 (Tangent Turning Signature)**.** *Let $\Gamma \in \mathcal{R}^2(\mathbb{R}^3)$ be a locally convex space curve and choose a fixed $p \in S^2 \backslash \operatorname{Ran} T$. By Γ_p we denote the projected curve given by*

$$\gamma_p := \Phi_p \circ T,$$

where T is the tangent vector function of the original curve Γ and the second map

$$\Phi_p : S^2 \backslash \{p\} \to \mathbb{R}^2$$

is the stereographic projection from p. We define the tangent turning parity $\mathcal{T}_\Gamma \in \mathbb{Z}_2$ *as*

$$\mathcal{T}_\Gamma \equiv \deg(T_p) \bmod 2,$$

where $\deg(T_p)$ *is the degree of the Gauss map for the curve* Γ_p*, also referred to as the turning number of* Γ_p *or as the winding number of the tangent vector function* $T_p \colon S^1 \to S^1$*.*

Remark 3.1.2. *Note that in Definition 3.2 from the original article [MB22b], we used an alternative but equivalent notion of tangent turning sign with values in* $\{\pm 1\}$*.*

The construction of the tangent turning signature in Definition 3.1.1 is based on an arbitrary choice of the point p. This ambiguity is represented in Figure 3.1 and in this diagram:

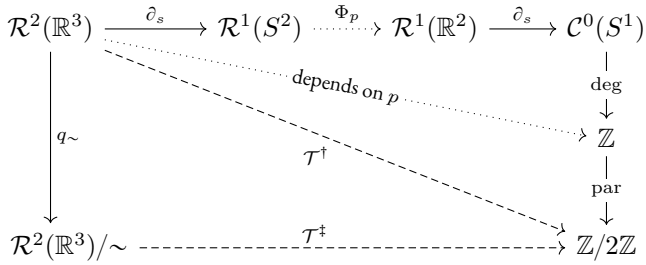

In this diagram, dotted arrows represent maps that are not uniquely determined. Specifically, they depend on the choice of the point p. In the following pages, we aim to show that this ambiguity is resolved by the parity operation and that both the dashed arrows are legitimate.

The first dashed line tagged with † represents the definition of the tangent turning signature and its well-definedness will be resolved in the next proposition. The second dashed arrow labeled by ‡ is resolved later, when we show that the value of the tangent turning signature is preserved under nondegenerate homotopy and can thus be defined on the quotient space.

Proposition 3.1.3 (Proposition 3.3 from [MB22b])**.** *The tangent turning signature* $\mathcal{T}_\Gamma$ *of a locally convex curve* $\Gamma \in \mathcal{R}^2(\mathbb{R}^3)$ *does not depend on the choice of* p*; i.e.* $\mathcal{T}_\Gamma$ *is well-defined.*

Proof. To show that the value of $\mathcal{T}_\Gamma$ does not depend on the choice of p, let us consider two different points $p_1, p_2 \in S^2 \backslash \operatorname{Ran} T$. In the trivial case, both points p_1 and p_2 lie in the same path-connected component $K \subset S^2 \backslash \operatorname{Ran} T$. By definition there must exist a regular path $\pi : [0,1] \to K$ such that $\pi(0) = p_1$ and $\pi(1) = p_2$, which defines regular homotopy

$$h_t := \Phi_{\pi(t)} \circ T$$

between the projected curves Γ_{p_1} and Γ_{p_2}. Thus, by the Whitney-Graustein Theorem from [Whi37], we even have $\deg(T_{p_1}) = \deg(T_{p_2})$ and the parity equality is trivially achieved.

In the second case, points p_1 and p_2 lie in different connected components C_1 and C_2 of $S^2 \backslash \operatorname{Ran} T$, respectively. Without loss of generality, assume they share a common border, i.e.

$$C_1 \cap C_2 = \varnothing \neq \partial C_1 \cap \partial C_2.$$

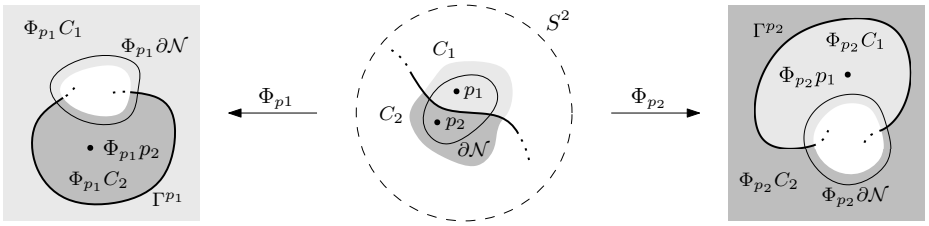

(a) Differences in topology caused by the change of the singular point of stereographic projection.

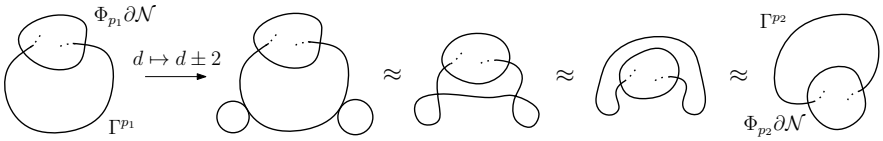

(b) Attaching two identically oriented loops to Γ_{p_1} allows us to construct regular homotopy to Γ_{p_2}.

Figure 3.2: Ideas from the proof of Proposition 3.1.3. Adapted from [MB22b].

In this configuration there must be a neighbourhood $\mathcal{N} \subset S^2$ such that $p_1, p_2 \in \mathcal{N}$ and

$$\mathcal{N} \setminus \operatorname{Ran} T \subset C_1 \cup C_2. \tag{3.4}$$

The projections Φ_{p_1} and Φ_{p_2} now indeed lead to different turning numbers. This difference is caused by the common border of $\partial C_1 \cap \partial C_2$, which is projected in two different ways. However, adding two loops of the same orientation to Γ_{p_1} makes it possible to construct the regular homotopy between the two projections Γ_{p_1} and Γ_{p_2} as suggested in Figure 3.2b. The additional loops affect the total signed curvature by $\pm 4\pi$ and thus

$$|\deg(T_{p_1}) - \deg(T_{p_2})| = 2.$$

The parity of the turning number thus remains constant, which means that the tangent turning signature $\mathcal{T}_\Gamma$ from Definition 3.1.1 is defined properly. □

3.2 Ramifications

Having introduced this topological framework for describing locally convex curves, the focus now shifts back to issues related to geometric flows. In the following, we aim to use the notion of tangent turning signature to investigate their long-term properties.

3.2.0 Invariance

As suggested before, we aim to prove that $\mathcal{T}_\Gamma$ does not change during any Frenet frame dependent flow. The following lemma serves as a basis for the proof of this statement.

Lemma 3.2.1 (Lemma 3.5 from [MB22b]). *Let h_t be a nondegenerate homotopy and denote $\{\Gamma_t\}_{t\in[0,1]}$ the associated family of curves from $\mathcal{R}^2(\mathbb{R}^3)$. Then for each $t \in [0,1]$ there is a*

neighbourhood H of t and $p \in S^2$ such that the tangent vector map $T(\cdot, t)$ satisfies

$$p \notin T[S^1 \times (H \cap [0,1])], \tag{3.5}$$

where the square brackets denote the image, e.i. the set $\{T(u,t)\colon u \in S^1, t \in H \cap [0,1]\}$.

Proof. For a fixed t from $[0,1]$, the tangent indicatrix $T(\cdot, t)$ is differentiable and

$$T[S^1 \times \{t\}] \neq S^2,$$

because there are no differentiable, space-filling functions [Mor87]. Since the domain $S^1 \times \{t\}$ is closed, and so is the image of $S^1 \times \{t\}$, there must be $p \in S^2$ and $\varepsilon > 0$ such that

$$T[S^1 \times \{t\}] \cap B_p^\varepsilon = \varnothing,$$

where B_p^ε is the ball $\{x \in S^2\colon \|x - p\| < \varepsilon\}$. Since T is continuous and we have

$$\min_{S^1} \|T(\cdot, t) - p\| \geqslant \varepsilon,$$

there exists neighbourhood H of t on which we can lower bound the tangent vector map as

$$\inf_{S^1 \times (H \cap [0,1])} \|T - p\| \geqslant \frac{\varepsilon}{2}.$$

Thus we constructed point $p \in S^2$ and neighbourhood H such that (3.5) is satisfied. □

Lemma 3.2.1 allows us to prove the invariance of $\mathcal{T}_\Gamma$ under nondegenerate homotopy. Showing that $\mathcal{T}$ is a meaningful notion even on the space of equivalence classes $\mathcal{M}/\sim$. This will complete the commutative diagram by proving that the bottom arrow is well-defined indeed.

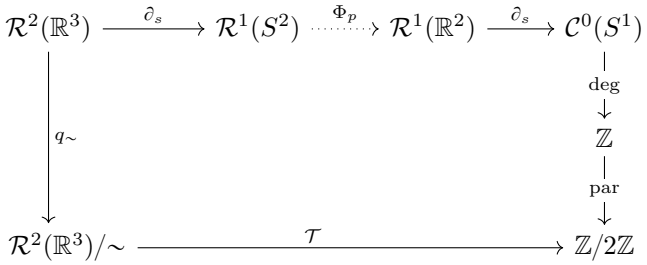

Theorem 3.2.2. *The tangent turning signature $\mathcal{T}_\Gamma$ of a locally convex space curve $\Gamma \in \mathcal{R}^2(\mathbb{R}^3)$ is invariant with respect to nondegenerate homotopy and is thus well-defined on $\mathcal{R}^2(\mathbb{R}^3)/\sim$.*

Proof. Let h_t be a nondegenerate homotopy and denote the set of curves generated by h_t as

$$\{\Gamma_t\}_{t \in [0,1]} \subset \mathcal{R}^2(\mathbb{R}^3).$$

Applying Lemma 3.2.1 for every t yields the following uncountable set of points on S^2:

$$\mathcal{P} = \{p_t\colon t \in [0,1]\} \subset S^2$$

and the corresponding open cover of $[0,1]$ made of neighbourhoods $H_t^* = H_t \cap [0,1]$:

$$\mathcal{S} = \{H_t^* \colon t \in [0,1]\} \subset \mathscr{P}([0,1]),$$

where $\mathscr{P}(M)$ is the powerset of M. Since the closed interval $[0,1]$ is compact, there exists a finite subcover of $\mathcal{S}' \subset \mathcal{S}$ of $[0,1]$ of cardinality $N \in \mathbb{N}$. Let us denote its elements by the strictly increasing sequence of $(t_i)_{i=1}^N \subset [0,1]$ with the corresponding set

$$\mathcal{S}' = \{H_{t_i}^*\}_{i=1}^N \subset \mathcal{S}.$$

Furthermore, denote by $\mathcal{P}' = \{p_i\}_{i=1}^N$ the associated subset of $\mathcal{P}$ such that each t_i satisfies

$$p_i \in S^2 \backslash T[S^1 \times H_{t_i}^*].$$

where $T(\cdot, t)$ is the tangent vector map of the curve Γ_t. Let us now construct a strictly increasing sequence $(k_i)_{i=1}^{N'}$ of integers between 1 and N such that the corresponding set

$$\mathcal{S}'' = \{H_{t_{k_i}}\}_{i=1}^{N'} \subset \mathcal{S}'$$

is a minimal subcover with respect to inclusion. As the sequence $(t_{k_i})_{i=1}^{N'}$ is increasing, the intersection in (3.6) is nonempty. The final configuration is depicted in Figure 3.3. Let

$$s_i \in H_{t_{k_i}}^* \cap H_{t_{k_{i+1}}}^* \tag{3.6}$$

and construct the following regular homotopy between the curves and $\Gamma_{p_{k_i}}^{s_i}$ and $\Gamma_{p_{k_i}}^{s_{i+1}}$:

$$\hat{h}_t := \Phi_{p_{k_i}} \circ T(\cdot, s_i + t(s_{i+1} - s_i)). \tag{3.7}$$

Each time interval $[s_i, s_{i+1}]$ is thus associated with following commutative diagram:

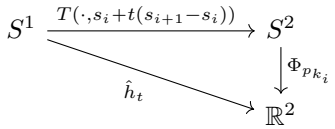

Note that the homotopy (3.7) is regular due to Observation 3.0.6. Thus, we prove that

$$\mathcal{T}_{\Gamma_{s_i}} = \mathcal{T}_{\Gamma_{s_{i+1}}}$$

for all nonnegative integers $i < N'$ and as this chain is finite, we have $\mathcal{T}_{\Gamma_0} = \mathcal{T}_{\Gamma_1}$. □

3.2.1 Geometric Flows

Theorem 3.2.2 immediately leads to the following important statement we aimed towards.

Corollary 3.2.3 (Corollary 3.6 from [MB22b]). *The tangent turning signature $\mathcal{T}_\Gamma$ of a locally convex space curve Γ is preserved under any Frenet frame dependent goemetric flow.*

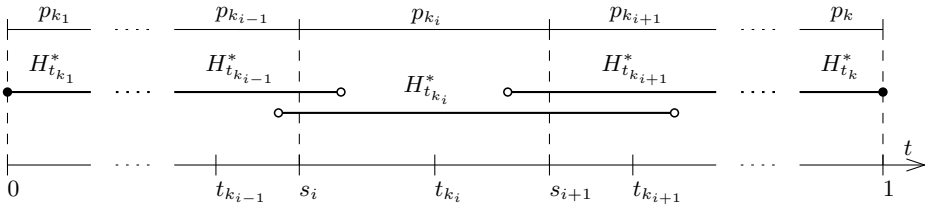

Figure 3.3: Objects from the proof of Theorem 3.2.2. Adapted from [MB22b].

Theorem 3.2.2 can also be applied in reverse. Specifically, if the tangent turning signature changes during smooth evolution, a point must exist where the curvature vanishes during the motion. The following example illustrates this scenario.

Example 3.2.4 (Example 4.2 from [MB22b]). *Consider the example adapted from [Gol+10] with the transformation of a doubly covered circle to a simple circle, parameterized as*

$$\gamma(u,t) := \begin{bmatrix} -t\cos u + (1-t)\cos(2u) \\ t\sin u + (1-t)\sin(2u) \\ -2t(1-t)\sin u \end{bmatrix},$$

where $u \in S^1$ *and* $t \in [0,1]$. *Given that the tangent turning signature of* Γ_0 *is* $[0]$ *and it changes during the homotopy to* $[1]$, *there must be* $(u,t) \in S^1 \times [0,1]$ *such that* $\kappa(u,t) = 0$.

The definition of Frenet frame dependent geometric flow can be further restricted to higher-order regularity conditions. For example, the Minimal surface generating flow, introduced in Chapter 2, demands that both curvature and torsion be non-zero at every point along the curve. In the notation introduced in this chapter, all evolving curves must live in the space $\mathcal{R}^3(\mathbb{R}^3)$. For more examples of flows demanding non-zero torsion see e.g. [RK02].

The space of third-order nondegenerate homotopy classes has been examined in [Lit71]. In this situation, four distinct equivalence classes emerge because the orientation of the curve becomes significant. These four classes are uniquely defined by the combination of the tangent turning parity $\mathcal{T}_\Gamma$ and the sign of the torsion τ. It's worth noting that since the torsion τ is continuous and never zero, its sign remains consistent at every point along the curve.

3.3 Conclusion

This chapter introduces the tangent turning signature from [MB22b] as a topological invariant for understanding locally convex space curves in three-dimensional space. This new quantity complements existing invariants like the turning number in plane curves.

We further establish a link between nondegenerate homotopy theory and Frenet frame dependent flows. Specifically, the tangent turning signature differentiates nondegenerate homotopy classes of locally convex space curves and thus remains constant during such flows.

Future research can extend the applicability of the tangent turning signature to broader categories of geometric flows, possibly accommodating manifolds in higher-dimensional spaces or those embedded in different ambient spaces.

4

Framed Curvature Flow

This chapter covers results from the most recent work [MB23], which introduces Framed curvature flow. Curvature-driven geometric flows have been extensively studied for their many favorable properties and various applications across multiple pure and applied fields. We aim to take advantage of these benefits by keeping the magnitude of the local velocity equal to curvature, but at the same time expand and generalise this family of flows by letting the velocity direction be dictated by an associated time-dependent moving frame. We refer to this new class of geometric flows as the *framed curvature flow*.

Even though our formulation is based on the Frenet frame, the velocity vector is well defined even in the presence of vanishing curvature, where the normal and binormal vectors are undefined. In the language of Definition 2.2 from [MB22b], the framed curvature flow is not a Frenet frame dependent geometric flow. In this way, it is a modification of the minimal surface generating flow from [MB22a], where both torsion and curvature must remain positive. Another advantage over [MB22a] is the rich configuration space enabled by the additional degrees of freedom from the moving velocity direction field. To demonstrate the expressivity of this approach we derive variations of the flow that trace out various surfaces of interest in the latter part of this chapter.

In this work, we formulate the coupled dynamics of the moving frame and the curvature-driven motion, establish local existence and uniqueness for a simplified case of this motion law, provide useful global estimates for geometric and topological quantities, classify possible singularities formed during the flow and analyse generated trajectory surfaces.

The Chapter is organised as follows. Section 4.0 introduces the framed curvature flow and prepares the notation and lemmas required for further analysis of the flow and its trajectory surfaces. The analysis itself is divided into Sections 4.1 and 4.2. While the former deals with local behaviour including the local existence and formation of singularities, the latter (Sec-

tion 4.2) focuses on long-term behaviour by means of length and area estimates and explores the effects of the moving frame topology. Section 4.3 then showcases interesting examples of flows from the configuration space of the framed curvature flow framework. Specifically, we explore flows leading to trajectory surfaces of constant mean and Gaussian curvature.

4.0 Introduction

Consider a family of closed curves $\{\Gamma_t\}_{t\in[0,\underline{t})}$ evolving in the time interval $[0,\underline{t})$, where $\underline{t} > 0$ is the terminal time. For a given time $t \in [0,\underline{t})$, the curve Γ_t is represented by a parametrization $\gamma(\cdot,t)\colon S^1 \to \mathbb{R}^3$, where $S^1 = \mathbb{R}/2\pi\mathbb{Z}$ is the unit circle. We use the standard Frenet frame notation, where T, N, and B denote the tangent, normal, and binormal vectors, respectively. The curvature and torsion, given by the Frenet-Serret formulae, are denoted by κ and τ, respectively. Furthermore, $g := \|\partial_u\gamma\|$ is the local rate of parametrization and $\mathrm{d}s = g\,\mathrm{d}u$ is the arclength element.

4.0.0 Theta-Frame

There are many ways to frame a curve [Bis75]. The Frenet frame is in some sense canonical and easy to work with, but is ill-defined at points of vanishing curvature. We define a time-dependent moving frame that is derived from the Frenet frame using an angle functional θ. The normal vector associated with this moving frame will determine the direction of the velocity vector during the framed curvature flow.

Definition 4.0.1 (θ-frame)**.** *For an evolving curve $\{\Gamma_t\}_{t\in[0,\underline{t})}$ and a functional*

$$\theta \in \mathcal{C}^{1,2}(S^1 \times [0,\underline{t}); S^1),$$

*we define a θ-*frame *of Γ_t, with θ-*normal *ν_θ and θ-*binormal *β_θ, using a one-parameter group of rotation $\{\mathscr{R}_\theta\}$, as*

$$\begin{bmatrix}\nu_\theta\\ \beta_\theta\end{bmatrix} = \mathscr{R}_\theta \begin{bmatrix}N\\ B\end{bmatrix}, \text{ where } \mathscr{R}_\theta := \begin{bmatrix}\cos\theta & \sin\theta\\ -\sin\theta & \cos\theta\end{bmatrix} \in \mathrm{SO}(2).$$

We denote the moving framed curves as $\{(\Gamma_t,\theta_t)\}_{t\in[0,\underline{t})}$, where $\theta_t := \theta(\cdot,t)$.

Note that $\beta_\theta = T \times \nu_\theta$ and Frenet-Serret type formulae for the θ-frame read

$$\partial_s \begin{bmatrix}T\\ \nu_\theta\\ \beta_\theta\end{bmatrix} = \begin{bmatrix}0 & \kappa\cos\theta & -\kappa\sin\theta\\ -\kappa\cos\theta & 0 & \tau+\partial_s\theta\\ \kappa\sin\theta & -\tau-\partial_s\theta & 0\end{bmatrix} \begin{bmatrix}T\\ \nu_\theta\\ \beta_\theta\end{bmatrix} =: \begin{bmatrix}0 & \psi_1 & -\psi_2\\ -\psi_1 & 0 & \psi_3\\ \psi_2 & -\psi_3 & 0\end{bmatrix} \begin{bmatrix}T\\ \nu_\theta\\ \beta_\theta\end{bmatrix}.$$

In the context of the associated trajectory surface defined in section 4.0.2, ψ_1 and ψ_2 can be interpreted as the geodesic and normal curvatures of Γ_t immersed in Σ_t, respectively. Hereafter, we refer to ψ_3 as the generalised torsion.

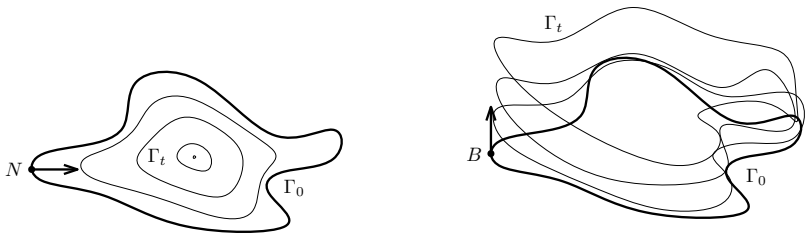

(a) Curve shortening flow.

(b) Vortex filament equation.

Figure 4.1: Classical examples of geometric motion laws for space curves.

4.0.1 Framed Flow

Definition 4.0.2 (Framed curvature flow)**.** *The family of evolving framed curves denoted by* $\{(\Gamma_t, \theta_t)\}_{t\in[0,\underline{t})}$ *is a solution to the* framed curvature flow *if the parametrization* γ *and the angle functional* θ *satisfy the following initial-value problem*

$$\partial_t\gamma = \kappa\nu_\theta \qquad \partial_t\theta = v_\theta \qquad \text{in } S^1 \times [0,\underline{t}), \tag{4.1a}$$

$$\gamma|_{t=0} = \gamma_0 \qquad \theta|_{t=0} = \theta_0 \qquad \text{in } S^1, \tag{4.1b}$$

where γ_0 *and* θ_0 *are the initial conditions and the* θ*-velocity*

$$v_\theta \in \mathcal{C}^1(S^1 \times [0,\underline{t}); \mathbb{R})$$

will be specified later in sections 4.1.2, 4.3.0 and 4.3.1.

Example 4.0.3. *The framed curvature flow subsumes the following classical geometric flows, depicted in Figure 4.1, as its special cases:*

(a) Curve shortening flow *studied e.g. in [AG92; Alt91]:*
When $\theta|_{t=0} = 0$ *and* $v_\theta|_{\theta=0} = 0$, (4.1) *reduces to* $\partial_t\gamma = \kappa N$.

(b) Vortex filament equation *studied e.g. in [Ric91]:*
When $\theta|_{t=0} = \frac{\pi}{2}$ *and* $v_\theta|_{\theta=\frac{\pi}{2}} = 0$, (4.1) *reduces to* $\partial_t\gamma = \kappa B$.

Remark 4.0.4. *The framed curvature flow* (4.1) *can also be viewed as a local harmonic combination of the* curve shortening flow *and the* vortex filament equation *from Examples 4.0.3(a) and 4.0.3(b), respectively. One can also write* (4.20) *as*

$$\partial_t\gamma = \cos\theta\ \partial_s^2\gamma + \sin\theta\ \partial_s\gamma \times \partial_s^2\gamma.$$

This formulation makes clear how the framed curvature flow (4.1) *is well-defined even when the curvature vanishes and the Frenet frame is undefined.*

Remark 4.0.5. *The set of equations* (4.1) *represents a case of geometric motion with an additional quantity, namely* θ*, whose velocity depends on the geometry, and vice versa. This kind of coupling has been studied in e.g. [Pad+19], where the the additional quantity represents the local radius of a bubble vortex tube.*

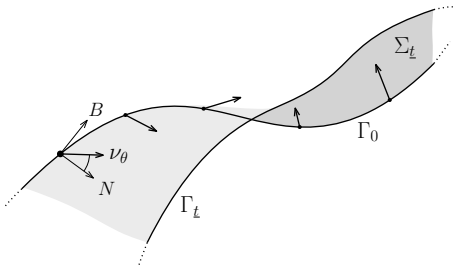

Figure 4.2: Trajectory surface generated by framed curvature flow.

4.0.2 Trajectory Surfaces

In the same way that a point mass moving in a homogeneous gravitational field generates a parabola, trajectory surfaces are generated by geometric flows of space curves. As the title suggests, these surfaces are one of the primary concerns of this chapter.

We argue that there are two main benefits to examining trajectory surfaces. First, the shape of the trajectory surface encodes the long-term properties of the associated motion law, and thus the knowledge of the generated surfaces may help us understand the overall behaviour of the original geometric flow. Conversely, this framework provides an alternative way to generate and study surfaces with prescribed characteristics, potentially enabling new ways to categorize and understand these surfaces and possibly help tackle various open problems. The formal meaning of trajectory surface is clarified below.

Definition 4.0.6 (Trajectory surface, [MB22a])**.** *For a given θ-velocity v_θ, terminal time $\underline{t}$ and initial curve Γ_0, we formally define the trajectory surface $\Sigma_{\underline{t}}$ as*

$$\Sigma_{\underline{t}} := \bigcup_{t\in[0,\underline{t})} \Gamma_t,$$

i.e. $\Sigma_{\underline{t}}$ is a surface parametrized by $\gamma(u,t)$ for $t \in [0,\underline{t})$ and $u \in S^1$.

Trajectory surfaces have been studied in [HM16] for the special case of inextensible flows, i.e. geometric flows satisfying $\partial_t g = 0$. An important example of such motion law is the vortex filament equation, mentioned in Example 4.0.3. Surfaces generated by this motion law, referred to as Hasimoto surfaces, have been previously considered in [AHY12].

Closely related to the trajectory surface is the concept of worldsheet from physics. In the context of string theory, particles sweep out worldlines and strings sweep out worldsheets in Minkowski space. The equations of motion are induced from the Nambu-Goto action or the Polyakov action [Nam95; Got71]. In our case, time is not treated as another dimension as in general relativity, but rather as another parameter.

In this Chapter, we are specifically interested in trajectory surfaces of constant curvature (see Section 4.3). In light of this, the following lemma states the formulas for the mean and the Gaussian curvature of surfaces generated by (4.1).

Lemma 4.0.7. *Mean curvature H and the Gaussian curvature K of the trajectory surface Σ_t*

obtained from the curve Γ_t evolving according to (4.1) *can be expressed in the form*

$$H = -\psi_2 + \chi \text{ and } K = -\psi_3^2 - \psi_2\chi,$$

respectively. The auxiliary variable χ used in the formulae above reads

$$\chi := \frac{v_\theta}{\kappa} + \frac{\kappa\partial_s\psi_3 + 2\partial_s\kappa\psi_3}{\kappa^3}\psi_1 + \frac{\partial_s^2\kappa - \kappa\partial_s\psi_3^2}{\kappa^3}\psi_2.$$

Proof. The first and the second fundamental form I and II of Σ_t are given by

$$\mathrm{I} = \begin{bmatrix} \mathscr{E} & \mathscr{F} \\ \mathscr{F} & \mathscr{G} \end{bmatrix} = \begin{bmatrix} g_{uu} & g_{vu} \\ g_{uv} & g_{vv} \end{bmatrix} = \begin{bmatrix} g^2 & 0 \\ 0 & \kappa^2 \end{bmatrix}, \qquad \mathrm{II} = \begin{bmatrix} \mathscr{L} & \mathscr{M} \\ \mathscr{M} & \mathscr{N} \end{bmatrix},$$

where (g_{ij}) is the metric tensor of Σ_t, and II contains $\mathscr{L} = -g^2\psi_2$, $\mathscr{M} = g\psi_3\kappa$ and

$$\mathscr{N} = \kappa v_\theta + \psi_1\frac{\kappa\partial_s\psi_3 + 2\partial_s\kappa\psi_3}{\kappa} + \psi_2\frac{\partial_s^2\kappa - \kappa\psi_3^2}{\kappa}.$$

Finally, the mean curvature H and the Gaussian curvature K are

$$K = \frac{\det \mathrm{II}}{\det \mathrm{I}} = \frac{\mathscr{L}\mathscr{N} - \mathscr{M}^2}{\mathscr{E}\mathscr{G} - \mathscr{F}^2}, \qquad H = \operatorname{tr}\left(\mathrm{II}\left(\mathrm{I}^{-1}\right)\right) = \frac{\mathscr{L}}{\mathscr{E}} + \frac{\mathscr{N}}{\mathscr{G}}.$$

For more details, we refer the reader to Section 2 in [MB22a]. □

Remark 4.0.8. *The principle curvatures of the trajectory surface $\Sigma_{\underline{t}}$ generated during* (4.1) *are*

$$\kappa_{1,2} = -\psi_2 + \chi \pm \sqrt{\zeta},$$

where $\zeta := \psi_2^2 - \psi_2\chi + \chi^2 + \psi_3^2$ and χ is the auxiliary variable from Lemma 4.0.7.

Further analysis of trajectory surfaces has been recently carried out in [ZZW22], where the authors describe the properties of u-curves, i.e. curves given by $\gamma(u, \cdot)$ with fixed $u \in S^1$.

4.1 Local Analysis

This section focuses on local properties, both in time and parameter space, of the solution to the framed curvature flow Equation (4.1). In particular, we state the evolution equations of the local geometric quantities in Section 4.1.0, study the effects of non-trivial tangential redistribution in Section 4.1.1 and with the help of these preliminary results we establish the local existence and uniqueness of the solution in Section 4.1.2. The Section 4.1.3 provides an overview of possible singularities formed during curvature blow-up events.

4.1.0 Evolution Equations

Evolution equations for local geometric quantities, like the rate of parametrisation or curvature, during general geometric flows of space curves have been extensively studied in many pieces of literature before. See e.g. [Olv08] for a general algebraic approach or [BKŠ22] for the treatment of geometric motion law similar to (4.1). We nevertheless state these equations and adopt them for the specific case of framed curvature flow for reader's convenience.

Lemma 4.1.1. *The arc-length commutator during the framed curvature flow* (4.1) *with the angle functional θ is given by*

$$[\partial_t, \partial_s] := \partial_t\partial_s - \partial_s\partial_t = \kappa^2 \cos\theta\ \partial_s. \tag{4.2}$$

Equivalently, $\partial_t g = -\kappa^2 \cos\theta\ g = -\kappa\psi_1 g$.

Proof. The statement is a special case of Proposition 1 from [BKŠ22]. □

Lemma 4.1.2. *The Frenet frame during the framed curvature flow* (4.1) *satisfies*

$$\partial_t \begin{bmatrix} T \\ N \\ B \end{bmatrix} = \begin{bmatrix} 0 & \xi_1 & -\xi_2 \\ -\xi_1 & 0 & \xi_3 \\ \xi_2 & -\xi_3 & 0 \end{bmatrix} \begin{bmatrix} T \\ N \\ B \end{bmatrix}, \qquad \begin{aligned} \xi_1 &:= \partial_s\psi_1 - \tau\psi_2, \\ \xi_2 &:= -\partial_s\psi_2 - \tau\psi_1, \\ \xi_3 &:= \kappa^{-1}(\psi_1\partial_s\tau + \partial_s^2\psi_2 - \tau^2), \end{aligned}$$

while the evolution of θ-normal ν_θ and θ-binormal β_θ can be expressed as

$$\partial_t \begin{bmatrix} T \\ \nu_\theta \\ \beta_\theta \end{bmatrix} = \begin{bmatrix} 0 & \zeta_1 & -\zeta_2 \\ -\zeta_1 & 0 & \zeta_3 \\ \zeta_2 & -\zeta_3 & 0 \end{bmatrix} \begin{bmatrix} T \\ \nu_\theta \\ \beta_\theta \end{bmatrix}, \qquad \begin{aligned} \zeta_1 &:= \partial_s\kappa, \\ \zeta_2 &:= -\psi_3\kappa, \\ \zeta_3 &:= v_\theta + \xi_3. \end{aligned}$$

Finally, the curvature κ and torsion τ evolve as

$$\partial_t\kappa = \kappa^2\psi_1 + \kappa^{-1}\left(\partial_s^2\psi_1 - \partial_s\tau\psi_2 - 2\tau\partial_s\psi_2 + \tau\psi_1\right), \tag{4.3}$$

$$\partial_t\tau = \kappa\psi_1(\tau + \psi_3) + \partial_s\left[\kappa^{-2}\left(\partial_s^2\psi_2 + 2\partial_s\kappa\psi_1\psi_3 - \kappa\psi_2\psi_3 + \kappa\psi_1\partial_s\psi_2\right)\right]. \tag{4.4}$$

Proof. The result can be obtained by substitution to Example 5.7 from [Olv08]. □

The evolution equations for the θ-frame local quantities ψ_1, ψ_2 and ψ_3 are more involved:

$$\begin{aligned} \partial_t\psi_1 &= \partial_t\kappa\cos\theta - \psi_2 v_\theta, \\ \partial_t\psi_2 &= \partial_t\kappa\sin\theta + \psi_1 v_\theta, \\ \partial_t\psi_3 &= \partial_t\tau + \partial_s v_\theta + \kappa\psi_1\partial_s\theta. \end{aligned}$$

Here, $\partial_t\kappa$ and $\partial_t\tau$ shall be substituted from (4.3) and (4.4).

4.1.1 Tangential Redistribution

To simplify previous calculations, we ignored the tangential velocity in (4.1) by setting $v_T := \langle\partial_t\gamma, T\rangle = 0$. Apart from advection of the θ-frame along the curve, this choice does not affect the geometry of the moving curve. Non-trivial tangential velocity can, however, be useful for improving numerical stability and for existence analysis. We wish to do the latter in the following section. Hence we introduce and analyse appropriate tangential term here. Specifically, we use the tangential velocity term developed and used in [HLS94; Kim97; MŠ01] and modify it for our motion law in the following lemma.

Lemma 4.1.3. *Assume that for all $t \in [0, \underline{t})$ and all $s \in \mathbb{R}/L(\Gamma_t)\mathbb{Z}$ the tangential velocity v_T satisfies the following integro-differential equation*

$$v_T(s,t) = v_{T,0}(t) + \int_0^s \kappa\psi_1 \,\mathrm{d}\bar{s} - \frac{s}{L(\Gamma_t)} \int_{\Gamma_t} \kappa\psi_1 \,\mathrm{d}\bar{s}, \tag{4.5}$$

where $v_{T,0}(t) = v_T(0,t)$ is any differentiable function $v_{T,0} \in \mathcal{C}^1([0,\underline{t}))$. Then the quantity $L(\Gamma_t)^{-1}g$ is constant during the framed curvature flow (4.1).

Proof. With $\partial_t\gamma = \kappa\nu_\theta + v_T T$, the arc-length commutator from Lemma 4.1.1 is

$$[\partial_t, \partial_s] = (\kappa\psi_1 - \partial_s v_T)\partial_s$$

and we have $\partial_t g = (-\kappa\psi_1 + \partial_s v_T)g$. Note that the choice of v_T does not affect the time derivative of length $L(\Gamma_t)$, provided the curves Γ_t are closed. And thus

$$\partial_t \left(\frac{g}{L(\Gamma_t)} \right) = \frac{g}{L(\Gamma_t)^2} \left[(-\kappa\psi_1 + \partial_s v_T) L(\Gamma_t) + \int_{\Gamma_t} \kappa\psi_1 \,\mathrm{d}s \right].$$

Substitution of $\partial_s v_T$ from (4.5) yields the vanishing right-hand side. □

With a suitable choice of parametrization and the tangential velocity satisfying (4.5) we can achieve uniform parametrization throught the flow.

Proposition 4.1.4. *Assume that the initial curve Γ_0 is uniformly parametrized such that $g(0,u) = L(\Gamma_0)$ for all $u \in S^1$. Let $\{(\Gamma_t, \theta_t)\}_{t\in[0,\underline{t})}$ be a solution to the framed curvature flow with tangential velocity* (4.5). *Then the curve Γ_t is parametrized uniformly during the whole flow, i.e. $g(u,t) = L(\Gamma_t)$ for all $t \in [0,\underline{t})$ and $u \in S^1$.*

Proof. Straightforward application of Lemma 4.1.3. □

Note that v_T in (4.5) is indeed well defined on the periodic domain as one can easy verify that $v_T|_{s=0} \equiv v_T|_{s=L(\Gamma_t)}$ and $\partial_s v_T|_{s=0} \equiv \partial_s v_T|_{s=L(\Gamma_t)}$.

4.1.2 Local Existence

This section establishes local existence and uniqueness for the framed curvature flow constrained by assumptions outlined in Lemma 4.1.5 or Lemma 4.1.6. First, it is important to note that the right-hand side of (4.1) is well-defined even in the absence of the Frenet frame (see Remark 4.0.4).

The existence result is achieved by extending the method of abstract theory of analytic semiflows in Banach spaces from [DG79; Ang90b; Ang90a; Lun84]. In particular we formulate (4.1) in terms of an extended four-dimensional system by treating θ as another dimension, and follow the existence proof of a similar system of equations from [BKŠ22]. First, let $\hat{\gamma}\colon [0,\underline{t}) \times S^1 \to \mathbb{R}^4$ denote the extended parametrization $\hat{\gamma} := [\gamma_1, \gamma_2, \gamma_3, \theta]^T$. And consider the extended system of equations

$$\partial_t\hat{\gamma} = \hat{A}\partial_s^2\hat{\gamma} + f(\partial_s\hat{\gamma}, \hat{\gamma}), \tag{4.6}$$

where $f \in \mathcal{C}(\mathbb{R}^{4,4}; \mathbb{R}^4)$ and the principal part of the right-hand side reads

$$\hat{\mathcal{A}} = \left[\begin{array}{c|c} \mathcal{A} & 0 \\ \hline \beta^T & \alpha \end{array}\right], \quad \mathcal{A} = \cos\theta\, \mathbb{I} + \sin\theta\, [T]_\times = \begin{bmatrix} \cos\theta & -\sin\theta\, T_3 & \sin\theta\, T_2 \\ \sin\theta\, T_3 & \cos\theta & -\sin\theta\, T_1 \\ -\sin\theta\, T_2 & \sin\theta\, T_1 & \cos\theta \end{bmatrix},$$

where $\mathbb{I}_{ij} = \delta_{ij}$, $([T]_\times)_{ij} = \sum_k \varepsilon_{ijk} T_k$ for $i, j \in \{1, 2, 3\}$, and $\alpha \in \mathbb{R}^+$, $\beta \in \mathbb{R}^3$ are fixed parameters of the framed curvature flow (4.1) with the following θ-velocity

$$v_\theta = \alpha \partial_s^2 \theta + \kappa \langle \beta, N \rangle + f_4(\partial_s \hat{\gamma}, \hat{\gamma}). \tag{4.7}$$

We want the system (4.6) to be parabolic. As the spectrum of $\hat{\mathcal{A}}$ is

$$\sigma(\hat{\mathcal{A}}) = \sigma(\mathcal{A}) \cup \{\alpha\} = \{\alpha, \cos\theta, e^{\pm i\theta}\},$$

the eigenvalues α and $\cos\theta$ must be positive. In order to proceed towards the local existence result, additional constraints have to be laid down to ensure that this property is guaranteed. In the following lemmas, we provide two different ways to achieve this goal.

Lemma 4.1.5. *Let $\beta = 0$ and $\alpha > 0$ be fixed parameters of the extended system of equations (4.6) with $f_4 \equiv 0$ and assume that θ_0 satisfies $|\theta(0, u)| < \frac{\pi}{2}$ for all $u \in S^1$. Then any solution $\{(\Gamma_t, \theta_t)\}_{t \in [0, \underline{t}]}$ to (4.1) will satisfy $|\theta| < \frac{\pi}{2}$ everywhere and the extended system (4.6) will remain parabolic.*

Proof. The statement is a consequence of the weak maximum principle for the angle functional θ. Using the notation from Chapter 7.1.4 of [Eva10], we have

$$\partial_t \theta + \mathcal{L}\theta = 0, \tag{4.8}$$

where $\mathcal{L} := -\alpha \partial_s^2 = -\alpha g^{-2} \partial_u^2 + \alpha g^{-3} \partial_u g \partial_u$. Thanks to the trivial right-hand side of (4.8), we can use Theorem 8 from Chapter 7 of [Eva10] and conclude that

$$|\theta(u, t)| \leqslant \max_{\overline{u} \in S^1} |\theta(0, \overline{u})| < \frac{\pi}{2}$$

for all $(u, t) \in S^1 \times [0, \underline{t}]$. The last inequality holds due to the assumptions. □

Introducing additional assumptions on the curvature allows us to extend the result from Lemma 4.1.5 for the case of non-trivial β and f_4 from (4.7).

Lemma 4.1.6. *Assume that $|\theta_0| < \frac{\pi}{2}$ on S^1 and there exist $C_1, C_2 > 0$ such that for all $u \in S^1$ and all $t \in [0, \underline{t}]$ we have $\kappa(u, t) \leqslant C_1$ and $f_4(u, t) \leqslant C_2$, where*

$$\underline{t} := \frac{1}{C_1 |\beta| + C_2} \left(\frac{\pi}{2} - \max_{u \in S^1} |\theta_0(u)| \right).$$

Then $|\theta| < \frac{\pi}{2}$ holds everywhere on $S^1 \times [0, \underline{t}]$ and (4.6) remains parabolic.

Proof. The non-difusive term $v_\theta - \alpha\partial_s^2\theta$ of the equation (4.7) is bounded as

$$|v_\theta - \alpha\partial_s^2\theta| \leqslant C_3,$$

where $C_3 := C_1|\beta| + C_2$ is a positive constant. Using this value we construct

$$\theta_- := \min_{u\in S^1} |\theta_0(u)| - C_3, \qquad \theta_+ := \max_{u\in S^1} |\theta_0(u)| + C_3,$$

which are subsolution and supersolution to θ (see Lemma 4.1.5). Since $|\theta_\pm|$ stays bellow $\frac{\pi}{2}$ at all times $t \in [0, \underline{t}]$, we concur that $|\theta|$ is bounded by $\frac{\pi}{2}$ as well. □

To prepare for the existence proof, further notation needs to be introduced. For any $\varepsilon \in (0, 1)$ and any $k \in \{0, \frac{1}{2}, 1\}$ we define the following family of Banach spaces of Hölder continuous functions

$$\mathcal{E}_k := h^{2k+\varepsilon}(S^1) \times h^{2k+\varepsilon}(S^1) \times h^{2k+\varepsilon}(S^1) \times h^{2k+\varepsilon}(S^1),$$

where $h^{2k+\varepsilon}(S^1)$ is a little Hölder space (see Section 4.1 in [BKŠ22]). With the aid of the previous lemmas and the appropriate tangential velocity term described in Section 4.1.1, we can now state the local existence result.

Proposition 4.1.7. *Consider* (4.1) *with additional tangential velocity satisfying* (4.5) *from in section 4.1.1 and assume that*

(a) the initial extended parametrization $\hat{\gamma}|_{t=0}$ belongs to $\mathcal{E}_1$,

(b) the initial parametrization γ_0 satisfies $\|\partial_u\gamma_0\| = L(\Gamma_0)$ on S^1,

(c) f is $\mathcal{C}^2$ smooth and globally Lipschitz continuous,

(d) the assumptions of Lemma 4.1.5 or Lemma 4.1.6 are satisfied.

Then there exists $\underline{t} > 0$ and a unique family of framed curves $\{(\Gamma_t, \theta_t)\}_{t\in[0,\underline{t})}$ satisfying (4.6) *with tangential velocity* (4.5) *such that $\hat{\gamma} \in \mathcal{C}([0, \underline{t}); \mathcal{E}_1) \cap \mathcal{C}^1([0, \underline{t}); \mathcal{E}_0)$.*

Proof. We extend the proof of Theorem 4.1 from [BKŠ22] to the parametrization with the framing angle $\hat{\gamma}$. We rewrite the extended system (4.6) as an abstract parabolic equation:

$$\partial_t\hat{\gamma} + \mathscr{F}(\hat{\gamma}) = 0 \tag{4.9}$$

for $\hat{\gamma} \in \mathcal{E}_1$, where $\mathscr{F}$ is operator mapping from $\mathcal{E}_1$ to $\mathcal{E}_0$. Using Lemma 2.5 from [Ang90b] as in the proof of Proposition 4 from [BKŠ22], the Frechet derivative $\mathscr{F}'$ of the operator $\mathscr{F}$ from (4.9) belongs to the maximum regularity class $\mathcal{M}(\mathcal{E}_1, \mathcal{E}_0)$. The solution $\hat{\gamma}$ exists in

$$\mathcal{C}([0, \overline{t}]; \mathcal{E}_1) \cap \mathcal{C}^1([0, \overline{t}]; \mathcal{E}_0)$$

for any $\overline{t} \in (0, \underline{t})$ due to Theorem 2.7 from [Ang90b]. □

For more details, we refer the reader to [BKŠ22] or to the original literature [DG79; Ang90b; Ang90a; Lun84] of the abstract theory of analytic semi-flows in Banach spaces.

Proposition 4.1.8. *Let the assumptions of Proposition 4.1.7 hold and suppose that the maximal time of existence $\underline{t}$ is finite, then*

$$\limsup_{t\to\underline{t}} \max_{u\in S^1} \kappa(u,t) = +\infty \quad \vee \quad \limsup_{t\to\underline{t}} \max_{u\in S^1} |\partial_s^2\theta(u,t)| = +\infty.$$

Proof. For contradiction, assume that the maximal time of the existence $\underline{t}$ is finite and that both κ and $|\partial_s^2\theta|$ are bounded. Since the assumptions of Proposition 4.1.7 are satisfied, the solution $\hat{\gamma}$ belongs to $\mathcal{C}([0,\bar{t}];\mathcal{E}_1)\cap\mathcal{C}^1([0,\bar{t}];\mathcal{E}_0)$ for any $\bar{t}\in(0,\underline{t})$. Moreover, the term $\partial_s^2\hat{\gamma}$ is bounded by the assumptions because

$$\|\partial_s^2\hat{\gamma}\|^2 = \|\partial_s^2\gamma\|^2 + |\partial_s^2\theta|^2 = \kappa^2 + |\partial_s^2\theta|^2.$$

Thus, by the maximum regularity, the extended solution $\hat{\gamma}$ belongs to the space $\mathcal{C}([0,\underline{t}];\mathcal{E}_1)\cap\mathcal{C}^1([0,\underline{t}];\mathcal{E}_0)$ and can be continued beyond $[0,\underline{t})$, which contradicts the maximal time assumption. More details can be retrieved from the last part of Theorem 4.1 from [BKŠ22]. □

The behaviour of Γ_t during the curvature blow-up event described in Proposition 4.1.8 is detailed in the next section.

4.1.3 Formation of Singularities

The expressive power of the framed curvature flow framework enables unusual singularity types to occur during the curvature blow-up events. The study of singularities has played an important role in the understanding of behaviour of different geometric flows and will also prove significant in the later parts of this work.

Singularities of geometric flows have been studied in e.g. [Kha15; Cor16; Lit23; Ando2; IY03] or [AG92], where the motion of planar curve has been extended beyond curvature singularities via a higher dimensional flow of an associated space curve. The existence of flows past various singularities has also been addressed by other means such as by using the concept of viscosity solutions for the level-set formulation of curvature-driven flows in [OS88; GP], topological surgeries [Per03b] or by analysis of self-similar shrinkers in [Veg15].

In [Alt91], Altschuler showed that the blow-up limits of space curves under the curve shortening flow are planar. The situation for framed curvature flow is more complicated. The following definition clarifies the meaning of different types of singularities which may occur during the evolution driven by (4.1).

Definition 4.1.9 (Singularity typologies)**.** *The event at which the curvature κ approaches infinity at time $\underline{t}$ and $L(\Gamma_t)\to 0$ as t approaches $\underline{t}$ (the curve Γ_t shrinks to a point) during the framed curvature flow* (4.1) *is called:*

1. Flat singularity *if and only if* $\theta_t \rightrightarrows 0$ *as t approaches $\underline{t}$.*
   (θ-frame uniformly approaches the Frenet frame).
2. Cone singularity *if and only if* $\theta_t \rightrightarrows \Theta\in(-\frac{\pi}{2},\frac{\pi}{2})\backslash\{0\}$ *as t approaches $\underline{t}$.*
3. Pinch singularity *if and only if* $\theta_t \rightrightarrows \Theta\in\{\pm\frac{\pi}{2}\}$ *as t approaches $\underline{t}$.*

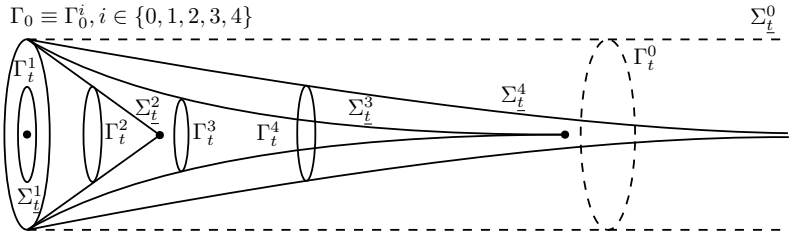

Figure 4.3: Depiction of singularity typologies from Definition 4.1.9 for circular initial condition Γ_0 and uniform theta angle. Upper indices 1 to 4 denote the flat, cone, pinch and infinite pinch scenario, respectively. The dashed line represents the trajectory of the vortex filament equation for reference.

Furthermore, when the trajectory surface $\Sigma_{\underline{t}}$ is unbounded, the case 3. is called infinite pinch singularity.

The flat singularity occurs in the classical example of curve shortening flow. For the case of simple planar curves, this singularity is guarantied by the Grayson-Gage-Hamilton theorem [GH86; Gra87]. Embedded space curves under the curve shortening flow do not necessarily shrink to a point, however the Grayson-Gage-Hamilton theorem can be extended in the case of simple spherical curves [MB20]. Other singularity types from Definition 4.1.9 are illustrated in the next set of analytical examples with simple evolution of circle.

Example 4.1.10 (Cone singularity)**.** *Let Γ_0 be a circle with radius $\rho_0 > 0$ and consider $v_\theta \equiv 0$ with $\theta_0 \equiv \phi \in (0, \frac{\pi}{2})$. This setup leads to the famous solution for shrinking circle with radius $\rho(t) = (\rho_0^2 - 2t\cos\phi)^{\frac{1}{2}}$ which vanishes at the terminal time $\underline{t} = (2\cos\phi)^{-1}\rho_0^2$. However, due to the non-trivial binormal velocity term $\langle \partial_t \gamma, B\rangle = \kappa \sin\phi \neq 0$, the singularity occurs at a point shifted in the binormal direction from the center of the initial circle by a distance*

$$\underline{z} = \left(\rho_0 - \left(\rho_0^2 - 2\underline{t}\cos\phi\right)^{\frac{1}{2}}\right)\tan\phi = \rho_0 \tan\phi.$$

This leads to a conical trajectory surface with a cone singularity.

Example 4.1.11 (Pinch singularity)**.** *Again, consider a circle Γ_0 with radius $\rho_0 > 0$ and $\theta_0 \equiv \phi \in (0, \frac{\pi}{2})$. To illustrate the pinch singularity, let*

$$\partial_t \theta = \frac{\tan\theta - 2\kappa\sqrt{\underline{t} - t}}{2(\underline{t} - t)},$$

where $\underline{t} = (\sin\phi)^{-2}\rho_0$. This θ-velocity is constructed in such a way that $\rho = \sin\theta\sqrt{\underline{t} - t}$ and $\partial_t z = \kappa \sin\theta = \sqrt{\underline{t} - t}$. Even tough the time derivative of the shift distance z diverges as t approaches $\underline{t}$, its definite integral is finite:

$$\lim_{t\to\underline{t}} z(t) = \lim_{t\to\underline{t}} \int_0^t \frac{1}{\sqrt{\underline{t} - \bar{t}}}\,\mathrm{d}\bar{t} = \lim_{t\to\underline{t}} \left[-2\sqrt{\underline{t} - \bar{t}}\right]_{\bar{t}=0}^{\bar{t}=t} = 2\sqrt{\underline{t}}.$$

The pitch singularity thus develops at a point located at a $2\sqrt{\underline{t}}$ distance form the center of the original circle.

Example 4.1.12 (Infinite pinch singularity)**.** *With the same setup of initial conditions as in the previous examples, we now consider* $\partial_t \theta = 2\rho_0^{-2}$*. This velocity leads to* $\theta(t) = 2t\rho_0^{-2}$ *and* $\rho(t) = \rho_0(1 - \sin(2\rho_0^{-1}t))^{\frac{1}{2}}$*. Thus the circle shrinks to a point at the time* $\underline{t} = \frac{1}{4}\pi\rho_0^2$ *and*

$$\partial_t z = \rho^{-1}\sin(2\rho_0^{-1}t)) = \rho_0^{-1}(1 - \sin(2\rho_0^{-1}t)))^{-\frac{1}{2}}\sin(2\rho_0^{-1}t)). \tag{4.10}$$

Unlike in the Example 4.1.11, the integral of (4.10) *diverges and thus the infinite pinch singularity is formed.*

All singularity typologies from Examples 4.1.10, 4.1.11 and 4.1.12 are depicted in Figure 4.3.

Remark 4.1.13. *Let us recall the definition of type-I and type-II singularity, studied in e.g. [Kha15; Cor16; Lit23]. This classification of curvature blow-up events is based on the comparison of the curvature growth near* $\underline{t}$ *with the function* $(\underline{t} - t)^{\frac{1}{2}}$*. Formally, a blow-up singularity is classified as type-I if*

$$\lim_{t\to\underline{t}} M_t(\underline{t} - t) := \lim_{t\to\underline{t}}[\max_{u\in S^1}\kappa^2(u,t)](\underline{t} - t) \tag{4.11}$$

is bounded, and as type-II otherwise. In terms of this classical notation, the singularities from Example 4.1.10 and 4.1.11 are type-I:

- *In Example 4.1.10, we have* $M_t = \rho^{-2}(t) = (\rho_0^2 - 2t\cos\phi)^{-1} = 2\cos\phi(\underline{t} - t)^{-1}$*, where the terminal time is* $\underline{t} = (2\cos\phi)^{-1}\rho_0^2$*. Thus*

$$\lim_{t\to\underline{t}} M_t(\underline{t} - t) = 2\cos\phi < +\infty.$$

- *Similarly in Example 4.1.11, the radius reads* $\rho = (\underline{t} - t)^{\frac{1}{2}}\sin\theta$ *and therefore*

$$\lim_{t\to\underline{t}} M_t(\underline{t} - t) = \lim_{t\to\underline{t}}\max_{u\in S^1}(\sin\theta_t(u))^{-2} = 1 < +\infty.$$

Whereas the infinite pinch singularity from Example 4.1.12 is type-II:

- *Since in Example 4.1.12, the radius is* $\rho(t) = \rho_0(1 - \sin(2\rho_0^{-1}t))^{-\frac{1}{2}}$*, the term* M_t *behaves as* $(\underline{t} - t)^2$ *near* $\underline{t}$ *and the limit* (4.11) *diverges.*

Further analysis of these connections is left for a future work.

The study of singularity formation is an extensive field of research, and this section offers only a brief exploration of potential blow-up scenarios within the context of the recently introduced framed curvature flow. Future work can involve for instance the analysis of singularity profiles leading to the self-shrinking Abresch–Langer curves [AL86].

4.2 Global Analysis

This section studies the global aspects of the solutions to the framed curvature flow, focusing on properties of global geometric quantities and their long term behaviour. First, several global estimates for the length and the generated surface area are provided in section 4.2.0, the evolution of the largest projected algebraic area is studied in section 4.2.1 and selected useful facts related to the topology of the θ-framing are provided in section 4.2.2.

4.2.0 Global Estimates

We aim to derive useful estimates for global geometric quantities such as the length and the generated area. To this end, we first prepare evolution equations for these quantities, then state assumptions upon which we base the bounds in the later parts of this section.

Lemma 4.2.1. *The evolution of the length $L(\Gamma_t)$ of the curve Γ_t and the total area $A(\Sigma_t)$ of the trajectory surface Σ_t during (4.1) is*

$$\frac{\mathrm{d}}{\mathrm{d}t}L(\Gamma_t) = -\int_{\Gamma_t} \kappa\psi_1 \,\mathrm{d}s, \qquad \frac{\mathrm{d}}{\mathrm{d}t}A\left(\Sigma_t\right) = \int_{\Gamma_t} \kappa \,\mathrm{d}s. \tag{4.12}$$

Proof. The first part of (4.12) is obtained from (4.2), the second one follows from

$$\frac{\mathrm{d}}{\mathrm{d}t}\int_{\Sigma_t} \mathrm{d}A = \frac{\mathrm{d}}{\mathrm{d}t}\int_0^t \int_{\Gamma_{\bar{t}}} \kappa \,\mathrm{d}s \,\mathrm{d}\bar{t},$$

where $\mathrm{d}A$ is obtained from $\mathscr{E} = g^2$, $\mathscr{F} = 0$ and $\mathscr{G} = v_N^2 + \gamma^2 = \kappa^2$ as

$$\mathrm{d}A = \sqrt{\mathscr{E}\mathscr{G} - \mathscr{F}^2}\,\mathrm{d}u \wedge \mathrm{d}t = g\kappa \,\mathrm{d}u \wedge \mathrm{d}t.$$

Particular details of the computations are in the proof of Lemma 4.0.7. □

Without any assumptions on the initial curve, we can bound the generated area from below by a linear function of time.

Corollary 4.2.2. *The Fenchel Theorem implies $A\left(\Sigma_t\right) \geqslant 2\pi t$ for all $t \in [0, \underline{t})$. Furthermore, when the curve is knotted on $[0, \underline{t})$, we get $A\left(\Sigma_t\right) \geqslant 4\pi t$ by the Milnor-Fáry Theorem [Fár49].*

Lemma 4.2.3. *The evolution of the total torsion τ and the total generalized torsion ψ_3 of Γ_t during the framed curvature flow (4.1) is*

$$\frac{\mathrm{d}}{\mathrm{d}t}\int_{\Gamma_t} \tau \,\mathrm{d}s = \frac{\mathrm{d}}{\mathrm{d}t}\int_{\Gamma_t} \psi_3 \,\mathrm{d}s = \int_{\Gamma_t} \psi_1\psi_3\kappa + \psi_2\partial_s\kappa \,\mathrm{d}s. \tag{4.13}$$

Proof. Since Γ_t is closed, both integrals are equal, i.e.

$$\int_{\Gamma_t} \psi_3 \,\mathrm{d}s = \int_{\Gamma_t} \tau \,\mathrm{d}s + \int_{\Gamma_t} \partial_s\theta \,\mathrm{d}s = \int_{\Gamma_t} \tau \,\mathrm{d}s.$$

The right-hand side of (4.13) is obtained from (4.2) and (4.4). □

The estimates below are based a subset of the following *assumptions*:

I. There exists a fixed $\varepsilon > 0$ such that $|\theta| \leqslant \frac{\pi}{2} - \varepsilon$. In this case we define a constant $K_{\mathrm{I.}} := \cos\left(\frac{\pi}{2} - \varepsilon\right) > 0$ which will bound $\cos\theta$ from below.

II. The curvature κ is uniformly bounded from bellow by a constant $K_{\mathrm{II.}} > 0$, i.e. $\kappa(u,t) \geqslant K_{\mathrm{II.}}$ for all $t \in [0, \underline{t})$ and $u \in S^1$.

Note that assumption *I.* is also needed for the existence proof in section 4.1.2 and follows from the assumptions given in Lemma 4.1.5, or alternatively Lemma 4.1.6. Assumption *II.*, on the other hand, can only be enforced up to a time t away from the singularity $\underline{t}$, where the curvature blows up.

Proposition 4.2.4. *Let Γ_t be a solution to* (4.1)*. If assumption* I. *holds, then*

$$L(\Gamma_t) \leqslant \left(L^2(\Gamma_0) - 8\pi^2 K_{\mathrm{I.}} t\right)^{\frac{1}{2}} \tag{4.14}$$

and thus the terminal time can be bounded from above as

$$\underline{t} \leqslant \left(8\pi^2 K_{\mathrm{I.}}\right)^{-1} L^2(\Gamma_0). \tag{4.15}$$

Moreover, assuming the curve is knotted on $[0, \underline{t})$, the $8\pi^2$ term in both (4.14) *and* (4.15) *estimates can be replaced by $32\pi^2$ as in Corollary 4.2.2.*

Proof. From assumption *I.* and the first part of Lemma 4.2.1 we have

$$\frac{\mathrm{d}}{\mathrm{d}t} L(\Gamma_t) = -\int_{\Gamma_t} \kappa^2 \cos\theta \ \mathrm{d}s \leqslant -K_{\mathrm{I.}} \int_{\Gamma_t} \kappa^2 \, \mathrm{d}s.$$

Using the Fenchel Theorem and Cauchy-Schwarz inequality, we obtain

$$\frac{\mathrm{d}}{\mathrm{d}t} L(\Gamma_t) \leqslant -\frac{K_{\mathrm{I.}}}{L(\Gamma_t)} \left(\int_{\Gamma_t} \kappa \, \mathrm{d}s\right)^2 \leqslant -\frac{4\pi^2 K_{\mathrm{I.}}}{L(\Gamma_t)}.$$

The result follows from the ODE comparison theorem. □

Proposition 4.2.5. *Let Γ_t be a solution to* (4.1) *and let Σ_t denote its associated trajectory surface. If assumptions* I. *and* II. *are satisfied, then we get*

$$A(\Sigma_t) \leqslant \frac{K_{\mathrm{II.}}}{12\pi^2 K_{\mathrm{I.}}} \left(L^3(\Gamma_0) - \left(L^2(\Gamma_0) - 8\pi^2 K_{\mathrm{I.}} t\right)^{\frac{3}{2}}\right).$$

Furthermore, as $\underline{t}$ is bounded by (4.15)*, we get a global bound*

$$A(\Sigma_{\underline{t}}) \leqslant \frac{K_{\mathrm{II.}} L^3(\Gamma_0)}{12\pi^2 K_{\mathrm{I.}}}.$$

Proof. Assuming *I.* and *II.* and using Lemma 4.2.1 and Proposition 4.2.4 yields

$$\frac{\mathrm{d}}{\mathrm{d}t} A(\Sigma_t) \leqslant K_{\mathrm{II.}} L(\Gamma_t) \leqslant K_{\mathrm{II.}} \left(L^2(\Gamma_0) - 8\pi^2 K_{\mathrm{I.}} t\right)^{\frac{1}{2}}.$$

Integrating the inequality yields the result. □

4.2.1 Projected Area

In this section, we consider the following quantity

$$A_p(\Gamma_t) := \frac{1}{2}\int_{\Gamma_t} \gamma \times \partial_s \gamma \,\mathrm{d}s = \frac{1}{2}\int_{S^1} \gamma \times \partial_u \gamma \,\mathrm{d}u \tag{4.16}$$

and use it to extend our area estimates for $\Sigma_{\underline{t}}$. The geometric interpretation of this quantity is revealed in following lemma.

Lemma 4.2.6. *For a given curve Γ_t, the quantity $A_p(\Gamma_t)$ defined in* (4.16) *is the largest algebraic area enclosed by any orthogonal projection of Γ_t.*

Proof. For any unit normal vector $\nu \in S^2$, let $\pi(\nu)$ be the projection operator onto $\{\nu\}^\perp$, i.e. $\pi(\nu) = \mathbb{I} - \nu \cdot \nu^T$, and let $\pi(\nu)\Gamma_t$ denote the projected planar curve paramerized by $\pi(\nu)\gamma$. Then

$$\begin{aligned} A(\pi(\nu)\Gamma_t) &:= \left\| \int_{S^1} \pi(\nu)\gamma \times \partial_u(\pi(\nu)\gamma)\,\mathrm{d}u \right\| \\ &= \left\| A_p(\Gamma_t) - \int_{S^1} \langle \gamma, \nu\rangle \nu \times \partial_u \gamma \,\mathrm{d}u - \int_{S^1} \langle \partial_u \gamma, \nu\rangle \gamma \times \nu \,\mathrm{d}u \right\| \\ &= \left\| A_p(\Gamma_t) + \nu \times \int_{S^1} \langle \partial_u \gamma, \nu\rangle \gamma - \langle \gamma, \nu\rangle \partial_u \gamma \,\mathrm{d}u \right\|, \end{aligned}$$

where $A(\Gamma)$ denotes the algebraic area enclosed by a planar curve Γ. Double application of the triple vector product formula yields

$$\begin{aligned} A(\pi(\nu)\Gamma_t) &= \|A_p(\Gamma_t) + \nu \times (\nu \times A_p(\Gamma_t))\| \\ &= \|A_p(\Gamma_t) + \langle A_p(\Gamma_t), \nu\rangle \nu - \|\nu\|^2 A_p(\Gamma_t)\| \\ &= \|\langle A_p(\Gamma_t), \nu\rangle \nu\| = |\langle A_p(\Gamma_t), \nu\rangle|\,. \end{aligned}$$

Thus, due to the Cauchy-Schwarz inequality, we have:

1. $A(\pi(\nu)\Gamma_t) \leqslant A_p(\Gamma_t)$ for all ν in S^2,
2. $A(\pi(A_p(\Gamma_t)^{-1}A_p(\Gamma_t))\Gamma_t) = A_p(\Gamma_t)$ when $A_p(\Gamma_t) > 0$.

The conjunction of 1. and 2. proves the statement. □

Lemma 4.2.7. *The time derivative of $A_p(\Gamma_t)$ during* (4.1) *is*

$$\frac{\mathrm{d}}{\mathrm{d}t} A_p(\Gamma_t) = -\int_{\Gamma_t} \kappa\beta_\theta \,\mathrm{d}s. \tag{4.17}$$

Proof. The derivation of this integral quantity is simplified using the fact that

$$\int_{\Gamma_t} \gamma \times \partial_s \gamma \,\mathrm{d}s = \int_{S^1} \gamma \times \partial_u \gamma \,\mathrm{d}u,$$

where $\mathrm{d}s = g\,\mathrm{d}u$ and, formally, $\partial_u = g\partial_s$. Thus we have

$$\frac{\mathrm{d}}{\mathrm{d}t}A_p(\Gamma_t) = \frac{1}{2}\int_{S^1} \partial_t\gamma \times \partial_u\gamma + \gamma \times \partial_u\partial_t\gamma\,\mathrm{d}u = \frac{1}{2}\int_{\Gamma_t} \kappa\nu_\theta \times T + \gamma \times \partial_s(\kappa\nu_\theta)\,\mathrm{d}s,$$

where $\nu_\theta \times T = -\beta_\theta$ and both parts of the integral yield the same value as

$$\int_{\Gamma_t} \gamma \times \partial_s(\kappa\nu_\theta)\,\mathrm{d}s = \int_{\Gamma_t} \partial_s(\gamma \times \kappa\nu_\theta) - T \times \kappa\nu_\theta\,\mathrm{d}s = -\int_{\Gamma_t} \kappa\beta_\theta\,\mathrm{d}s.$$

Adding these integrals leads to (4.17). □

Proposition 4.2.8. *Let $\{(\Gamma_t, \theta_t)\}_{t\in[0,\underline{t})}$ develop a flat singularity at time $\underline{t}$, then*

$$A(\Sigma_{\underline{t}}) \geqslant \max_{t\in[0,\underline{t})} \|A_p(\Gamma_t)\|.$$

Proof. Let $x \in \mathbb{R}^3$ be the point to which the curve Γ_t shrinks towards as the time t approaches $\underline{t}$. Since $\Sigma_{\underline{t}} \cup \{x\}$ spans the initial curve Γ_0, its area must be at least that of a minimal spanning surface, which has locally larger area than the projection. Formally, let $\mathrm{d}A'$ denote the area element of $\pi(\nu)\Gamma_t$, then

$$\mathscr{E}' = \|\partial_u\pi(\nu)\gamma\|^2 \leqslant \|\!|\pi(\nu)|\!\|^2\|\partial_u\gamma\|^2 = g^2,$$
$$\mathscr{G}' = \|\partial_t\pi(\nu)\gamma\|^2 \leqslant \|\!|\pi(\nu)|\!\|^2\|\partial_t\gamma\|^2 = \kappa^2.$$

With $\|\!|\cdot|\!\|$ being the spectral norm, $\|\!|\pi(\nu)|\!\| = \max(\sigma(\pi(\nu))) = 1$ and thus

$$\mathrm{d}A' = \sqrt{\mathscr{E}'\mathscr{G}' - \mathscr{F}'^2}\,\mathrm{d}u \wedge \mathrm{d}t \leqslant \sqrt{\mathscr{E}'\mathscr{G}'}\,\mathrm{d}u \wedge \mathrm{d}t \leqslant g\kappa\,\mathrm{d}u \wedge \mathrm{d}t = \mathrm{d}A.$$

Note that the algebraic area of the projection is even smaller as the overlapping parts can annihilate. □

Proposition 4.2.9. *Let Γ_t be a solution to* (4.1) *and assume* I. *and* II., *then*

$$\frac{\mathrm{d}}{\mathrm{d}t}\|A_p(\Gamma_t)\| \leqslant 2K_{\mathrm{I}.}K_{\mathrm{II}.}L(\Gamma_t).$$

Proof. Applying the assumptions and Cauchy-Schwarz inequality yields

$$\frac{\mathrm{d}}{\mathrm{d}t}\|A_p(\Gamma_t)\| = \left\langle \frac{A_p(\Gamma_t)}{\|A_p(\Gamma_t)\|}, \frac{\mathrm{d}}{\mathrm{d}t}A_p(\Gamma_t) \right\rangle \leqslant \left\| \frac{\mathrm{d}}{\mathrm{d}t}A_p(\Gamma_t) \right\| \leqslant 2K_{\mathrm{I}.}K_{\mathrm{II}.} \left\| \int_{\Gamma_t} \beta_\theta\,\mathrm{d}s \right\|.$$

The statement then follows from the fact that $\mathscr{R}_\theta$ is unitary. □

Since the area of any surface enclosed by the curve Γ_t is smaller than $\|A_p(\Gamma_t)\|$ (see proof of Proposition 4.2.8), the above proposition provides an upper bound on the growth of the minimal spanning surface area.

Remark 4.2.10. *Note that for $\theta \equiv \frac{\pi}{2}$, both the length $L(\Gamma_t)$ and the projected area $A_p(\Gamma_t)$ remain constant during* (4.1), *as shown in [AH65]. On the other hand, for $\theta \equiv 0$ the motion is an L^2-gradient flow for the length functional (see [Kim08]).*

4.2.2 Frame Topology

Let us consider the topology of the moving θ-frame and its possible ramifications on the long-term behaviour of the framed curvature flow. We do so by analysing the time evolution of two geometric quantities, named writhe and twist, which are closely connected to the topology of the moving frame. Writhe of an embedded curve is an averaged sum of all signed crossings over the space of all orthogonal projections, but can also be written using Gauss formula as

$$\mathrm{W_r}(\Gamma_t) = \frac{1}{4\pi} \iint\limits_{\Gamma_t \times \Gamma_t} \frac{\langle \gamma(s,t) - \gamma(s',t), T(s,t) \times T(s',t) \rangle}{\|\gamma(s,t) - \gamma(s',t)\|^3} \,\mathrm{d}s \wedge \mathrm{d}s'.$$

The second important geometric quantity describing the frame topology is the total twist of the θ-frame, which reads

$$\begin{aligned} \mathrm{T}^{\theta}_{\mathrm{w}}(\Gamma_t) &= \frac{1}{2\pi} \int_{\Gamma_t} \langle \nu_\theta \times \partial_s \nu_\theta, T \rangle \,\mathrm{d}s \\ &= \frac{1}{2\pi} \int_{\Gamma_t} -\psi_1 \langle \nu_\theta \times T, T \rangle + \psi_3 \langle \nu_\theta \times \beta_\theta, T \rangle \,\mathrm{d}s \\ &= \frac{1}{2\pi} \int_{\Gamma_t} \psi_3 \,\mathrm{d}s = \mathrm{T}^{F}_{\mathrm{w}}(\Gamma_t) + \frac{1}{2\pi} \deg(\theta_t), \end{aligned}$$

where $\deg(\theta_t)$ is the topological degree of $\theta_t \colon S^1 \to S^1$ and $\mathrm{T}^{F}_{\mathrm{w}}(\Gamma_t)$ is the normalized total twist (i.e. total twist assiciated with the Frenet frame):

$$\mathrm{T}^{F}_{\mathrm{w}}(\Gamma_t) = \frac{1}{2\pi} \int_{\Gamma_t} \tau \,\mathrm{d}s.$$

The writhe and twist are connected via the Călugăreanu–White–Fuller Theorem [Căl61; Whi69] which states that

$$\mathrm{S}^{\bullet}_{\mathrm{Lk}}(\Gamma_t) = \mathrm{W_r}(\Gamma_t) + \mathrm{T}^{\bullet}_{\mathrm{w}}(\Gamma_t), \tag{4.18}$$

where $\bullet$ represents either F or θ and $\mathrm{S}^{\theta}_{\mathrm{Lk}}(\Gamma_t)$, $\mathrm{S}^{F}_{\mathrm{Lk}}(\Gamma_t)$ are the self-linking numbers for the Frenet frame and the θ-frame, respectively. With the help of this theorem, we can describe the evolution of writhe for embedded curves.

Proposition 4.2.11. *Let $\{(\Gamma_t, \theta_t)\}_{t \in [0,\underline{t})}$ be a solution to (4.1). Consider $t \in [0, \underline{t})$ such that $\Gamma_t \hookrightarrow \mathbb{R}^3$ (i.e. Γ_t is embedded) and $\kappa(u,t) > 0$ for all $u \in S^1$. Then*

$$\frac{\mathrm{d}}{\mathrm{d}t} \mathrm{W_r}(\Gamma_t) = -\frac{1}{2\pi} \int_{\Gamma_t} \psi_1 \psi_3 \kappa + \psi_2 \partial_s \kappa \,\mathrm{d}s. \tag{4.19}$$

Proof. The assumptions imply that the time derivative of $\mathrm{S}^{F}_{\mathrm{Lk}}(\Gamma_t)$ exists and is equal to 0. Thus, we may differentiate (4.18) to obtain

$$\frac{\mathrm{d}}{\mathrm{d}t} \mathrm{W_r}(\Gamma_t) = \frac{\mathrm{d}}{\mathrm{d}t} \left[\mathrm{S}^{F}_{\mathrm{Lk}}(\Gamma_t) - \mathrm{T}^{F}_{\mathrm{w}}(\Gamma_t) \right] = -\frac{1}{2\pi} \frac{\mathrm{d}}{\mathrm{d}t} \int_{\Gamma_t} \tau \,\mathrm{d}s.$$

The formula (4.19) then follows from Lemma 4.2.3. □

Remark 4.2.12. *Note that since v_θ is continuous, the degree of θ cannot change during the flow and the difference $\mathrm{S}^\theta_{\mathrm{Lk}}(\Gamma_t) - \mathrm{S}^F_{\mathrm{Lk}}(\Gamma_t)$ is a constant integer.*

The following proposition provides a necessary topological condition needed to close the trajectory surface in the sense of ending the flow in a flat singularity described in section 4.1.3.

Proposition 4.2.13. *Assume that $\{(\Gamma_t, \theta_t)\}_{t\in[0,\underline{t})}$ develops a flat singularity and (Γ_0, θ_0) is not a Seifert framing. Then there must exist $t \in [0, \underline{t})$ such that either $\kappa(u, t) = 0$ at some point $u \in S^1$ or Γ_t is not embedded.*

Proof. The Seifert framing must have zero self-linking number, see [SCR21]. □

4.3 Generated Surfaces

By adjusting the definition of the θ-velocity, the framed curvature flow can be formulated such that its associated trajectory surface has various interesting properties. These specific formulations are explored in this section. We first consider trajectory surfaces of constant mean curvature in section 4.3.0 and then constant Gauss curvature in section 4.3.1. Other special surfaces, such as surfaces of a constant ratio of principle curvatures, proposed in [Liu+22], fall outside the scope of this manuscript and may be the subject of future work.

4.3.0 Constant Mean Curvature

In this section, we consider the use of framed curvature flow as a means of solving the Björling problem for minimal surfaces and its generalisation for non-minimal surfaces of constant mean curvature (see [BD10]).

Proposition 4.3.1. *For a fixed constant $H \in \mathbb{R}$, consider the framed curvature flow (4.1) with the θ-velocity given by*

$$v_\theta = \kappa H - (\kappa\partial_s\psi_3 + 2\partial_s\kappa\psi_3)\kappa^{-2}\psi_1 + (\kappa^3 + \kappa\psi_3^2 - \partial_s^2\kappa)\kappa^{-2}\psi_2. \tag{4.20}$$

The trajectory surface $\Sigma_{\underline{t}}$ generated by this flow has a constant mean curvature equal to the prescribed value H.

Proof. Substitution of (4.20) to Lemma 4.0.7. □

The following results are all related to the Flux theorem introduced in [Kus87; Kus91].

Proposition 4.3.2 (Flux Theorem)**.** *Let $\{(\Gamma_t, \theta_t)\}_{t\in[0,\underline{t})}$ be a solution to the framed curvature flow with θ-velocity defined in (4.20). Then for any $a \in \mathbb{R}^3$*

$$H\int_{\partial\Sigma_t}\langle\gamma\times T, a\rangle\,\mathrm{d}s + \int_{\partial\Sigma_t}\langle\nu_\theta, a\rangle\,\mathrm{d}s = 0, \tag{4.21}$$

where $\partial\Sigma_t = \Gamma_0 \cup \Gamma_t$ is the boundary of the associated trajectory surface Σ_t.

Proof. Multiple proofs can be found in e.g. [Lóp13], where the unit conormal vector from Theorem 5.1.1. is equivalent to the θ-normal ν_θ. □

Combining the Flux theorem with the evolution equations for the projected area A_p leads to a simple formula for the derivative of total θ-normal.

Corollary 4.3.3. *For any solution* $\{(\Gamma_t, \theta_t)\}_{t\in[0,\underline{t})}$ *to* (4.1) *with* v_θ *from* (4.20) *we have*

$$\frac{\mathrm{d}}{\mathrm{d}t}\int_{\Gamma_t} \nu_\theta \,\mathrm{d}s = 2H\int_{\Gamma_t} \kappa\beta_\theta \,\mathrm{d}s.$$

Proof. The boundary $\partial\Sigma_t$ consists of Γ_t and Γ_0, but the former is static. Differentiation of the Flux theorem (4.21) thus leads to

$$H\frac{\mathrm{d}}{\mathrm{d}t}\int_{\Gamma_t} \gamma \times T \,\mathrm{d}s + \frac{\mathrm{d}}{\mathrm{d}t}\int_{\Gamma_t} \nu_\theta \,\mathrm{d}s = 0. \tag{4.22}$$

The result is then obtained by rearranging (4.22) and using Lemma 4.2.7. □

The Flux theorem enables the following two necessary conditions for flat singularity formation during the flow that generates CMC surfaces.

Corollary 4.3.4. *When* $\{(\Gamma_t, \theta_t)\}_{t\in[0,\underline{t})}$ *develops a flat singularity at the terminal time* $\underline{t}$*, the surface* $\Sigma_{\underline{t}}$ *only has one non-trivial boundary* Γ_t*, and thus*

$$A_p(\Gamma_0) = -\frac{1}{H}\int_{\Gamma_0} \nu_\theta \,\mathrm{d}s$$

Corollary 4.3.5. *Assume that* $\{(\Gamma_t, \theta_t)\}_{t\in[0,\underline{t})}$ *solves the framed curvature flow with* v_θ *from* (4.20) *and develops a flat singularity. Then*

$$L(\Gamma_0) \geqslant 2H\|A_p(\Gamma_0)\|.$$

In particular, if Γ_0 *is simple planar curve enclosing area* A*, then*

$$L(\Gamma_0) \geqslant 2HA.$$

Proof. For any unit vector $a \in S^2$, we have $2H|\langle A_p(\Gamma_0), a\rangle| \leqslant L(\Gamma_0)$ from Corollary 5.1.7 of [Lóp13]. □

Important subclass of surfaces with constant mean curvature are the minimal surfaces [MP12; Pér16] characterised by $H = 0$. In nature, minimal surfaces emerge in the context of soap films [Gol+10; Gol+14], cell membranes [LL14], the crystallographic structure of zeolites [AHB85; And+88; Scr76] and as the apparent horizon of a black hole [HI01].

For the case of minimal surfaces, many of the previous results derived from the Flux theorem significantly simplify. Moreover, when the flow develops a flat singularity, the associated trajectory surface effectively represents a valid solution to the Plateau problem with a single boundary curve Γ_0.

Corollary 4.3.6 (Corollary 5.1.5 from [Lóp13]). *For minimal surfaces with $H = 0$, we have even stricter conditions, namely for all $a \in \mathbb{R}^3$*

$$\int_{\partial\Sigma_t} \langle \nu_\theta, a \rangle \, \mathrm{d}s = 0, \qquad \int_{\partial\Sigma_t} \langle \nu_\theta, \gamma \times a \rangle \, \mathrm{d}s = 0.$$

We end this section with an analysis of specific examples of solutions to (4.20) with simple initial configurations. First example illustrates the configuration that leads to the simplest minimal surface, which is a subset of the flat plane.

Example 4.3.7. *Let the initial curve Γ_0 be a closed convex planar curve and $\theta_0 \equiv 0$. Then the framed curvature flow with θ-velocity from* (4.20) *and $H = 0$ is equivalent to the curve shortening flow and generates a flat surface $\Sigma_{\underline{t}}$ equivalent to the convex hull of Γ_0 in a finite time $\underline{t}$ when the Γ_t shrinks down to a round point (see [GH86; Gra87]).*

More analytical examples can be obtained by considering configurations with helical and cylindrical symmetries.

Example 4.3.8 (Helical symmetry). *For a constant θ_0 consider evolving helix curve*

$$\gamma_0(u) := \begin{bmatrix} \varrho_0 \cos u \\ \varrho_0 \sin u \\ wu \end{bmatrix}, \qquad \gamma(u,t) := \begin{bmatrix} \varrho(t) \cos(u + \upsilon(t)) \\ \varrho(t) \sin(u + \upsilon(t)) \\ wu + \omega(t) \end{bmatrix},$$

where ρ_0 and w are positive constants and ρ, υ, ω are functions of time t. Since $\kappa = \varrho g^{-2}$ and $\tau = w g^{-2}$, the problem (4.20) *reduces to the following system*

$$\frac{\mathrm{d}}{\mathrm{d}t} \begin{bmatrix} \theta \\ \varrho \\ \omega \\ \upsilon \end{bmatrix} = \frac{1}{g^3} \begin{bmatrix} g \sin\theta + \rho g H \\ -g\rho \cos\theta \\ \rho^2 \sin\theta \\ -w \sin\theta \end{bmatrix}, \qquad \begin{bmatrix} \theta \\ \varrho \\ \omega \\ \upsilon \end{bmatrix}\Bigg|_{t=0} = \begin{bmatrix} \theta_0 \\ \varrho_0 \\ 0 \\ 0 \end{bmatrix}, \tag{4.23}$$

where $g^2 = \varrho^2 + w^2$. Similar helicoidal surfaces of constant mean curvature were studied in e.g. [HK20].

Considering cylindrically symmetrical configurations leads to the family of Delaneu surfaces, first classified in [Del41].

Example 4.3.9 (Cylindrical symmetry). *Setting $w = 0$ reduces the system* (4.23) *to*

$$\frac{\mathrm{d}}{\mathrm{d}t} \begin{bmatrix} \theta \\ \varrho \\ \omega \end{bmatrix} = \frac{1}{\varrho^2} \begin{bmatrix} \sin\theta + \varrho H \\ -\varrho \cos\theta \\ \varrho \sin\theta \end{bmatrix}, \qquad \begin{bmatrix} \theta \\ \varrho \\ \omega \end{bmatrix}\Bigg|_{t=0} = \begin{bmatrix} \theta_0 \\ \varrho_0 \\ 0 \end{bmatrix}.$$

Nodoid surface generated by the flow from Example 4.3.9 is depicted in Figure B.5.

4.3.1 Constant Gaussian Curvature

Unlike the mean curvature flow or the minimal surface generating flow [MB22a], the framed curvature flow can be used for generating developable surfaces or surfaces of any other prescribed Gaussian curvature.

Proposition 4.3.10. *For a fixed constant $K \in \mathbb{R}$, consider a framed curvature flow* (4.1) *with the θ-velocity given by*

$$v_\theta = -\kappa\psi_2^{-1}K - (\kappa\partial_s\psi_3 + 2\partial_s\kappa\psi_3)\kappa^{-2}\psi_1 \tag{4.24a}$$
$$-\kappa\psi_2^{-1}\psi_3^2 - (\partial_s^2\kappa - \kappa\psi_3^2)\kappa^{-2}\psi_2. \tag{4.24b}$$

The trajectory surface $\Sigma_{\underline{t}}$ generated by this flow has a constant Gaussian curvature equal to the prescribed value K.

Proof. Substitution of (4.24) to Lemma 4.0.7. □

Important examples of surfaces with constant Gaussian curvature are developable surfaces. For this specific case, the Gauss-Bonnet formula significantly simplifies and can be used to uncover an unexpected integral of motion.

Proposition 4.3.11. *Let $\{(\Gamma_t, \theta_t)\}_{t\in[0,\underline{t})}$ be a solution to the framed curvature flow with θ-velocity defined in* (4.24) *with K set to* 0*. Then the integral of ψ_1 over the curve Γ_t at any time $t \in [0, \underline{t})$ is preserved.*

Proof. The Gauss-Bonnet theorem states that

$$\int_{\Sigma_t} K \,\mathrm{d}A + \int_{\partial\Sigma_t} \kappa_g \,\mathrm{d}s = 2\pi\chi(\Sigma_t), \tag{4.25}$$

where $\mathrm{d}A = \kappa g \,\mathrm{d}u \wedge \mathrm{d}t$ (see proof of Proposition 4.2.8), κ_g is the geodesic curvature at the boundary $\partial\Sigma_t = \Gamma_0 \cup \Gamma_t$ and $\chi(\Sigma_t) = 0$ is the Euler characteristic of an annulus. Differentiation of (4.25) and subsequent substitution yields

$$\frac{\mathrm{d}}{\mathrm{d}t}\int_{\Gamma_t} \psi_1 \,\mathrm{d}s = -\int_{\Gamma_t} \kappa K \,\mathrm{d}s,$$

where ψ_1 is the geodesic curvature of Γ_t on Σ_t and the integrand on the right hand side is 0 by the assumption that $K = 0$. □

As in the previous section, we construct analytical examples using configurations with helical and cylindrical symmetries.

Example 4.3.12 (Helical symmetry)**.** *For a constant θ_0 consider evolving helix curve*

$$\gamma_0(u) := \begin{bmatrix} \varrho_0 \cos u \\ \varrho_0 \sin u \\ wu \end{bmatrix}, \qquad \gamma(u,t) := \begin{bmatrix} \varrho(t)\cos(u+\upsilon(t)) \\ \varrho(t)\sin(u+\upsilon(t)) \\ wu + \omega(t) \end{bmatrix},$$

where ρ_0 and w are positive constants and ρ, υ, ω are functions of time t. Since $\kappa = \varrho g^{-2}$ and $\tau = w g^{-2}$, the problem (4.24) *reduces to the following system*

$$\frac{\mathrm{d}}{\mathrm{d}t}\begin{bmatrix}\theta\\ \varrho\\ \omega\\ \upsilon\end{bmatrix} = \frac{1}{g^3}\begin{bmatrix}\frac{Kg^4+w^2\cos^2\theta}{g\sin\theta}\\ -g\rho\cos\theta\\ \rho^2\sin\theta\\ -w\sin\theta\end{bmatrix}, \qquad \begin{bmatrix}\theta\\ \varrho\\ \omega\\ \upsilon\end{bmatrix}\Bigg|_{t=0} = \begin{bmatrix}\theta_0\\ \varrho_0\\ 0\\ 0\end{bmatrix}, \tag{4.26}$$

where $g^2 = \varrho^2 + w^2$. This solution leads to a family of helical trajectory surfaces of constant Gaussian curvature.

Example 4.3.13 (Cylindrical symmetry)**.** *Setting $w = 0$ reduces the system* (4.26) *to*

$$\frac{\mathrm{d}}{\mathrm{d}t}\begin{bmatrix}\theta\\ \varrho\\ \omega\end{bmatrix} = \frac{1}{\varrho^2}\begin{bmatrix}(\sin\theta)^{-1}Kg^3\\ -\varrho\cos\theta\\ \varrho\sin\theta\end{bmatrix}, \qquad \begin{bmatrix}\theta\\ \varrho\\ \omega\end{bmatrix}\Bigg|_{t=0} = \begin{bmatrix}\theta_0\\ \varrho_0\\ 0\end{bmatrix}.$$

The examples above can be used to generate surfaces similar to the one depicted in Figure B.5.

4.4 Conclusion

In conclusion, the framed curvature flow is a promising generalisation of the classical curvature-driven geometric flows of space curves and its configuration space contains exciting motion laws with possible use cases in the analysis of surfaces with prescribed curvature.

However, more analysis is required, especially with respect to local existence for larger subspace of the possible settings of the θ-velocity. Other future work may entail the study of motion laws generating other types of surfaces such as the surfaces with constant principle curvature ratio [Liu+22] or surfaces minimising energies other than the surface area, such as the Willmore energy or various repulsive energies.

Another possible direction of future work is to generalize the concept of framed curvature flow to higher dimensional space with more than one codimension and look for possible connections between the generated trajectory varieties and the Open book decomposition.

Further intuition and knowledge can be obtained by means of a proper numerical analysis and experiments with different settings of the θ-velocity. Finally, the simple examples of different types of singularities involving curvature blow-up, that were presented in Subsection 4.1.3, ought to be extended and studied in much more detail.

5 Conclusions

This thesis explores the geometry and topology of curves evolving in three-dimensional Euclidean space. Geometric flows, notably in this lower-dimensional setting, are intrinsic to the understanding of manifold natural phenomena and engineering applications. While a significant part of this research field focused on higher-dimensional or intrinsic flows, this work aims to fill the gaps in our understanding of evolving space curves by extending the toolkit available for their study.

The thesis consolidates and presents key findings drawn from the following research articles:

[MKB19] J. Minarčík, M. Kimura, and M. Beneš. "Comparing motion of curves and hypersurfaces in $\mathbb{R}^m$". In: *Discrete and Continuous Dynamical Systems Series B* 24 (2019), pp. 4815–4826.

[MB20] J. Minarčík and M. Beneš. "Long-term behavior of curve shortening flow in $\mathbb{R}^3$". In: *SIAM Journal on Mathematical Analysis* 52 (2020), pp. 1221–1231.

[MB22a] J. Minarčík and M. Beneš. "Minimal surface generating flow for space curves of non vanishing torsion". In: *Discrete and Continuous Dynamical Systems - Series B* 27 (2022), pp. 6605–6617.

[MB22b] J. Minarčík and M. Beneš. "Nondegenerate Homotopy and Geometric Flows". In: *Homology, Homotopy and Applications* 24 (2022), pp. 255–264.

[MB23] J. Minarčík and M. Beneš. "Trajectory Surfaces of Framed Curvature Flow". *Preprint* 2023.

Main Results

The thesis presents several new notions and contains many individual results, detailed in the published articles listed above. All of them fall into the category of evolving space curves but the key contributions can be grouped into the following subthemes:

- **Analysis of higher codimension curve shortening flow:** We presented several new and non-trivial results related to the long-term behaviour of spherical and convex curves, including a generalized Avoidance principle and a new Comparison theorem for evolving space curves and hypersurfaces.
- **Trajectory surfaces:** We introduced and studied surfaces traced out by general geometric flows, which is useful for understanding the global properties of specific surface classes or curve flows. By introducing the Minimal surface generating flow we showed how specific surfaces can be created via simple local motion laws.
- **Framed curvature flow:** To overcome the limitations of the Minimal surface generating flow, we proposed a motion law for framed curves. After establishing local existence and several global estimates, we showed how this flow can be used for generating surfaces of constant mean or Gaussian curvature.
- **Tangent turning signature:** When dealing with flow in higher codimension, one encounters several topological problems related to the ambiguity of the normal vector or knotted configurations. The thesis introduced a new invariant, called tangent turning signature, which helps us capture some of these complexities.

Future Work

The analytical tools introduced in this thesis lay the groundwork for numerous future research directions. These opportunities for further studies are not only mathematically rich but also bear potential for various applications in science and engineering:

- **Higher-dimensional cases:** The current study has been largely confined to three-dimensional Euclidean space. However, many of the findings may be extended into higher dimensions or more general ambient spaces as in [Smo12].
- **Application-specific models:** Motion laws and tools introduced in this work may find applications in fields like robotics, computational geometry, or fluid dynamics.
- **Computational methods:** The development of efficient numerical methods for solving these motion laws, especially, those involving the approximation of torsion.
- **Topological changes:** Changes in topology are often linked to critical scientific phenomena. While reconnection or annihilation through self-contact is well-studied, spontaneous branching during growth still lacks proper mathematical treatment.

Each of these potential studies could leverage the analytical and topological tools developed in this thesis, contributing further to the understanding of geometric flows of low-dimensional manifolds in various dimensions.

Bibliography

A

[AH65] R. J. Arms and F. R. Hama. "Localized Induction Concept on a Curved Vortex and Motion of an Elliptic Vortex Ring". In: *Physics of Fluid* 8 (1965), pp. 553–559.

[AHB85] S. Andersson, S. T. Hyde, and J. O. Bovin. "On the periodic minimal surfaces and the conductivity mechanism of α-AgI". In: *Zeitschrift für Kristallographie* 173 (1985), pp. 97–99.

[AL86] U. Abresch and J. Langer. "The normalized curve shortening flow and homothetic solutions". In: *J. Differential Geom.* 23.2 (1986), pp. 175–196.

[And+88] S. Andersson et al. "Minimal Surfaces and Structures: From Inorganic and Metal Crystals to Cell Membranes and Biopolymers". In: *Chemical Reviews* 88 (1988), pp. 221–242.

[Ang90a] S. Angenent. "Nonlinear analytic semi-flows". In: *Proc. R. Soc. Edinb., Sect. A* 115 (1990), pp. 91–107.

[Ang90b] S. Angenent. "Parabolic equations for curves on surfaces. I: Curves with p integrable curvature". In: *Ann. Math.* 132.2 (1990), pp. 451–483.

[Alt91] S. J. Altschuler. "Singularities for the curve shortening flow for space curves". In: *Journal of Differential Geometry* 34 (1991), pp. 491–514.

[AG92] S. J. Altschuler and M. A. Grayson. "Shortening space curves and flow through singularities". In: *Journal of Differential Geometry* 35 (1992), pp. 283–298.

[AS96] L. Ambrosio and H. M. Soner. "A level set approach to the evolution of surfaces of any codimension". In: *Journal of Differential Geometry* 43 (1996), pp. 693–737.

[Abr+01] A. Abrams et al. "Circles minimize most knot energies". In: *Topology* 42 (2001), pp. 381–394.

[And02] B. Andrews. "Singularities in crystalline curvature flows". In: *Asian J. Math.* 6 (2002), pp. 101–122.

[Ale+03] M. Alexa et al. "Computing and rendering point set surfaces". In: *IEEE Transactions on Visualization and Computer Graphics* 9.1 (2003), pp. 3–15. DOI: 10.1109/TVCG.2003.1175093.

[Ada04] C. C. Adams. *The Knot Book: An Elementary Introduction to the Mathematical Theory of Knots*. American Mathematical Society, 2004. ISBN: 978-0-8218-3678-1.

[AB11] B. Andrews and P. Bryan. "Curvature bound for curve shortening flow via distance comparison and a direct proof of Grayson's theorem". In: *J. Reine Angew. Math.* 653 (2011), pp. 179–187.

[AHY12] N. H. Abdel-All, R. A. Hussien, and T. Youssef. "Hasimoto Surfaces". In: *Life Science Journal* 9 (2012), pp. 556–560.

[Alt+13] D. J. Altschuler et al. "The zoo of solitons for curve shortening in $\mathbb{R}^n$". In: *Nonlinearity* 26 (2013), pp. 1189–1226.

[AY18] S. Angenent and Q. You. "Ancient solutions to curve shortening with finite total curvature". In: *Transactions of the American Mathematical Society* (2018). Corpus ID: 59366007. DOI: 10.1090/tran/8186.

B

[Bis75] R. L. Bishop. "There is More than One Way to Frame a Curve". In: *The American Mathematical Monthly* 82.3 (1975), pp. 246–251.

[Bra78] K. Brakke. *The motion of a surface by its mean curvature*. Vol. 20. Mathematical Notes. Princeton, N.J.: Princeton University Press, 1978.

[Bra92] K. A. Brakke. "The Surface Evolver". In: *Experimental Mathematics* 1.2 (1992), pp. 141–165. URL: http://www.susqu.edu/brakke/evolver/evolver.html.

[BW95] L. Bronsard and B. T. R. Wetton. "A Numerical Method for Tracking Curve Networks Moving with Curvature Motion". In: *Journal of Computational Physics* 120 (1995), pp. 66–87.

[BP96] G. Bellettini and M. Paolini. "Anisotropic motion by mean curvature in the context of Finsler geometry". In: *Hokkaido Mathematical Journal* 25.3 (1996), pp. 537–566.

[Bar+97] C. F. Barenghi et al. "Superfluid vortex lines in a model of turbulent flow". In: *Physics of Fluids* 9.9 (1997), pp. 2631–2643.

[Bal+99] J. M. Ball et al. *Fundamental contributions to the continuum theory of evolving phase interfaces in solids*. Springer–Verlag, Berlin, 1999.

[Bou00] M. Boutin. "Numerically Invariant Signature Curves". In: *International Journal of Computer Vision* 40 (2000), pp. 235–248.

[Ben01] M. Beneš. "Mathematical analysis of phase-field equations with numerically efficient coupling terms". In: *Interfaces Free Bound.* 3.2 (2001), pp. 201–212. DOI: 10.4171/IFB/38.

[Bur+01] P. Burchard et al. "Motion of curves in three spatial dimensions using a level set approach". In: *Journal of Computational Physics* 170 (2001), pp. 720–741.

[BCM04] M. Beneš, V. Chalupecký, and K. Mikula. "Geometrical image segmentation by the Allen-Cahn equation". In: *Applied Numerical Mathematics* 51 (2004), pp. 187–205.

[Bre05] S. Brendle. "Convergence of the Yamabe flow for arbitrary initial energy". In: *Journal of Differential Geometry* 69.2 (2005), pp. 217–278. DOI: 10.4310/jdg/1121449107. URL: https://doi.org/10.4310/jdg/1121449107.

[BHS06] A. Bobenko, T. Hoffmann, and B. Springborn. "Minimal surfaces from circle patterns: Geometry from combinatorics". In: *Annals of Mathematics* 164 (2006), pp. 231–264.

[BS07] I. Bakas and C. Sourdis. "Dirichlet sigma models and mean curvature flow". In: *Journal of High Energy Physics* 2007.06 (2007), p. 057.

[Bet+07] L. M. A. Bettencourt et al. "Growth, innovation, scaling, and the pace of life in cities". In: *Proceedings of the National Academy of Sciences* 104 (2007), pp. 7301–7306.

[Ben+08] M. Beneš et al. "Application of a curvature adjusted method in image segmentation". In: *Bulletin of the Institute of Mathematics, Academia Sinica (New Series)* 3.4 (2008), pp. 509–523.

[Ber+08] M. Bergou et al. "Discrete elastic rods". In: *ACM SIGGRAPH* 63 (2008).

[BPW09] U. Bauer, K. Polthier, and M. Wardetzky. "Uniform Convergence of Discrete Curvatures from Nets of Curvature Lines". In: *Discrete and Computational Geometry* 43 (2009), pp. 1221–1231.

[BS09] S. Brendle and R. Schoen. "Manifolds with 1/4-pinched curvature are space forms". In: *J. Amer. Math. Soc.* 22 (2009), pp. 287–307.

[BD10] D. Brander and J. F. Dorfmeister. "The Björling problem for non-minimal constant mean curvature surfaces". In: *Comm. Anal. Geom.* 18 (2010), pp. 171–194.

[Bal+12] M. Balažovjech et al. "Lagrangean method with topological changes for numerical modelling of forest fire propagation". In: *Proceedings of ALGORITMY* (2012), pp. 42–52.

[Bur+15] M. J. Burin et al. "On filament structure and propagation within a commercial plasma globe". In: *Physics of Plasmas* 22 (2015), p. 053509.

[Bae+17] C. Baek et al. "Form finding in elastic gridshells". In: *Proceedings of the National Academy of Sciences* 115 (2017), pp. 66–87.

[Bla18] S. Blatt. "The gradient flow of O'Hara's knot energies". In: *Mathematische Annalen* 370 (2018). Published 17 April 2017, pp. 993–1061. URL: https://link.springer.com/article/10.1007/s00208-017-1540-4.

[BR20] S. Bartels and P. Reiter. "Numerical solution of a bending-torsion model for elastic rods". In: *Numerische Mathematik* 146 (2020), pp. 661–697.

[BLS20] K. Brazda, L. Lussardi, and U. Stefanelli. "Existence of varifold minimizers for the multiphase Canham–Helfrich functional". In: *Calc. Var.* 59 (2020), p. 93.

[BK22] R. Bamler and B. Kleiner. "Ricci flow and diffeomorphism groups of 3-manifolds". In: *Journal of the American Mathematical Society* 36.1 (2022).

[BKŠ22] M. Beneš, M. Kolář, and D. Ševčovič. “Qualitative and Numerical Aspects of a Motion of a Family of Interacting Curves in Space”. In: *SIAM Journal on Applied Mathematics* 82 (2022).

[Bän+23] E. Bänsch et al. *Interfaces: Modeling, Analysis, Numerics*. Vol. 51. Oberwolfach Seminars. Covers a vast array of different mathematical methods to deal with interfaces and free boundaries. Includes in-depth numerical analysis of geometric partial differential equations and free boundary problems. Provides a first systematic introduction to interfaces which combines modeling, analysis and computation. Birkhäuser, 2023. URL: https://www.springer.com/gp/book/9783030942800.

[Bac] T. Bachoff. *Frenet frames and theorems of Jacobi and Milnor for space polygons (Global geometry of polygons. III)*. URL: https://www.maths.ed.ac.uk/~v1ranick/papers/banchoff6.pdf.

C

[CH58] J. W. Cahn and J. E. Hilliard. “Free energy of a nonuniform system. I. Interfacial free energy”. In: *The Journal of Chemical Physics* 28.2 (1958), pp. 258–267.

[Căl61] G. Călugăreanu. “Sur les classes d’isotopie des noeuds tridimensionels et leurs invariants”. In: *Czech. Math. J.* 11 (1961), pp. 588–625.

[Chr70] J. Christiansen. “Numerical solution of ordinary simultaneous differential equations of the 1st order using a method for automatic step change”. In: *Numerische Mathematik* 14 (1970), pp. 317–324.

[Car76] M. D. do Carmo. *Differential Geometry of Curves and Surfaces*. Corpus ID: 35089975. Prentice-Hall, 1976. DOI: 10.1007/b137116.

[Cag86] G. Caginalp. “An analysis of a phase field model of a free boundary”. In: *Arch. Rational Mech. Anal.* 92 (1986), pp. 205–245.

[Cho93] D. L. Chopp. “Computing Minimal Surfaces via Level Set Curvature Flow”. In: *Journal of Computational Physics* 106 (1993), pp. 77–91.

[CD98] B. Chopard and M. Droz. *Cellular automata modeling of physical systems*. Cambridge University Press, 1998.

[Cao03] F. Cao. *Geometric Curve Evolution and Image Processing*. Springer, 2003.

[Cam+10] M. D. Campanell et al. “Measurements of the motion of filaments in a plasma ball”. In: *Physics of Plasmas* 17 (2010), p. 053507.

[Che+16] A. Chern et al. “Schrödinger’s Smoke”. In: *ACM Transactions on Graphics* 35.4 (2016). Article No.: 77, pp. 1–13. DOI: 10.1145/2897824.2925868.

[Cor16] K. Corrales. “Non existence of type II singularities for embedded and unknotted space curves”. arXiv preprint arXiv:1605.03100. 2016.

[CW17] K. Crane and M. Wardetzky. “A Glimpse into Discrete Differential Geometry”. In: *Notices of the American Mathematical Society* 64 (2017), pp. 1153–1159.

[CDR22] C. Coupette, S. Dalleiger, and B. Rieck. "Ollivier-Ricci Curvature for Hypergraphs: A Unified Framework". In: *Proceedings of the International Conference on Learning Representations (ICLR)*. Accepted as a poster at ICLR 2023. Oct. 2022. URL: https://arxiv.org/abs/2210.12048.

D

[Del41] Ch. Delaunay. "Sur la surface de révolution dont la courbure moyenne est constante". In: *Journal de Mathématiques Pure et Appliquée* 16 (1841), pp. 309–321.

[Dzi90] G. Dziuk. "An algorithm for evolutionary surfaces". In: *Numerische Mathematik* 58 (1990), pp. 603–611.

[Dzi94] G. Dziuk. "Convergence of a semi-discrete scheme for the curve shortening flow". In: *Mathematical Models and Methods in Applied Sciences* 4 (1994).

[DO07] E. Demainea and J. O'Rourke. *Geometric folding algorithms. Linkages, origami, polyhedra*. Cambridge Univ. Press, 2007.

[DHS10] P. Daskalopoulos, R. Hamilton, and N. Sesum. "Classification of compact ancient solutions to the curve shortening flow". In: *Journal of Differential Geometry* 84.3 (Mar. 2010), pp. 455–464. DOI: 10.4310/jdg/1279114297.

[ĐGM13] B. Đurickovic, A. Goriely, and J. H. Maddocks. "Twist and Stretch of Helices Explained via the Kirchhoff-Love Rod Model of Elastic Filaments". In: *Physical Review Letters* 111 (2013), pp. 108103 1–5. DOI: 10.1103/PhysRevLett.111.108103.

[DS23] P. Daskalopoulos and M. Saez. "Uniqueness of entire graphs evolving by mean curvature flow". In: *Journal für die reine und angewandte Mathematik (Crelles Journal)* (Jan. 2023). Requires Authentication. DOI: 10.1515/crelle-2022-0085. URL: https://doi.org/10.1515/crelle-2022-0085.

E

[Eul44] L. Euler. *Methodus Inveniendi Lineas Curvas Maximi Minimive Proprietate Gaudentes*. Appendix: De curvis elasticis. Lausanne, Switzerland: M.-M. Bousquet, 1744.

[EG92] L. C. Evans and R. F. Gariepy. *Measure Theory and Fine Properties of Functions*. Boca Raton, FL: CRC Press, 1992.

[Eva10] L. C. Evans. *Partial differential equations*. Second. Vol. 19. Graduate Studies in Mathematics. Providence, RI: American Mathematical Society, 2010.

[ELW22] C. G. Evans, B. Lambert, and A. Wood. “Lagrangian mean curvature flow with boundary”. In: *Calculus of Variations and Partial Differential Equations* 61 (2022). Published 07 April 2022. DOI: https://doi.org/10.1007/s00526-022-02229-0. URL: https://link.springer.com/article/10.1007/s00526-022-02229-0.

F

[Fár49] I. Fáry. “Sur la courbure totale d’une courbe gauche faisant un noeud”. In: *Bulletin de la Société Mathématique de France* 77 (1949), pp. 128–138.

[Fey55] R. P. Feynman. “Application of Quantum Mechanics to Liquid Helium”. In: *Progress in Low Temperature Physics*. Vol. 1. Elsevier, 1955, pp. 17–53.

[Fel68] E. A. Feldman. “Deformations of closed space curves”. In: *Journal of Differential Geometry* 2 (1968), pp. 67–75.

[Fir74] W. J. Firey. “Shapes of worn stones”. In: *Mathematika* 21 (1974), pp. 1–11.

[Fur88] D. J. Furbish. “River-bend curvature and migration: How are they related?” In: *Geology* 16.8 (1988), pp. 752–755.

[Fur91] D. J. Furbish. “Spatial autoregressive structure in meander evolution”. In: *Geological Society of America Bulletin* 103.12 (1991), pp. 1576–1589.

[FT99] D. Fuchs and S. Tabachnikov. “More on paperfolding”. In: *Amer. Math. Monthly* 106 (1999), pp. 27–35.

[FL13] A. Frascati and S. Lanzoni. “A mathematical model for meandering rivers with varying width”. In: *Journal of Geophysical Research: Earth Surface* 118 (2013), pp. 1641–1657.

[FGC23] N. Feng, M. Gillespie, and K. Crane. “Winding Numbers on Discrete Surfaces”. In: *ACM Trans. Graph.* XX.X (2023).

G

[Got71] T. Gotō. “Relativistic Quantum Mechanics of One-Dimensional Mechanical Continuum and Subsidiary Condition of Dual Resonance Model”. In: *Progress of Theoretical Physics* 46 (5 1971), pp. 1560–1569.

[GH86] M. Gage and R. S. Hamilton. “The heat equation shrinking convex plane curves”. In: *Journal of Differential Geometry* 23 (1986), pp. 69–96.

[Gra87] M. Grayson. “The heat equation shrinks embedded plane curves to round points”. In: *Journal of Differential Geometry* 26 (1987), pp. 285–314.

[Gur93] M. E. Gurtin. *Thermomechanics of evolving phase boundaries in the plane*. Oxford Mathematical Monographs. Oxford University Press, 1993.

[Gol+10] R. E. Goldsteina et al. “Soap-film Möbius strip changes topology with a twist singularity”. In: *Proceedings of the National Academy of Sciences of the United States of America* 107 (2010), pp. 21979–21984.

[Gol+14] R. E. Goldstein et al. “Boundary singularities produced by the motion of soap films”. In: *Proceedings of the National Academy of Sciences of the United States of America* 111 (2014), pp. 8339–8344.

[Gho19] M. Ghomi. *Classical open problems in differential geometry*. 2019.

[GMP20] H. Garcke, J. Menzel, and A. Pluda. “Long time existence of solutions to an elastic flow of networks”. In: *Communications in Partial Differential Equations* 45 (2020), pp. 1253–1305.

[Gar+23] H. Garcke et al. “Phase-field methods for spectral shape and topology optimization”. In: *ESAIM: COCV* 29.10 (2023). Published online 19 January 2023, pp. 1–57. DOI: https://doi.org/10.1051/cocv/2022090.

[GP] Y. Giga and N. Požár. “A level set crystalline mean curvature flow of surfaces”. In: *Adv. Differential Equations* 21 (7/8), pp. 631–698.

H

[Hel98] H. S. Hele-Shaw. “The Flow of Water”. In: *Nature* 58.1489 (1898), pp. 34–36. DOI: 10.1038/058034a0.

[Has72] H. Hasimoto. “A soliton on a vortex filament”. In: *Journal of Fluid Mechanics* 51.3 (1972), pp. 477–485. DOI: 10.1017/S0022112072002307. URL: https://doi.org/10.1017/S0022112072002307.

[Ham82] R. S. Hamilton. “Three-manifolds with positive Ricci curvature”. In: *Journal of Differential Geometry* 17.2 (1982), pp. 255–306.

[Hui84] G. Huisken. “Flow by mean curvature of convex surfaces into spheres”. In: *Journal of Differential Geometry* 20 (1984), pp. 237–266.

[Hol+86] M. Holodniok et al. *Methods of Analysis of Nonlinear Dynamical Models*. Acad. Praha, 1986.

[Hui90] G. Huisken. “Asymptotic behavior for singularities of the mean curvature flow”. In: *J. Differential Geom.* 31.1 (1990), pp. 285–299.

[OHa91] J. O’Hara. “Energy of a knot”. In: *Topology* 30.2 (1991), pp. 241–247. DOI: 10.1016/0040-9383(91)90010-2.

[OHa92] J. O’Hara. “Energy Functionals of Knots”. In: *Topology Hawaii (Honolulu. HI, 1990)*. River Edge: World Science Publication, 1992, pp. 201–204.

[HLS94] T. Y. Hou, J. Lowengrub, and M. Shelley. “Removing the stiffness from interfacial flows and surface tension”. In: *J. Comput. Phys.* 114 (1994), pp. 312–338.

[Ham95] R. S. Hamilton. “Harnack estimate for the mean curvature flow”. In: *Journal of Differential Geometry* 41.1 (1995), pp. 215–226.

[Hui98] G. Huisken. "A distance comparison principle for evolving curves". In: *Asian J. Math.* 2.1 (1998), pp. 127–133.

[HI01] G. Huisken and T. Ilmanen. "The inverse mean curvature flow and the Riemannian Penrose inequality". In: *Journal of Differential Geometry* 59 (3 2001), pp. 353–437.

[Hat02] A. Hatcher. *Algebraic Topology*. New York: Cambridge University Press, 2002. ISBN: 9780521795401.

[Hal12] H. P. Halldorsson. "Self-similar solutions to curve shortening flow". In: *Transactions of the American Mathematical Society* 364.10 (Oct. 2012), pp. 5285–5309. DOI: 10.1090/S0002-9947-2012-05632-7.

[He12] S. He. "Distance comparison principle and Grayson type theorem in the three dimensional curve shortening flow, preprint". arXiv:1209.5146v1. 2012.

[Has16] R. Haslhofer. "Lectures on curve shortening flow". In: 2016. URL: https://api.semanticscholar.org/CorpusID:43500498.

[HM16] R. A. Hussien and S. G. Mohamed. "Generated Surfaces via Inextensible Flows of Curves in $\mathbb{R}^3$". In: *Journal of Applied Mathematics* 2016 (2016), pp. 1–8.

[HK20] Y. Hatakeyama and M. Koiso. "Stability of helicoidal surfaces with constant mean curvature". In: *International Journal of Mathematics for Industry* 12 (2020).

I

[IPS81] S. Ikeda, G. Parker, and K. Sawai. "Bend theory of river meanders: Part I, Linear development". In: *Journal of Fluid Mechanics* 112 (1981), pp. 363–377.

[IY03] T. Ishiwata and S. Yazaki. "On the blow-up rate for fast blow-up solutions arising in an anisotropic crystalline motion". In: *Journal of Computational and Applied Mathematics* 159.1 (Oct. 2003), pp. 55–64.

J

[Jol02] I. T. Jolliffe. *Principal Component Analysis*. 2nd ed. Springer Series in Statistics. eBook ISBN: 978-0-387-22440-4, Softcover ISBN: 978-1-4419-2999-0. Springer New York, NY, 2002. ISBN: 978-0-387-95442-4. DOI: 10.1007/b98835.

[JKS13] A. Jacobson, L. Kavan, and O. Sorkine-Hornung. "Robust Inside-Outside Segmentation Using Generalized Winding Numbers". In: *ACM Trans. Graph.* 32.4 (July 2013). ISSN: 0730-0301. DOI: 10.1145/2461912.2461916.

K

[Kus87] R. Kusner. “Global Geometry of Extremal Surfaces in Three-Space”. PhD thesis. University of California, Berkeley, 1987.

[Kee88] J. P. Keener. “The dynamics of three-dimensional scroll waves in excitable media”. In: *Physica D* 31 (1988), pp. 269–276.

[Kus91] R. Kusner. “Bubbles, conservation laws, and balanced diagrams”. In: *Math. Sci. Res. Inst. Publ., Springer, New York* 17 (1991), pp. 103–108.

[Kim97] M. Kimura. “Numerical analysis for moving boundary problems using the boundary tracking method”. In: *Jpn. J. Indust. Appl. Math.* 14 (1997), pp. 373–398.

[KS97] R. B. Kusner and J. M. Sullivan. “Möbius energies for knots and links, surfaces and submanifolds”. In: *Geometric Topology (Athens, GA, 1993)*. Vol. 2. AMS/IP Stud. Adv. Math. Providence, RI: Amer. Math. Soc., 1997, pp. 570–604.

[Kim08] M. Kimura. “Geometry of hypersyrfaces and moving hypersurfaces in Rm for the study of moving boundary problems”. In: *Jindřich Nečas Center for Mathematical Modeling Lecture notes* 4.2 (2008), pp. 39–93.

[Kha15] G. Khan. “A condition ensuring spatial curves develop type-II singularities under curve shortening flow”. In: *arXiv:1209.4072v3* (2015).

[AAR16] O. Al-Ketan, R. K. A. Al-Rub, and R. Rowshan. “Mechanical Properties of a New Type of Architected Interpenetrating Phase Composite Materials”. In: *Advanced Materials Technologies* 2 (2016).

[KBŠ17] M. Kolář, M. Beneš, and D. Ševčovič. “Area preserving geodesic curvature driven flow of closed curves on a surface”. In: *Discrete and Continuous Dynamical Systems - Series B* 22 (2017), pp. 3671–3689.

[Kol+18] M. Kolář et al. “Modeling of Double Cross-Slip by Means of Geodesic Curvature Driven Flow”. In: *Acta Physica Polonica Series A* 134.3 (2018), pp. 667–670.

[Kol+21] M. Kolář et al. “Analysis of Kuramoto-Sivashinsky Model of Flame/Smoldering Front by Means of Curvature Driven Flow”. In: *Numerical Mathematics and Advanced Applications ENUMATH 2019*. Ed. by F.J. Vermolen and C. Vuik. Vol. 139. Lecture Notes in Computational Science and Engineering. Cham: Springer, 2021. DOI: 10.1007/978-3-030-55874-1_60.

L

[Lit71] J. A. Little. “Third order nondegenerate homotopies of space curves”. In: *Journal of Differential Geometry* 5 (1971), pp. 503–515.

[LS84] J. Langer and D. A. Singer. “The total squared curvature of closed curves”. In: *Journal of Differential Geometry* 20.1 (1984), pp. 1–22.

[Lun84] A. Lunardi. “Abstract quasilinear parabolic equations”. In: *Math. Ann.* 267 (1984), pp. 395–416.

[Lóp11] R. López. "The theorem of Schur in the Minkowski plane". In: *Journal of Geometry and Physics* 61 (2011), pp. 342–346.

[Lóp13] R. López. *Constant Mean Curvature Surfaces with Boundary*. Springer Monographs in Mathematics. 2013.

[LL14] M. Larsson and K. Larsson. "Periodic minimal surface organizations of the lipid bilayer at the lung surface and in cubic cytomembrane assemblies". In: *Advances in Colloid and Interface Science* 205 (2014), pp. 68–73.

[Liu+22] Y. Liu et al. "On Helical Surfaces with a Constant Ratio of Principal Curvatures". In: *arxiv* (2022). URL: https://doi.org/10.48550/arXiv.2204.06443.

[Lit23] F. Litzinger. "Singularities of low entropy high codimension curve shortening flow". In: *arXiv preprint arXiv:2304.02487* (2023). URL: https://doi.org/10.48550/arXiv.2304.02487.

M

[Mul56] W. W. Mullins. "Two-dimensional motion of idealized grain boundaries". In: *Journal of Applied Physics* 27.6 (1956), pp. 900–904.

[Mor87] M. Morayne. "On differentiability of Peano type functions". In: *Colloquium Mathematicae* 53 (1987), pp. 129–132.

[Mur87] T. Mura. *Micromechanics of Defects in Solids*. Springer Netherlands, 1987.

[MŠ01] K. Mikula and D. Ševčovič. "Evolution of plane curves driven by a nonlinear function of curvature and anisotropy". In: *SIAM J. Appl. Math.* 61 (2001), pp. 1473–1501.

[Mik02] K. Mikula. "Image processing with partial differential equations". In: *NATO Science Series* 75 (2002), pp. 283–322.

[MKF09] V. Mallet, D. E. Keyes, and F. E. Fendell. "Modeling wildland fire propagation with level set methods". In: *Computers & Mathematics with Applications* 57.7 (Apr. 2009), pp. 1089–1101. DOI: 10.1016/j.camwa.2008.10.089.

[MP12] W. H. Meeks III and J. Pérez. *A Survey on Classical Minimal Surface Theory*. Vol. 60. University Lecture Series. 2012, p. 182.

[MN14] F. C. Marques and A. Neves. "Min-Max theory and the Willmore conjecture". In: *Annals of Mathematics* 179 (2014), pp. 683–782.

[MU14] K. Mikula and J. Urbán. "A new tangentially stabilized 3D curve evolution algorithm and its application in virtual colonoscopy". In: *Adv. Comput. Math.* 40 (2014), pp. 819–837.

[MSS15] F. Martín, A. Savas-Halilaj, and K. Smoczyk. "On the topology of translating solitons of the mean curvature flow". In: *Calculus of Variations and Partial Differential Equations* 54 (2015), pp. 2853–2882.

[MS16] F. Maucher and P. Sutcliffe. "Untangling Knots Via Reaction-Diffusion Dynamics of Vortex Strings". In: *Physical Review Letters* 116 (2016), p. 178101.

[Man+18] C. Mantegazza et al. “Evolution of networks with multiple junctions”. In: *arXiv: 1611.08254v2* (2018).

[Mac+19] T. Machon et al. “Aspects of Defect Topology in Smectic Liquid Crystals”. In: *Commun. Math. Phys.* 372 (2019), pp. 525–542.

[MS19] F. Maucher and P. Sutcliffe. “Dynamics of linked filaments in excitable media”. In: *Nonlinearity* 32.3 (2019), p. 942. DOI: 10.1088/1361-6544/aafbb3.

[MKB19] J. Minarčík, M. Kimura, and M. Beneš. “Comparing motion of curves and hypersurfaces in $\mathbb{R}^m$”. In: *Discrete and Continuous Dynamical Systems Series B* 24 (2019), pp. 4815–4826.

[MB20] J. Minarčík and M. Beneš. “Long-term behavior of curve shortening flow in $\mathbb{R}^3$”. In: *SIAM Journal on Mathematical Analysis* 52 (2020), pp. 1221–1231.

[MB22a] J. Minarčík and M. Beneš. “Minimal surface generating flow for space curves of non vanishing torsion”. In: *Discrete and Continuous Dynamical Systems - Series B* 27 (2022), pp. 6605–6617.

[MB22b] J. Minarčík and M. Beneš. “Nondegenerate Homotopy and Geometric Flows”. In: *Homology, Homotopy and Applications* 24 (2022), pp. 255–264.

[MB23] J. Minarčík and M. Beneš. “Trajectory Surfaces of Framed Curvature Flow”. Preprint. 2023.

N

[NPW84] L. Niemeyer, L. Pietronero, and H. J. Wiesmann. “Fractal Dimension of Dielectric Breakdown”. In: *Phys. Rev. Lett.* 52 (12 1984), p. 1033. DOI: https://doi.org/10.1103/PhysRevLett.52.1033.

[Nam95] J. Nambu. “Quark model and the factorization of the Veneziano amplitude”. In: *Broken Symmetry* (1995), pp. 258–267.

[Ni+19] C.-C. Ni et al. “Community Detection on Networks with Ricci Flow”. In: *Scientific Reports* 9.1 (July 2019). DOI: 10.1038/s41598-019-46380-9.

[NPP19] G. D. Nin, A. Pluda, and M. Pozzetta. *Lectures on Curvature Flow of Networks*. Springer, 2019.

[NPP20] G. D. Nin, A. Pluda, and M. Pozzetta. *Degenerate elastic networks, preprint*. 2020.

O

[OS88] S. Osher and J. A. Sethian. “Fronts Propagating with Curvature Dependent speed: Algorithms Based on Hamilton-Jacobi Formulation”. In: *Journal of Computational Physics* 79 (1988), pp. 12–49.

[Obe07] T. Oberhuber. “Finite difference scheme for the Willmore flow of graphs”. English. In: *Kybernetika* 43.6 (2007), pp. 855–867. ISSN: 0023-5954.

[OA08] A. Odgaard and J. Abad. “River Meandering and Channel Stability”. In: *Sedimentation Engineering: Processes, Measurements, Modeling, and Practice*. 2008, pp. 439–459.

[Olv08] P. J. Olver. “Invariant submanifold flows”. In: *Journal of Physics A: Mathematical and Theoretical* 41 (2008), p. 344017.

P

[DG79] G. Da Prato and P. Grisvard. “Equations d’évolution abstraites non linéaires de type parabolique”. In: *Ann. Mat. Pura Appl.* 4 (1979), pp. 329–396.

[PM87] P. Perona and J. Malik. “Scale space and edge detection using anisotropic diffusion”. In: *Proc. IEEE Computer Society Workshop on Computer Vision*. 1987.

[PP93] U. Pinkall and K. Polthier. “Computing Discrete Minimal Surfaces and Their Conjugates”. In: *Experimental Mathematics* 2 (1993), pp. 15–36.

[Per02] G. Perelman. *The entropy formula for the Ricci flow and its geometric applications*. arXiv:math/0211159. 2002. URL: https://arxiv.org/abs/math/0211159.

[Per03a] G. Perelman. *Finite extinction time for the solutions to the Ricci flow on certain three-manifolds*. arXiv:math/0307245. 2003. URL: https://arxiv.org/abs/math/0307245.

[Per03b] G. Perelman. *Ricci flow with surgery on three-manifolds*. arXiv:math/0303109. 2003. URL: https://arxiv.org/abs/math/0303109.

[Par+11] G. Parker et al. “A new framework for modeling the migration of meandering rivers”. In: *Earth Surface Processes and Landforms* 36.1 (2011), pp. 70–86.

[Pér16] J. Pérez. “A New Golden Age of Minimal Surfaces”. In: *Notices of the American Mathematical Society* 64.04 (2016).

[Pad+19] M. Padilla et al. “On Bubble Rings and Ink Chandeliers”. In: *ACM Transactions on Graphics (SIGGRAPH 2019)* 38 (2019), pp. 1–14.

[Pad+22] M. Padilla et al. “Filament based plasma”. In: *ACM Transactions on Graphics (TOG)* 41 (2022), pp. 1–14.

R

[RM89] J. R. Rice and M. Mu. “An experimental performance analysis for the rate of convergence of collocation on general domains”. In: *Numerical Methods for Partial Differential Equations* 5 (1989), pp. 45–52.

[Ric91] R. L. Ricca. "Rediscovery of Da Rios equations". In: *Nature* 352 (1991), pp. 561–562.

[RCV93] V. V. Rybenkov, N. R. Cozzarelli, and A. V. Vologodskii. "Probability of DNA knotting and the effective diameter of the DNA double helix". In: *Proceedings of the National Academy of Sciences* 90.11 (1993), pp. 5307–5311. DOI: 10.1073/pnas.90.11.5307. URL: https://doi.org/10.1073/pnas.90.11.5307.

[RK02] G. Richardson and J. R. King. "The evolution of space curves by curvature and torsion". In: *Journal of Physics A: Mathematical and General* 35 (2002), pp. 9857–9879.

[Ric05] R. L. Ricca. "Inflexional disequilibrium of magnetic flux-tubes". In: *Fluid Dynamics Research* 36 (2005), pp. 319–332.

[Rem+14] M. Remešíková et al. "Manifold evolution with tangential redistribution of points". In: *SIAM J. Sci. Comput.* 36.4 (2014), A1384–A1414.

[RS21] P. Reiter and H. Schumacher. "Sobolev Gradients for the Möbius Energy". In: *Archive for Rational Mechanics and Analysis* 242 (Nov. 2021), pp. 701–746. DOI: 10.1007/s00205-021-01680-1.

S

[Sch21] A. Schur. "Über, die Schwarzsche Extremaleigenschaft des Kreises unter den Kurven Konstanter Krümmung". In: *Math. Annalen* 83 (1921), pp. 143–148.

[Sch25] E. Schmidt. "Über das Extremum der Bogenlänge einer Raumkurve bei Vergeschriebenen Einschränkungen ihrer Krümmunge". In: *Sitzungsber. Akademia Berlin* (1925), pp. 485–490.

[Sma58] S. Smale. "A classification of immersions of the two-sphere". In: *Transactions of the American Mathematical Society* 90.2 (1958), pp. 281–290. ISSN: 0002-9947. DOI: 10.2307/1993205.

[Scr76] L. E. Scriven. "Equilibrium bicontinuous structure". In: *Nature* 263 (1976), pp. 123–125.

[Saf86] P. G. Saffman. "Viscous fingering in Hele-Shaw cells". In: *Journal of Fluid Mechanics* 173 (1986). S2CID 17003612, pp. 73–94.

[Sum86] D. W. Sumners. "The Role of Knot Theory in DNA Research". In: *Geometry and Topology*. 1st ed. CRC Press, 1986, p. 22. ISBN: 9781003072386. DOI: 10.1201/9781003072386-23.

[Sed94] V. D. Sedykh. "Four vertices of a convex space curve". In: *Bulletin of the London Mathematical Society* 26 (1994), pp. 177–180.

[Set96] J. A. Sethian. *Level Set Methods: Evolving Interfaces in Geometry, Fluid Mechanics, Computer Vision, and Materials Science*. Cambridge University Press, 1996.

[Sap01] G. Sapiro. *Geometric partial differential equations and image analysis*. Cambridge University Press, 2001.

[Sos04] A. Sossinsky. *Knots: Mathematics with a Twist*. Trans. by Giselle Weiss. Harvard University Press, Apr. 2004, p. 160. ISBN: 9780674013810.

[SMU07] D. Schwabe, A. I. Mizev, and M. Udhayasankar. "Formation of dynamic particle accumulation structures in oscillatory thermocapillary flow in liquid bridges". In: *Physics of Fluids* 19 (2007).

[Smo12] K. Smoczyk. "Mean Curvature Flow in Higher Codimension: Introduction and Survey". In: *Global Differential Geometry*. Ed. by C. Bär, J. Lohkamp, and M. Schwarz. Vol. 17. Springer Proceedings in Mathematics. Springer, Berlin, Heidelberg, 2012. DOI: 10.1007/978-3-642-22842-1_9.

[Sag+19] A. O. Sageman-Furnas et al. "Chebyshev nets from commuting Poly Vector fields". In: *ACM Transactions on Graphics* 38 (2019), pp. 1–16.

[SW19] H. Schumacher and M. Wardetzky. "Variational Convergence of Discrete Minimal Surfaces". In: *Numerische Mathematik* 141 (2019), pp. 173–213.

[SCR21] D. W. L. Sumners, I. Cruz-White, and R. L. Ricca. "Zero helicity of Seifert framed defects". In: *J. Phys. A.* 54 (2021), p. 295203.

[SSY22] K. Sakakibara, Y. Shimoji, and S. Yazaki. "A simple numerical method for Hele–Shaw type problems by the method of fundamental solutions". In: *Japan Journal of Industrial and Applied Mathematics* 39 (2022), pp. 869–887.

[Sch22] R. G. Scharein. *KnotPlot*. Hypnagogic Software. Originally part of the author's PhD thesis work at the Imager Computer Graphics Laboratory. 2022. URL: http://www.knotplot.com.

T

[Ter90] H. Terrones. "Computation of Minimal Surfaces". In: *Journal de Physique Colloques* 51 (1990), pp. 345–362.

[Top06] P. Topping. *Lectures on the Ricci flow*. Vol. 325. London Mathematical Society, 2006. ISBN: 0521689473.

V

[Vis96] A. Visintin. *Models of Phase Transitions*. 1st ed. Progress in Nonlinear Differential Equations and Their Applications. Boston, MA: Birkhäuser Boston, 1996, pp. X, 326. ISBN: 978-0-8176-3768-2. DOI: 10.1007/978-1-4612-4078-5.

[Veg15] L. Vega. "The dynamics of vortex filaments with corners". In: *Communications on Pure and Applied Analysis* 14.4 (2015), pp. 1581–1601.

W

[Whi37] H. Whitney. "On regular closed curves in the plane". In: *Compositio Mathematica* 4 (1937), pp. 276–284.

[Whi69] J. H. White. "Self-linking and the Gauss integral in higher dimensions". In: *Am. J. Math.* 91 (1969), pp. 693–728.

[Whi02] B. White. "Evolution of curves and surfaces by mean curvature". In: *Proceedings of the ICM*. Vol. 1. 2002, pp. 525–538.

[Whi05] B. White. "A local regularity theorem for mean curvature flow". In: *Ann. of Math. (2)* 161.3 (2005), pp. 1487–1519.

[WC06] J. J. van Wijk and A. M. Cohen. "Visualization of Seifert Surfaces". In: *IEEE Trans. on Visualization and Computer Graphics* 12 (2006), pp. 485–496.

Y

[Ye94] R. Ye. "Global existence and convergence of Yamabe flow". In: *Journal of Differential Geometry* 39.1 (1994), pp. 35–50. DOI: 10.4310/jdg/1214454674. URL: https://doi.org/10.4310/jdg/1214454674.

[YHW10] A. R. Yeates, G. Hornig, and A. L. Wilmot-Smith. "Topological constraints on magnetic relaxation". In: *Phys. Rev. Lett.* 105 (2010), p. 085002.

[Ye+20] K. Ye et al. "Penrose: From Mathematical Notation to Beautiful Diagrams". In: *ACM Trans. Graph.* 39.4 (2020).

[YSC21] C. Yu, H. Schumacher, and K. Crane. "Repulsive Curves". In: *ACM Trans. Graph.* 40 (2021).

[Yu+21] C. Yu et al. "Repulsive Surfaces". In: *ACM Trans. Graph.* 40 (2021).

Z

[Zha+22] Y. Zhang et al. "Nonconvex ancient solutions to Curve Shortening Flow". In: (2022). Comment: The same result was independently obtained by Charyyev, J. in arXiv:2204.05978. DOI: 10.48550/arXiv.2204.05253. arXiv: 2204.05253 [math.DG].

[ZZW22] S. Zhong, Z. Zhao, and X. Wan. "Geometry of solutions of the geometric curve flows in space". In: *Authorea* (2022). DOI: 10.22541/au.166756688.88270742/v1.

[ZR22] S. Zuccher and R. L. Ricca. "Creation of quantum knots and links driven by minimal surfaces". In: *Journal of Fluid Mechanics* 942 (2022), A8. DOI: 10.1017/jfm.2022.362.

Image Sources

[al85] Wasserman et al. *Knotted DNA*. Figure 4. Electron micrograph of a knotted loop of DNA. Reprinted with permission from The American Association for the Advancement of Science. 1985.

[Sul02] J. M. Sullivan. "Sphere Eversions: from Smale through "The Optiverse"". In: *Mathematical Visualization*. Springer, 2002. DOI: 10.1007/978-3-662-04909-9_22.

[Sla07] C. Slayden. *Ricci flow example*. Cosmocyte. Image courtesy Cameron Slayden of Cosmocyte. Available at https://www.cs.princeton.edu/~chazelle/media/AMSfeb07.htm. Feb. 2007.

[Thi09] M. Thirnbeck. *Meandering River*. [Online; accessed April 24, 2018], with kind permission of the author. 2009. URL: https://www.flickr.com/photos/39295360@N00/4007430076.

[WHB09] D. A. Winkler, J. D. Halley, and F. R. Burden. "Modelling for Regenerative Medicine: Systems Biology Meets Systems Chemistry". In: *CSIRO Molecular and Health Technologies* (2009). Received: September 5, 2008; Published: March 16, 2009. Contact: *dave.winkler@csiro.au.

[KR12] J. Kacher and I. M. Robertson. "Quasi-four-dimensional analysis of dislocation interactions with grain boundaries in 304 stainless steel". In: *Acta Materialia* 60.19 (2012). Reprinted by permission of Elsevier., pp. 6657–6672.

[Hal13] A. Hall. *Hele-Shaw cell No.25*. [Online; accessed April 24, 2018], with kind permission of the author. 2013. URL: http://www.antonyhall.net/works01/heleshaw02.html.

[KI13] D. Kleckner and W. T. M. Irvine. "Creation and dynamics of knotted vortices". In: *Nature Physics* 9.4 (2013). Reprinted by permission of Springer Nature.

[Ima14] Image from Google Maps. *Meandering Amazon River*. [Online; accessed November 4, 2023]. 2014. URL: https://www.ascentoftheamazon.com/wp-content/uploads/2014/07/image24.jpg.

[M A19] M. Aschwanden et al. *High-Resolution Imaging of the Solar Corona*. [Online; accessed November 4, 2023], with kind permission of the author. 2019. URL: https://knowablemagazine.org/article/physical-world/2019/solar-corona-temperature.

[Lib] K. Libbrecht. *Snowflakes*. [Online; accessed April 24, 2018], with kind permission of the author. URL: http://www.snowcrystals.com/photos/f0103a182B.

A

Appendix: Evolution of Filament Networks

This chapter addresses the topic of moving networks of curves, proven useful in diverse applications such as grain boundary evolution and engineered curved grid structures. Taking a step further, we introduce models of filament networks with adaptable topologies. By incorporating ideas from discrete differential geometry, our approach potentially expands the scope of useful applications in this field.

We present a formal definition of filament networks and introduce a novel energy functional based on material distribution systems. Utilizing discrete differential geometry methods, we derive conditions for optimizing these networks. These models are not only grounded in theory but also have practical implications, particularly in the optimization of tunnel systems and simulations of natural branching structures. The contents of this appendix constitute a yet unpublished work, offering a potential starting point for future research directions.

A.0 Introduction

This section introduces the main ideas and notation as well as provides a brief literature review of fields related to network optimisation problems and its practical applications.

A.0.0 Motivation

Moving networks of curves have been studied in both in $\mathbb{R}^2$ [NPP20; NPP19; BW95; Man+18] and $\mathbb{R}^3$ [GMP20]. The applications of these models include modelling of grain boundary evolution [Bal+99] and engineering curved grid structures [Bae+17; Sag+19].

We aim to advance this field by introducing models of filament networks with adaptable

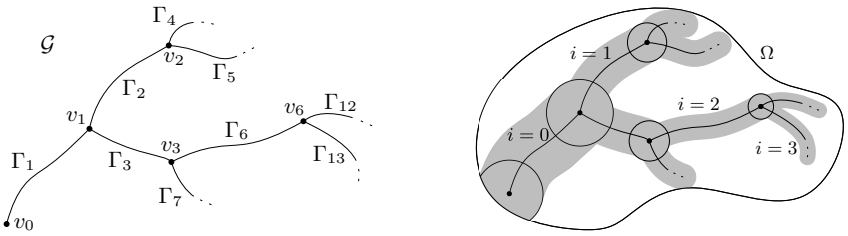

Figure A.1: Diagram depicting branching network notation (left) and explanation of the root system energy functional (right).

topologies. These models have potential applications ranging from optimizing tunnel systems to simulating various natural structures, such as root and vascular networks or Lichtenberg figures [NPW84]. This section describes a simplified model of branching tree structures optimizing energy inspired by material transport systems of fractal character found both in natural and industrial settings [Bet+07].

A.0.1 Formulation

Throughout this text we define filament network as an embedding of a directed graph $\mathcal{G} = (\mathcal{V}, \mathcal{E})$ with a collection of points $\mathcal{V} = \{v_i\}_i$ from $\mathbb{R}^n$ as vertices and edges $\mathcal{E} \subset \mathcal{V} \times \mathcal{V} \times \{\Gamma\}$. Where the curve Γ associated with vertex tuple $(v, w) \in \mathcal{V}^2$ is given by $\gamma\colon [0,1] \to \mathbb{R}^n$ such that $\gamma(0) = v$ and $\gamma(1) = w$.

This example is inspired by biological systems which distribute energy or materials via branching filament networks of binary tree structure. We aim to optimize the shape of this topological profile with respect to energy inspired by biology - defined later in this section. In this case, the filament network $\mathcal{G}$ has to satisfy the following set of conditions (see Figure A.1).

1. Γ_k is a curve parametrized by $\gamma_k\colon [0,1] \to \mathbb{R}^n$ for all $k \in \mathbb{N}$,
2. $\gamma_k(0) = v_l$ with $l = \left\lfloor \frac{k}{2} \right\rfloor$ and $\gamma_k(1) = v_k$ for all $k \in \mathbb{N}$,
3. for every non-negative integer k, and l greater than k, if $L(\Gamma_k) = k$ and there exists a positive integer n such that $\left\lfloor \frac{l}{2^n} \right\rfloor = k$, then the length $L(\Gamma_l)$ must be equal to 0.

We use the following nomenclature: *Tip Node* refers to a vertex of degree 1, *Body Node* refers to a vertex of degree 2, and finally, *Junction Node* refers to a vertex with degree 3. Note that vertices of degree higher than 3 are not considered.

A.0.2 Energy Functional

This section introduces an energy functional inspired by material distribution systems found in nature and engineering. The α-length is defined for $\alpha \in (0,1]$ as

$$L^\alpha(\mathcal{G}) = \sum_{i=1}^{+\infty} \alpha^i \sum_{j=2^i}^{2^{i+1}-1} L(\Gamma_i) \tag{A.1}$$

and the β-volume for $\beta \in (0, 1]$ is given by

$$V^{\beta}(\mathcal{G}) = \mathcal{M}\left[\bigcup_{i=1}^{+\infty}\bigcup_{j=2^i}^{2^{i+1}-1}\left(\Gamma_j \oplus B_{\beta^i}\right) \cap \Omega\right], \tag{A.2}$$

where $\mathcal{M}$ is the Lebesque measure, $\oplus$ denotes the dilation operator and B_r is a ball with radius r, i.e. $\Gamma_j \oplus B_{\beta^i} = \{x \colon \operatorname{dist}(x, \Gamma_j) < \beta^i\}$. Consider the energy functional

$$E(\mathcal{G}) = \phi(L^{\alpha}(\mathcal{G}), V^{\beta}(\mathcal{G})), \tag{A.3}$$

where $\phi \colon (0, L^{\alpha}_{max}) \times \mathbb{R}^+ \to \mathbb{R}^+$ for some fixed $L^{\alpha}_{max} > 0$, must satisfy

1. $\phi(x, y) \to +\infty$ as $x \to L^{\alpha}_{max}$ for all y in $\mathbb{R}^+$,
2. $\phi(x, \cdot)$ is decreasing on $\mathbb{R}^+$ for all x in $(0, L^{\alpha}_{max})$,
3. $\phi(\cdot, y)$ is increasing on $(0, L^{\alpha}_{max})$ for all y in $\mathbb{R}^+$.

The condition (1) represents the *finiteness of available resources* and the remaining monotonicity conditions (2) and (3) enforce the *expansion profitability* and the opposing *structural cost*, respectively.

We use the following form of ϕ for its simplicity.

$$\phi(L^{\alpha}, V^{\beta}) = \lambda(L^{\alpha}_{max} - L^{\alpha})^{-1} - V^{\beta}, \tag{A.4}$$

where the constant $\lambda > 0$ determines the *profit-cost ratio*.

A.1 Discretization

This section presents a discrete approach to the energy gradient flow of networks. We first derive the gradient in a discrete setting, thereby bypassing the need for solving continuous partial differential equations. Next, we explore the implications of this approach on determining optimal junction angles in networks. Finally, we introduce a branching condition that enables the addition of new branches to the network based on energy considerations.

A.1.0 Discrete Energy Gradient

Instead of defining the gradient flow analytically and then solving the corresponding partial differential equations numerically, we derive the gradient in the discrete setting. This approach related to discrete differential geometry is often used in computation-heavy domains such as computed graphics (see e.g. [CW17; YSC21]).

The gradient of the discrete energy functional at a point X is given by

$$\nabla E = \partial_{L^{\alpha}}\phi \nabla L^{\alpha} + \partial_{V^{\beta}}\phi \nabla V^{\beta} \tag{A.5}$$

$$= \partial_{L^{\alpha}}\phi \sum_X \nabla_X L^{\alpha} + \partial_{V^{\beta}}\phi \sum_X \nabla_X V^{\beta}, \tag{A.6}$$

where $\partial_{L^\alpha}\phi = \lambda(L^\alpha_{max} - L^\alpha)^{-2}$ and $\partial_{V^\beta}\phi = -1$. The point-wise gradients $\nabla_X L^\alpha$ and $\nabla_X V^\beta$ depend on the node type of X.

- Tip node with previous point X_p:

$$\nabla_X L^\alpha = \alpha^i \nabla_X \|X - X_p\|, \tag{A.7}$$
$$\nabla_X V^\beta = 2\beta^i \nabla_X \|X - X_p\|. \tag{A.8}$$

  Note that the factor 2 in (A.8) reflects that β^i is the radius, not the diameter.

- Body node with neighbouring points X_p and X_n:

$$\nabla_X L^\alpha = \alpha^i \nabla_X \left(\|X_n - X\| + \|X - X_p\|\right), \tag{A.9}$$
$$\nabla_X V^\beta \approx 0. \tag{A.10}$$

  The approximation (A.10) can be improved, however, it has a negligible effect on the numerical simulation.

- Junction node with neighbouring points X_p, X_l and X_r:

$$\nabla_X L^\alpha = \alpha^i \nabla_X \|X_p - X\| + \alpha^{i+1} \nabla_X \left(\|X_r - X\| + \|X - X_l\|\right), \tag{A.11}$$
$$\nabla_X V^\beta \approx 2\beta^i \nabla_X \|X_p - X\| + 2\beta^{i+1} \nabla_X \left(\|X_r - X\| + \|X - X_l\|\right). \tag{A.12}$$

  In (A.12), we assume that β^i is smaller than the discretization step.

Since the gradient $\nabla_X \|X - Y\|$ is pointing in the direction $X - Y$ and it is a unit vector, we can substitute $\nabla_X \|X - Y\| = \|X - Y\|^{-1}(X - Y)$ to all of the above equations.

A.1.1 Optimal Junction Angle

The classically studied length or elastic energy minimizing gradient flow of networks leads to Steiner trees with triple junctions satisfying the Herring condition (see e.g. [BW95; Man+18]). In our case, the optimal angles depend on the energy hyperparameters and the current α-length of $\mathcal{G}$.

Consider a discrete triple junction node X with neighbouring points X_p, X_l and X_r and let $s_\star := \|X - X_\star\|^{-1}(X - X_\star)$ for $\star \in \{p, l, r\}$. Then

$$\nabla_X E = \left[\frac{\lambda}{(L^\alpha_{max} - L^\alpha)^2}\alpha^i - 2\beta^i\right] s_p + \left[\frac{\lambda}{(L^\alpha_{max} - L^\alpha)^2}\alpha^{i+1} - 2\beta^{i+1}\right](s_l + s_r).$$

We assume that the neighbouring discrete points are symmetrical in the sense that $\|X_p - X_l\| = \|X_p - X_r\|$. Let $\mathcal{G}^{opt}$ denoted the network for which

$$\nabla_X E\left(\mathcal{G}^{opt}\right) = 0.$$

The symmetry assumption and the condition for $\mathcal{G}^{opt}$ imply that $s_l + s_r$ is parallel to s_p and

$$s_l + s_r = \langle s_l + s_r, s_p\rangle s_p = 2\langle s_{l,r}, s_p\rangle s_p,$$

where $s_{l,r}$ represents s_l or s_r. The energy gradient condition for the optimal graph $\mathcal{G}^{opt}$ is

$$0 = \left[\frac{\lambda}{(L^\alpha_{max} - L^\alpha)^2} \alpha^i - 2\beta^i + 2\langle s_{l,r}, s_p \rangle \left(\frac{\lambda}{(L^\alpha_{max} - L^\alpha)^2} \alpha^{i+1} - 2\beta^{i+1} \right) \right] s_p.$$

The optimal junction angle can be written as $\theta_{opt} = 2 \arccos\left(-\langle s_{l,r}, s_p \rangle\right)$, where

$$\langle s_{l,r}, s_p \rangle = -\frac{1}{2} \frac{\lambda\alpha^i - 2(L^\alpha_{max} - L^\alpha)^2 \beta^i}{\lambda\alpha^{i+1} - 2(L^\alpha_{max} - L^\alpha)^2 \beta^{i+1}}. \tag{A.13}$$

The asymptotic optimal junction angle can be evaluated as the following limit

$$\lim_{L^\alpha \to L^\alpha_{max}} \theta_{opt} = 2 \arccos\left(- \lim_{L^\alpha \to L^\alpha_{max}} \langle s_{l,r}, s_p \rangle \right) = 2 \arccos\left(\frac{1}{2\alpha} \right).$$

Thus the parameter α should be at least $\frac{1}{2}$ to obtain geometrically feasible critical networks.

A.1.2 Branching Condition

In case of favorable energy outcome, new branches are added to the tree. This topological change is triggered by the branching condition. The condition is derived from (A.13) by ensuring that $\langle s_{l,r}, s_p \rangle \in (-1, 0)$ which leads to

$$\left(\frac{\alpha}{\beta} \right)^i > \frac{2}{\lambda} \frac{1 - 2\beta}{1 - 2\alpha} \left(L^\alpha_{max} - L^\alpha \right)^2.$$

Assuming that $\alpha < \beta$, we can express the branching condition at level i as

$$i < \left[\log\left(\frac{\alpha}{\beta} \right) \right]^{-1} \left[\log\left(\frac{2}{\lambda} \right) + \log\left(\frac{1 - 2\beta}{1 - 2\alpha} \right) + 2 \log\left(L^\alpha_{max} - L^\alpha \right) \right].$$

This gives us a lower bound for the maximum branch degree possible for a given configuration of parameters and the current α-length.

A.2 Conclusion

The chapter outlines the evolution and optimization of filament networks, which are described as moving networks of curves. It proposes an approach incorporating discrete differential geometry and a novel energy functional inspired by biological systems. This energy functional accounts for both the limitations in available resources and the interplay between structural cost and expansion profitability.

By using a discrete approach to compute energy gradients, this framework enables the handling of branching topological changes which can lead to interesting and useful dynamics. The work thus serves as an unpublished foundation for future research in this field.

B

Appendix: Computational Experiments

This appendix presents a collection of selected computational experiments that complement the main text and provide validation to some of the most important theoretical results. It touches on topics from all previous Chapters and provides additional resources.

We first describe our discretization approach and methods used for approximation of important quantities in Section B.0. The numerical integration scheme and supporting algorithms are provided in Section B.1. Finally, the computational results are presented in Section B.2.

B.0 Discrete Geometry

This section serves as a technical foundation, outlining the notation and approximation methods used in the simulations of this appendix. We initiate the discussion with a general overview of the numerical approach and basic notation.

In this work, geometric flows of curves in $\mathbb{R}^3$ are numerically treated in a way similar to [KBŠ17]. We discretize spatial derivatives by means of the osculating circles and then solve the resulting system of time-dependent ODE's by means of the Runge-Kutta-Merson scheme.

A discrete curve $\tilde{\Gamma}$ is a finite set of nodes $\{\tilde{\gamma}_i\}_{i=0}^{N-1}$ connected by linear segments, where $N \in \mathbb{N}$ is the number of nodes. In order to simplify further notation for closed curves, we set $\tilde{\gamma}_{-1} := \tilde{\gamma}_{N-1}$ and $\tilde{\gamma}_N := \tilde{\gamma}_0$. The vector KN can be approximated by means of the geometrical approach based on osculating circles. The approximate values of K and N at the node $\tilde{\gamma}_i$ are denoted by $\tilde{K}_i$ and $\tilde{N}_i$, respectively.

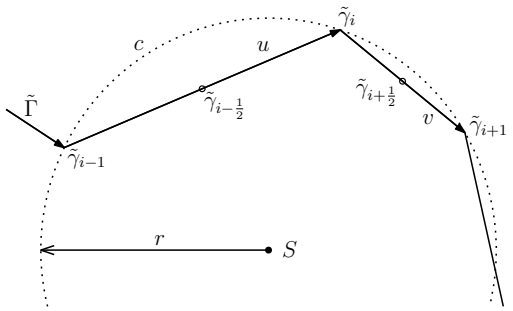

Figure B.1: Visualization of the geometric quantities defined in the osculating plane.

B.0.0 Discrete Curvature

This subsection describes the curvature approximation scheme from [MKB19] used in the subsequent simulations. This approach uses a discrete osculating circle given by three subsequent points along the discretized curve.

Consider a particular node $\tilde{\gamma}_i \in \tilde{\Gamma}$, where $0 \leqslant i < N$. We define

$$u := \tilde{\gamma}_i - \tilde{\gamma}_{i-1}, \qquad \tilde{\gamma}_{i-\frac{1}{2}} := \tfrac{1}{2}(\tilde{\gamma}_{i-1} + \tilde{\gamma}_i),$$
$$v := \tilde{\gamma}_{i+1} - \tilde{\gamma}_i, \qquad \tilde{\gamma}_{i+\frac{1}{2}} := \tfrac{1}{2}(\tilde{\gamma}_i + \tilde{\gamma}_{i+1}),$$

as shown in Figure B.1. In order to approximate the curvature K, we find the center S of the circle c defined by the points $\tilde{\gamma}_{i-1}$, $\tilde{\gamma}_i$ and $\tilde{\gamma}_{i+1}$. Since c is the circumscribed circle of the triangle with the vertices $\tilde{\gamma}_{i-1}$, $\tilde{\gamma}_i$ and $\tilde{\gamma}_{i+1}$ and lies in the osculating plane, the point S has to satisfy the following conditions:

$$S - \tilde{\gamma}_i \in \{u, v\}_{span}, \tag{B.1}$$
$$S - \tilde{\gamma}_{i-\frac{1}{2}} \perp u, \tag{B.2}$$
$$S - \tilde{\gamma}_{i+\frac{1}{2}} \perp v. \tag{B.3}$$

First condition (B.1) implies the existence of $t_1, t_2 \in \mathbb{R}$, such that $S = \tilde{\gamma}_i + t_1 u + t_2 v$. This allows us to rewrite (B.2) and (B.3) as

$$\langle S - \tilde{\gamma}_{i-\frac{1}{2}}, u\rangle = t_1\|u\|^2 + t_2\langle u, v\rangle - \langle \tilde{\gamma}_{i-\frac{1}{2}} - \tilde{\gamma}_i, u\rangle = 0,$$
$$\langle S - \tilde{\gamma}_{i+\frac{1}{2}}, v\rangle = t_1\langle u, v\rangle + t_2\|v\|^2 - \langle \tilde{\gamma}_{i+\frac{1}{2}} - \tilde{\gamma}_i, v\rangle = 0.$$

The parameters t_1 and t_2 can be obtained by solving the following linear system:

$$\mathbb{A} \cdot \begin{bmatrix} t_1 \\ t_2 \end{bmatrix} := \begin{bmatrix} \|u\|^2 & \langle u, v\rangle \\ \langle u, v\rangle & \|v\|^2 \end{bmatrix} \cdot \begin{bmatrix} t_1 \\ t_2 \end{bmatrix} = \begin{bmatrix} \langle \tilde{\gamma}_{i-\frac{1}{2}} - \tilde{\gamma}_i, u\rangle \\ \langle \tilde{\gamma}_{i+\frac{1}{2}} - \tilde{\gamma}_i, v\rangle \end{bmatrix} = \begin{bmatrix} -\frac{1}{2}\|u\|^2 \\ \frac{1}{2}\|v\|^2 \end{bmatrix}. \tag{B.4}$$

When $\|u\|^2\|v\|^2 = \langle u, v\rangle^2$ and the determinant $\det \mathbb{A}$ vanishes, the points $\tilde{\gamma}_{i-1}$, $\tilde{\gamma}_i$ and $\tilde{\gamma}_{i+1}$ are collinear and we set $\tilde{K}_i := 0$. Otherwise, the system (B.4) has a unique solution

$$t_1 = -\frac{\|v\|^2(\|u\|^2 + \langle u, v\rangle)}{2\det \mathbb{A}}, \qquad t_2 = \frac{\|u\|^2(\|v\|^2 + \langle u, v\rangle)}{2\det \mathbb{A}}.$$

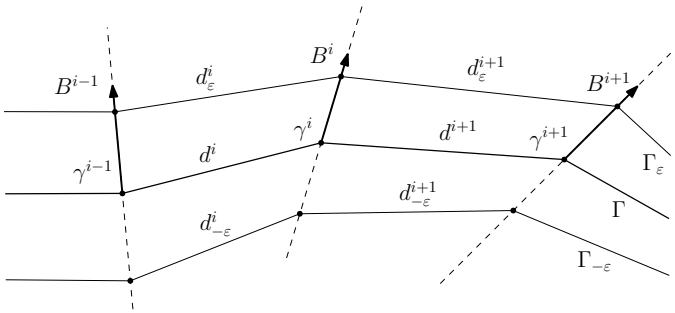

Figure B.2: Discretization scheme for torsion.

The discrete curvature $\tilde{K}_i$ is then calculated from the radius r of the osculation circle c as

$$\tilde{K}_i := \tfrac{1}{r} = \|\tilde{\gamma}_i - S\|^{-1} = \|t_1 u + t_2 v\|^{-1}.$$

The principal normal vector N is approximated by the expression

$$\tilde{N}_i := \tilde{K}_i(S - \tilde{\gamma}_i).$$

The geometrical setting is illustrated in Figure B.1.

B.0.1 Discrete Torsion

There are various approximation techniques for curvature, ranging from classic finite differences to approaches based on discrete differential geometry [CW17]. Even though there are some techniques to discretize torsion [Bac; Bou00], the literature on this subject is relatively sparse. To this end, we present a novel approximation method for discrete torsion, inspired by the curvature approximations detailed in [CW17].

Consider a family of curves Γ_ε derived from a given space curve Γ by ε-expansion in the binormal direction. Each curve Γ_ε is then prescribed by the following parametric function:

$$\gamma_\varepsilon := \gamma + \varepsilon B.$$

Using the Frenet-Serret equations and the Taylor's theorem we get

$$\|\partial_u \gamma_\varepsilon\| = \|gT - \varepsilon g\tau N\| = \sqrt{1+\varepsilon^2\tau^2}\,\|\partial_u\gamma\| = (1 + \tfrac{1}{2}\varepsilon^2\tau^2)\|\partial_u\gamma\| + \mathcal{O}(\varepsilon^4),$$

where $g := \|\partial_u\gamma\|$. Thus the length of the expanded curve Γ_ε satisfies

$$\frac{\mathrm{d}}{\mathrm{d}\varepsilon}\left(\int_{\Gamma_\varepsilon} \mathrm{d}s\right)\Big|_{\varepsilon=0} = 0 \qquad \frac{\mathrm{d}^2}{\mathrm{d}\varepsilon^2}\left(\int_{\Gamma_\varepsilon} \mathrm{d}s\right)\Big|_{\varepsilon=0} = \int_\Gamma \tau^2\,\mathrm{d}s,$$

and τ^2 can be expressed as the following limit

$$\tau^2 = \frac{\partial_\varepsilon^2\|\partial_u\gamma_\varepsilon\|}{\|\partial_u\gamma\|}\Big|_{\varepsilon=0} = \lim_{\varepsilon\to 0}\frac{\|\partial_u\gamma_\varepsilon\| - 2\|\partial_u\gamma\| + \|\partial_u\gamma_{-\varepsilon}\|}{\varepsilon^2\|\partial_u\gamma\|} =: \lim_{\varepsilon\to 0}\tau_\varepsilon^2.$$

In the following, we define discrete torsion from three consecutive points on a discrete curve denoted by γ^{i-1}, γ^i and γ^{i+1}. The idea is to discretize τ_ε^2 instead of τ^2 and find the limit of the discretized value as ε approaches zero. The process is summarized as follows:

$$\begin{array}{ccc} \tau_\varepsilon^i & \xrightarrow{\varepsilon\to 0} & \tau^i \\ \uparrow & & \uparrow \\ \tau_\varepsilon & \xrightarrow{\varepsilon\to 0} & \tau \end{array} \qquad \text{discretization}$$

To aid with the definition of τ_ε^2, we introduce the following discrete variables:

$$B^i := \frac{(\gamma_{i+1}-\gamma_i)\times(\gamma_i-\gamma_{i-1})}{\|(\gamma_{i+1}-\gamma_i)\times(\gamma_i-\gamma_{i-1})\|}, \qquad d_\varepsilon^i := \|(\gamma^i+\varepsilon B^i)-(\gamma^{i-1}+\varepsilon B^{i-1})\|,$$
$$l_\varepsilon^i := d_\varepsilon^{i+1}+d_\varepsilon^i, \qquad (\tau_\varepsilon^i)^2 := \frac{l_\varepsilon^i-2l_0^i+l_{-\varepsilon}^i}{\varepsilon^2 l_0^i}.$$

After algebraic manipulation, the square of d_ε^i can be rewritten using d_0^i in the form

$$\begin{aligned}(d_\varepsilon^i)^2 &= (d_0^i)^2 + 2\varepsilon\langle\gamma^i-\gamma^{i-1}, B^i-B^{i-1}\rangle + \varepsilon^2\|B^i-B^{i-1}\|^2 \\ &= (d_0^i)^2 + 2\varepsilon\langle\gamma^i-\gamma^{i-1}, H^i\times(\gamma^i-\gamma^{i-1})\rangle + \varepsilon^2\|H^i\times(\gamma^i-\gamma^{i-1}\|^2 \\ &= (d_0^i)^2\left[1+(\varepsilon\sin\alpha^i\|H^i\|)^2\right],\end{aligned}$$

where α_i is the angle between H^i and $\gamma^i-\gamma^{i-i}$, and the term H^i is given by

$$H^i := \frac{\gamma^{i+1}-\gamma^i}{\|(\gamma^{i+1}-\gamma^i)\times(\gamma^i-\gamma^{i-1})\|} + \frac{\gamma^{i-1}-\gamma^{i-2}}{\|(\gamma^i-\gamma^{i-1})\times(\gamma^{i-1}-\gamma^{i-2})\|}.$$

Using the Taylor theorem, we can estimate d_ε^i and l_ε^i for ε close to 0 as

$$\begin{aligned} d_\varepsilon^i &= d_0^i\sqrt{1+(\varepsilon\sin\alpha^i\|H^i\|)^2} = d_0^i\left[1+\tfrac{1}{2}\varepsilon^2(\sin\alpha^i\|H^i\|)^2\right]+\mathcal{O}(\varepsilon^4), \\ l_\varepsilon^i &= l_0^i + \tfrac{1}{2}\varepsilon^2\left[d_0^{i+1}(\sin\alpha^{i+1}\|H^{i+1}\|)^2 + d_0^i(\sin\alpha^i\|H^i\|)^2\right]+\mathcal{O}(\varepsilon^4).\end{aligned}$$

Finally, we define the approximation of $(\tau^i)^2$ at the point γ^i as

$$(\tau^i)^2 := \lim_{\varepsilon\to 0}(\tau_\varepsilon^i)^2 = \frac{d_0^{i+1}(\sin\alpha^{i+1}\|H^{i+1})^2 + d_0^i(\sin\alpha^i\|H^i)^2}{d_0^{i+1}+d_0^i}.$$

Note that this approximation does not provide us with the sign of the torsion, but it is not required for the minimal surface generating flow due to Proposition 2.1.2.

B.1 Numerical Integration

In this section, we focus on numerical integration method for solving time-dependent ODEs in our geometrical setting. We describe the semi-discrete scheme as a foundational step, followed by an application of the Runge-Kutta-Merson scheme for time integration. The section also addresses the order of convergence and the challenges posed by topological changes.

B.1.0 Semi-discrete Scheme

For numerical integration of the initial value problem

$$\frac{\mathrm{d}\tilde{\gamma}_i}{\mathrm{d}t} = \tilde{K}_i^2(S_i - \tilde{\gamma}_i), \tag{B.5}$$

$$\tilde{\gamma}_i|_{t=0} = \gamma_0\left(\frac{2\pi i}{N}\right), \tag{B.6}$$

we use the 4th order accurate Runge-Kutta-Merson method with an automatic time step adjustment as in [Chr70].

Denoting $\tilde{\gamma} = (\tilde{\gamma}_0, \ldots, \tilde{\gamma}_{N-1})^T$ and $F_i(\tilde{\gamma}) = \tilde{K}_i\tilde{N}_i$, system (B.5-B.6) reduces to

$$\tilde{\gamma}_i'(t) = F_i(\tilde{\gamma}(t)).$$

We denote the time step $\tau > 0$ and the time level $\tilde{t}$. The next time level is given by the formula

$$\tilde{\gamma}(\tilde{t} + \tau) = \tilde{\gamma}(\tilde{t}) + \tfrac{1}{6}(k_1 + 4k_4 + k_5),$$

where $k_j = (k_{j,0}, \ldots, k_{j,N-1})^T$ can be computed using the following set of formulas

$$\begin{aligned}
k_{1,i} &= F_i(\tilde{\gamma}(\tilde{t})),\\
k_{2,i} &= F_i(\tilde{\gamma}(\tilde{t}) + \tfrac{\tau}{3}k_1),\\
k_{3,i} &= F_i(\tilde{\gamma}(\tilde{t}) + \tfrac{\tau}{6}(k_1 + k_2)),\\
k_{4,i} &= F_i(\tilde{\gamma}(\tilde{t}) + \tfrac{\tau}{8}(k_1 + 3k_3)),\\
k_{5,i} &= F_i(\tilde{\gamma}(\tilde{t}) + \tfrac{\tau}{2}(k_1 - 3k_3 + 4k_4)).
\end{aligned}$$

The time step τ is updated at each iteration as in the page 246 of [Hol+86].

$$\tau_{new} = \left(\frac{\delta}{\varepsilon}\right)^{\frac{1}{5}}\omega\tau, \quad \text{where } \varepsilon = \max_{0\leqslant i<N}\frac{1}{3}\left\|\frac{1}{5}k_{1,i} - \frac{9}{10}k_{3,i} + \frac{4}{5}k_{4,i} - \frac{1}{10}k_{5,i}\right\|.$$

The control parameters ω and δ must satisfy $0 < \omega < 1$ and $\delta > 0$.

B.1.1 Order of Convergence

We assume that Γ_0 is embedded in a unit sphere centered at the origins. The deviation of the discretized curve from the shrinking sphere radius is characterized by

$$\mathcal{E}_\infty(N) := \max_{\tilde{t}}\max_{0\leqslant i<N}\left|\|\tilde{\gamma}_i(\tilde{t})\| - \sqrt{1-2\tilde{t}}\right|,$$

$$\mathcal{E}_p(N) := \max_{\tilde{t}}\left(\frac{1}{L(\tilde{t})}\sum_{i=0}^{N-1}\frac{l_{i+1}(\tilde{t}) + l_i(\tilde{t})}{2}\left|\|\tilde{\gamma}_i(\tilde{t})\| - \sqrt{1-2\tilde{t}}\right|^p\right)^{\frac{1}{p}},$$

where $p \in \mathbb{N}$, $L(\tilde{t}) := \sum_{i=0}^{N-1} l_i(\tilde{t})$ and $l_i(\tilde{t}) := \|\tilde{\gamma}_i(\tilde{t}) - \tilde{\gamma}_{i-1}(\tilde{t})\|$.

The Experimental Order of Convergence (EOC) used in [RM89; Dzi94] is calculated as

$$\mathrm{EOC}_p(N_1, N_2) := -\frac{\log(\mathcal{E}_p(N_2)) - \log(\mathcal{E}_p(N_1))}{\log N_2 - \log N_1}$$

where $p \in \mathbb{N}$ or $p = \infty$. The following numerical simulations were performed by using the semi-discrete scheme (B.5-B.6) with the control parameters $\delta = 10^{-5}$ and $\omega = 0.8$ as suggested in [Hol+86], page 246.

B.2 Computational Experiments

In the final section of this appendix, we present a series of computational experiments to support and validate our theoretical results. These experiments span topics from all chapters of this thesis, from spherical verification and minimal surfaces to more complex configurations like filament networks and coupled dynamics. Each experiment aims to empirically substantiate the analytical and numerical methods discussed earlier.

B.2.0 Spherical Verification

The first couple of examples are related to the curve shortening flow of space curves, studied in Chapter 1. Let us restate Definition 1.0.1 for reader's convenience:

Definition B.2.1 (Curve shortening flow)**.** *Let $\{\Gamma_t\}_{t\in[0,\underline{t})}$ with $\underline{t} > 0$ be a family of evolving curves. The curve shortening flow is defined as the following initial-value problem:*

$$\begin{aligned} \partial_t \gamma &= \kappa N && \text{on } S^1 \times [0, \underline{t}), \\ \gamma|_{t=0} &= \gamma_0 && \text{in } S^1, \end{aligned}$$

where $\gamma_0 \in \mathcal{C}^2(S^1; \mathbb{R}^3)$ is the parametrization of the initial curve Γ_0.

We include two computational examples serving both as verification of the numerical scheme from Section B.1 and testing of the properties of moving spherical curves. According to Corollary 1.1.5, spherical curves under the curvature flow should remain embedded in a shrinking sphere. Both examples follow the curve shortening flow redefined above.

Example B.2.2. *The initial curve Γ_0 for the first example is given by the parametrization*

$$\gamma\left(\tfrac{u+\pi}{2\pi}, 0\right) = \begin{bmatrix} \cos(6u)\sin u \\ \sin(6u)\sin|u| \\ -\cos u \end{bmatrix}, \qquad u \in [-\pi, \pi].$$

The results of the numerical simulation are presented in Table B.1 and Figure B.3.

Example B.2.3. *The initial curve Γ_0 for the second example is given by the parametrization*

$$\gamma\left(\tfrac{u}{2\pi}, 0\right) = \frac{1}{\sqrt{1 + (5\cos(10u))^2}} \begin{bmatrix} \cos u \\ \sin u \\ 5\cos(10u) \end{bmatrix}, \qquad u \in [0, 2\pi].$$

The results of the numerical simulation are presented in Table B.2 and Figure B.4.

Table B.1: Results of the numerical computation from Example B.2.2. The error measurements were taken during time interval $[0, 0.45]$.

N	$\mathcal{E}_\infty(N)$	EOC_∞	$\mathcal{E}_1(N)$	EOC_1	$\mathcal{E}_2(N)$	EOC_2
100	$1.0205 \cdot 10^{-2}$		$9.3770 \cdot 10^{-3}$		$6.4629 \cdot 10^{-3}$	
200	$2.5018 \cdot 10^{-3}$	2.0283	$2.2581 \cdot 10^{-3}$	2.0540	$1.5292 \cdot 10^{-3}$	2.0794
400	$6.5329 \cdot 10^{-4}$	1.9372	$5.8649 \cdot 10^{-4}$	1.9449	$3.8876 \cdot 10^{-4}$	1.9758
800	$1.6623 \cdot 10^{-4}$	1.9746	$1.4426 \cdot 10^{-4}$	2.0234	$9.7702 \cdot 10^{-5}$	1.9924
1600	$5.0943 \cdot 10^{-5}$	1.7062	$3.5888 \cdot 10^{-5}$	2.0071	$2.4118 \cdot 10^{-5}$	2.0183

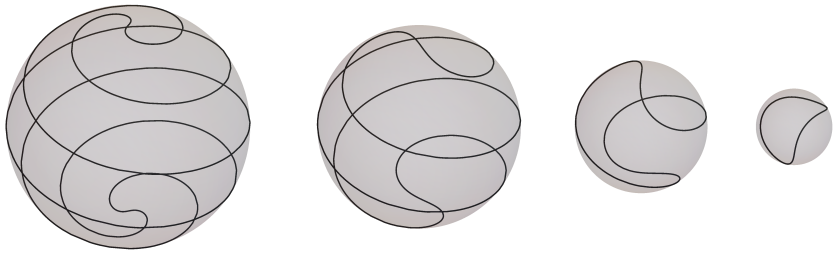

(a) $\tilde{t} = 0$ (b) $\tilde{t} = 0.15$ (c) $\tilde{t} = 0.35$ (d) $\tilde{t} = 0.45$

Figure B.3: Results of the numerical simulation from Example B.2.2. The discretized curve is visualized at four different time levels along with the corresponding sphere.

B.2.1 Minimal Surfaces

We move to the Minimal surface generating flow introduced in Chapter 2. Let us restate Definition 2.0.6 of the motion law for easier reference:

Definition B.2.4 (Minimal surface generating flow)**.** *Let Γ_0 be a closed space curve with positive curvature and torsion. We say that a family of curves $\{\Gamma_t\}_{t\in[0,\underline{t})}$ is evolving according to the minimal surface generating flow if its parametrization γ satisfies the initial value problem:*

$$\partial_t \gamma = \tau^{-\frac{1}{2}} N \qquad \text{in } S^1 \times (0, \underline{t}), \tag{B.7}$$

$$\gamma|_{t=0} = \gamma_0 \qquad \text{in } S^1, \tag{B.8}$$

where γ_0 is parametrization of the initial curve Γ_0 and τ is the torsion of the curve.

We accompany Example 2.2.1 which was given analyticaly by a result obtained by means of the numerical approximation. The evolution for local quantities g, κ and τ, given in Equations (2.5-2.8), have been numerically solved by the explicit Euler first-order method using the finite difference approximations along the parametric interval.

The results presented in Figure B.10 show the evolution of initial curve with parametrization

$$\gamma_0(u) = [\cos u(r_1 + r_2 \cos(mu)), \sin u(r_1 + r_2 \cos(mu)), r_2 \sin u]^T \tag{B.9}$$

Table B.2: Results of the numerical computation from Example B.2.3. The error measurements were taken during time interval $[0, 0.45]$.

N	$\mathcal{E}_\infty(N)$	EOC_∞	$\mathcal{E}_1(N)$	EOC_1	$\mathcal{E}_2(N)$	EOC_2
400	$1.1538 \cdot 10^{-1}$		$1.1538 \cdot 10^{-1}$		$1.0340 \cdot 10^{-1}$	
800	$2.9575 \cdot 10^{-2}$	1.9639	$2.9574 \cdot 10^{-2}$	1.9640	$2.2146 \cdot 10^{-2}$	2.2232
1200	$1.2998 \cdot 10^{-2}$	2.0276	$1.2996 \cdot 10^{-2}$	2.0280	$9.4608 \cdot 10^{-3}$	2.0975
1600	$7.2659 \cdot 10^{-3}$	2.0218	$7.2636 \cdot 10^{-3}$	2.0222	$5.2386 \cdot 10^{-3}$	2.0547
2000	$4.6211 \cdot 10^{-3}$	2.0281	$4.6209 \cdot 10^{-3}$	2.0269	$3.3186 \cdot 10^{-3}$	2.0459

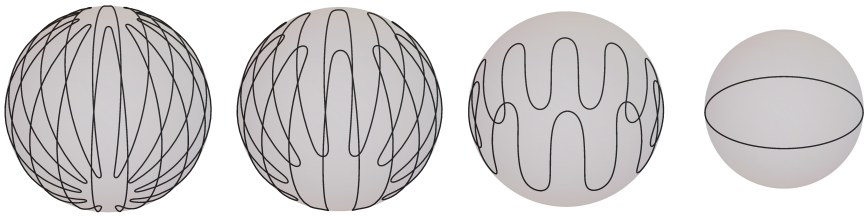

(a) $\tilde{t} = 0$ (b) $\tilde{t} = 0.01$ (c) $\tilde{t} = 0.05$ (d) $\tilde{t} = 0.2$

Figure B.4: Results of the numerical simulation from Example B.2.3. The discretized curve is visualized at four different time levels along with the corresponding sphere.

for all $u \in S^1$. This specific experiment used parameters $m = 10$, $r_1 = 1$ and $r_2 = \frac{1}{10}$. The initial condition for the values of g, κ and τ was analytically derived from (B.9). The experiment was run with time step $\Delta t = 10^{-6}$ and the curve was discretized with 10^3 points.

The validity of the numerical results was partially verified by several sanity checks and the numerical scheme was partially validated using the known solution described in Example 2.2.1. During the experiment, the integral $\sqrt{\tau}$ deviated from its initial value by less than $2 \cdot 10^{-14}$, which is in accordance to Corollary 2.2.2. The length was monotonically decreasing (see Proposition 2.2.3) while the torsion τ was increasing at every fixed $u \in S^1$ (see Proposition 2.1.2). Even though, the assumptions for Proposition 2.3.3 were not satisfied by the initial configuration, the averaged curvature κ_{ave} eventually became lower than the minimum of torsion τ_{min}. The curvature vanished in finite time as shown in Proposition 2.3.3.

B.2.2 Tangent Turning Signature

This section presents multiple examples to demonstrate the computation of the tangent turning signature, as introduced in Chapter 3. To facilitate easier referencing, we restate Definition 3.1.1 where this invariant was first introduced.

Definition B.2.5 (Tangent turning signature)**.** *Let $\Gamma \in \mathcal{R}^2(\mathbb{R}^3)$ be a locally convex space curve and choose a fixed $p \in S^2 \backslash \mathrm{Ran}\, T$. By Γ_p we denote the projected curve given by*

$$\gamma_p := \Phi_p \circ T,$$

where T is the tangent vector function of the original curve Γ and the second map

$$\Phi_p : S^2 \backslash \{p\} \to \mathbb{R}^2$$

is the stereographic projection from p. We define the tangent turning parity $\mathcal{T}_\Gamma \in \mathbb{Z}_2$ *as*

$$\mathcal{T}_\Gamma \equiv \deg(T_p) \bmod 2,$$

where $\deg(T_p)$ is the degree of the Gauss map for the curve Γ_p, also referred to as the turning number of Γ_p or as the winding number of the tangent vector function $T_p \colon S^1 \to S^1$.

The following example shows the construction of the projected curve Γ^p and the corresponding value of the tangent turning signature $\mathcal{T}_\Gamma$ for several specific curves from $\mathcal{M}$.

Example B.2.6. *Consider the following set of parametric functions of locally convex curves:*

$$\gamma_1(u) = \frac{1}{2}\begin{bmatrix} 1+\cos(2u) \\ \sin(2u) \\ 2\sin u \end{bmatrix}, \qquad \gamma_2(u) = \frac{1}{6}\begin{bmatrix} \cos(2u)(5+\cos(3u)) \\ \sin(2u)(5+\cos(3u)) \\ \sin(3u) \end{bmatrix},$$
$$\gamma_3(u) = \begin{bmatrix} \cos(4u)\cos u \\ \sin(4u)\cos u \\ \sin u \end{bmatrix}, \qquad \gamma_4(u) = \frac{1}{6}\begin{bmatrix} \cos u(5+\cos(10u)) \\ \sin u(5+\cos(10u)) \\ \sin(10u) \end{bmatrix},$$

for $u \in 2S^1$. The curves defined by these functions are shown in Figure B.6 along with their tangent indicatrices and their stereographical projections from the point $p = (0,0,1)^T$.

Since the turning numbers read $d(\Gamma_1^p) = d(\Gamma_2^p) = 2$, $d(\Gamma_3^p) = 5$ and $d(\Gamma_4^p) = 11$, the tangent turning signature is equal to the equivalence class $[0]$ for the first two curves Γ_1 and Γ_2, and to the equivalence class $[1]$ for the remaining curves Γ_3 and Γ_4.

B.2.3 Constant Mean Curvature Surfaces

Finally, we show how the Framed curvature flow presented in Chapter 4 can be used to generate surfaces of constant mean curvature. To improve readability, we restate Example 4.3.9 which uses the specific θ-velocity that leads to constant mean curvature surfaces. In this case, we assume cylindrically symmetrical configurations that lead to Delaneu surfaces [Del41].

Example B.2.7 (Cylindrical symmetry)**.** *Setting $w = 0$ reduces the system* (4.23) *to*

$$\frac{\mathrm{d}}{\mathrm{d}t}\begin{bmatrix} \theta \\ \varrho \\ \omega \end{bmatrix} = \frac{1}{\varrho^2}\begin{bmatrix} \sin\theta + \varrho H \\ -\varrho\cos\theta \\ \varrho\sin\theta \end{bmatrix}, \qquad \begin{bmatrix} \theta \\ \varrho \\ \omega \end{bmatrix}\Bigg|_{t=0} = \begin{bmatrix} \theta_0 \\ \varrho_0 \\ 0 \end{bmatrix}.$$

Figure B.5 depicts the results of the numerical simulation for the initial configuration that leads to the nodoid surface. All other Delaneu surfaces can be obtained by adjusting the initial angle θ and the prescribed mean curvature H. The simulation used discrete torsion from Section B.0.1, and the created surface was ported to Blender for realistic rendering.

Figure B.5: Rendering of nodoid trajectory surface with constant mean curvature from Example 4.3.9. The black circle is the initial condition Γ_0. The rendering was made in Blender.

B.2.4 Evolving Networks

This subsection contains selected numerical simulations related to the motion of curve networks. The first couple of experiments illustrate the motion by curve shortening flow with triple junction points and fixed boundary points. The final example depicts the branching network described in Appendix A.

Figures B.7 and B.8 show the evolution due to the curve shortening flow of networks with fixed endpoints. The first example is in $\mathbb{R}^2$ (Figure B.7) and the second example (Figure B.8) shows evolving networks of space curves. The final shapes converge to Steiner trees.

Figure B.9 shows a branching tree evolving according to the discrete gradient flow described in Subsection A.1.0. All simulations were performed using the Runge-Kutta-Merson method described in Section B.1. The branching topological changes occur spontaneously via the mechanism described in Subsection A.1.2.

B.3 Conclusions

This appendix supplements the main text with additional computational experiments and methodological discussions. It has offered validation for selected theoretical results and provided further insights for various curve flows covered in the preceding chapters.

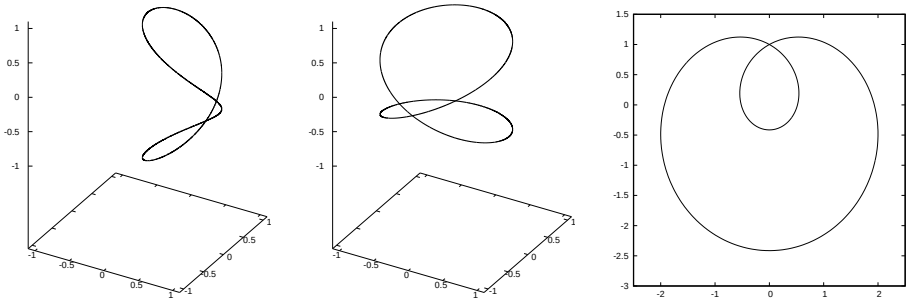

(a) Viviani curve Γ_1. (b) Tantrix of Γ_1. (c) Projection Γ_1^p.

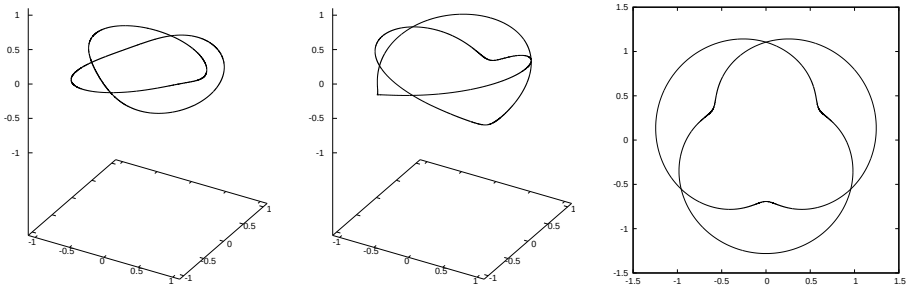

(d) Trefoil curve Γ_2. (e) Tantrix of Γ_2. (f) Projection Γ_2^p.

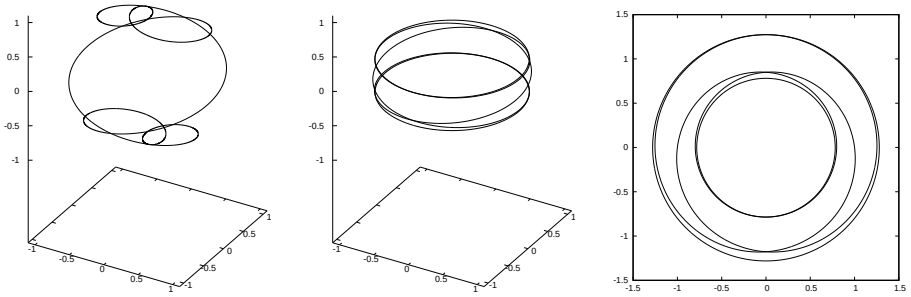

(g) Curve Γ_3. (h) Tantrix of Γ_3. (i) Projection Γ_3^p.

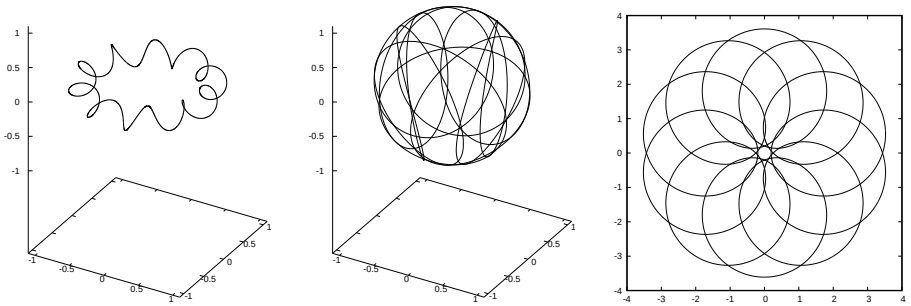

(j) Curve Γ_4. (k) Tantrix of Γ_4. (l) Projection Γ_4^p.

Figure B.6: Locally convex curves from Example B.2.6. Figures adapted from [MB22b].

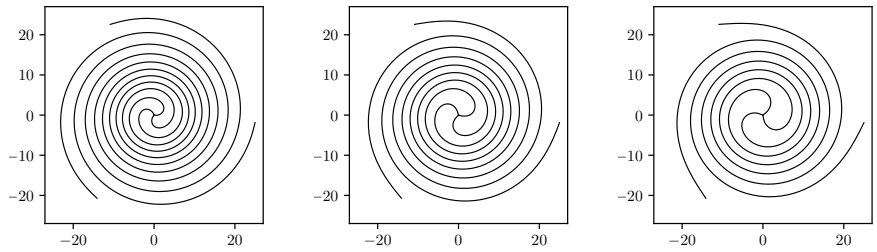

(a) Step 0 ($t = 0$). (b) Step 250 ($t = 25$). (c) Step 500 ($t = 50$).

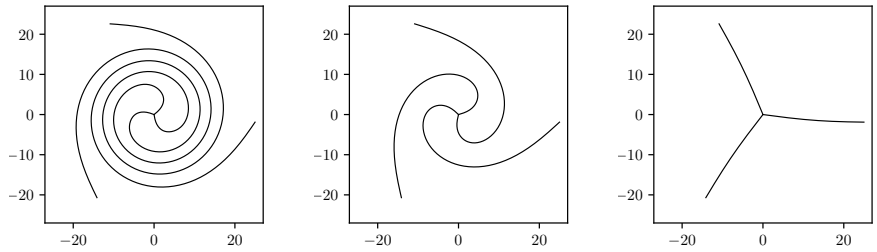

(d) Step 1000 ($t = 100$). (e) Step 2000 ($t = 200$). (f) Step 5000 ($t = 500$).

Figure B.7: Curve network with triple junction and fixed endpoints evolving according to the curve shortening flow. Parameters: $\Delta t = 0.0$, $\delta = 10^{-4}$ and $\omega = 0.8$.

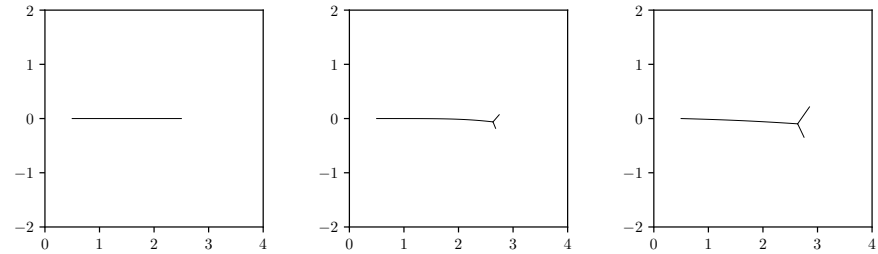

(a) Step 0 ($t = 0.00$). (b) Step 5 ($t = 0.05$). (c) Step 20 ($t = 0.20$).

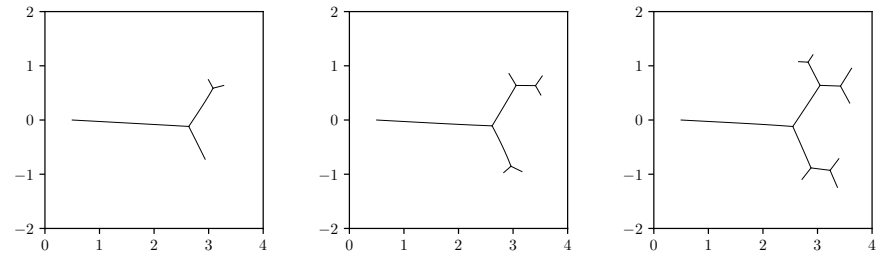

(d) Step 55 ($t = 0.55$). (e) Step 65 ($t = 0.65$). (f) Step 80 ($t = 0.80$).

Figure B.8: Evolution of network with parameters $\alpha = 0.6$, $\beta = 0.5$, $C = 2$, $L^{\alpha}_{max} = 10$.

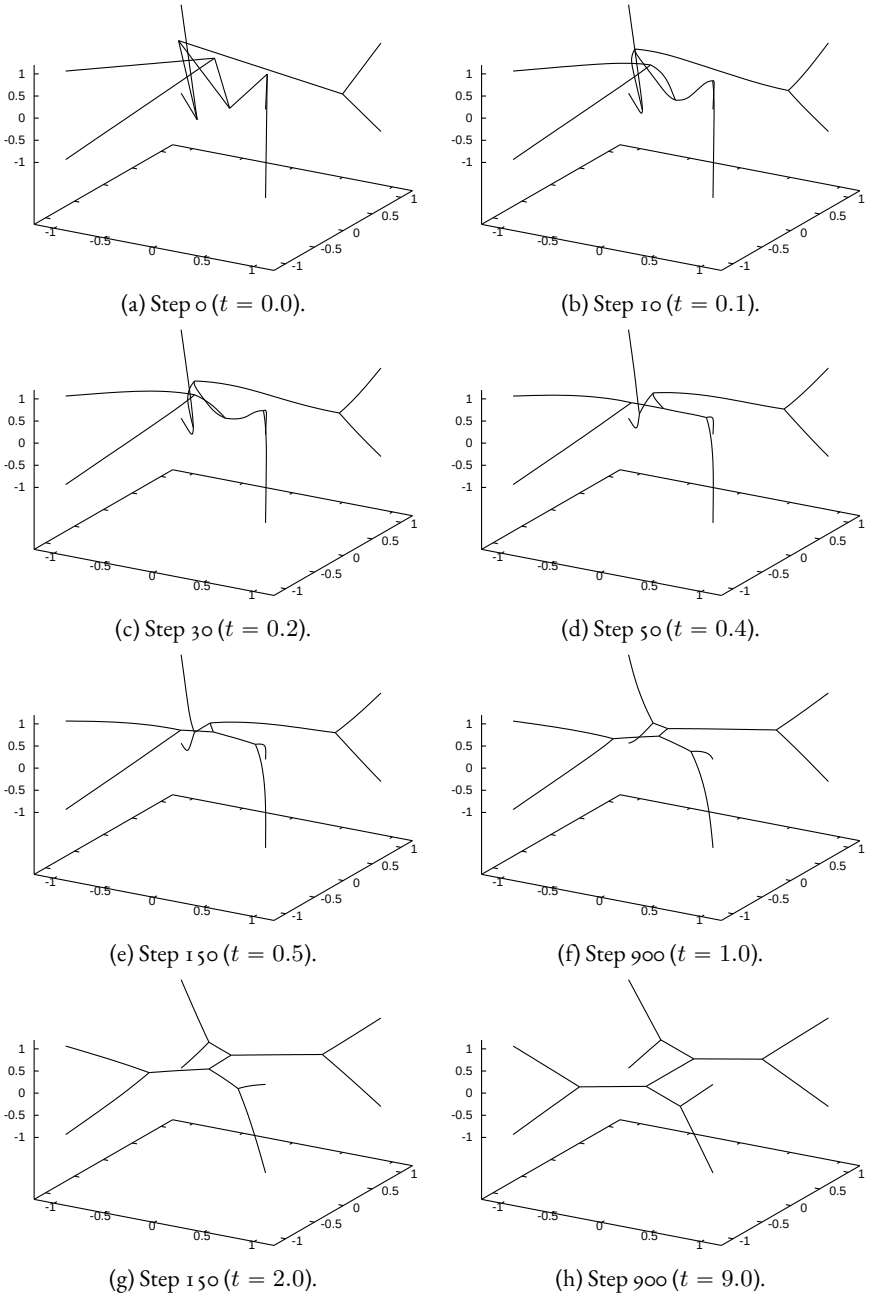

(a) Step 0 ($t = 0.0$). (b) Step 10 ($t = 0.1$).

(c) Step 30 ($t = 0.2$). (d) Step 50 ($t = 0.4$).

(e) Step 150 ($t = 0.5$). (f) Step 900 ($t = 1.0$).

(g) Step 150 ($t = 2.0$). (h) Step 900 ($t = 9.0$).

Figure B.9: Example of space curve network with fixed endpoints evolving according to the curve shortening flow. The simulation ran with timestep $\Delta t = 0.01$ and the Runge-Kutta-Merson controlling parameters $\delta = 10^{-4}, \omega = 0.8$.

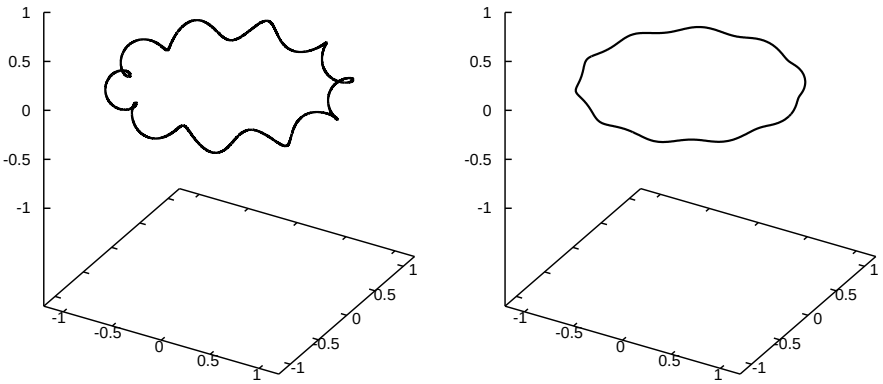

(a) Initial curve Γ_0 (up to rotation).

(b) Final curve $\Gamma_{\underline{t}}$(up to rotation).

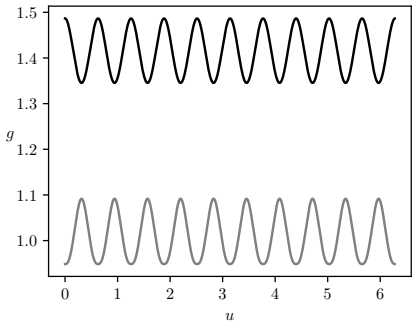

(c) $g|_{t=0}$ (black) and $g|_{t=\underline{t}}$ (gray).

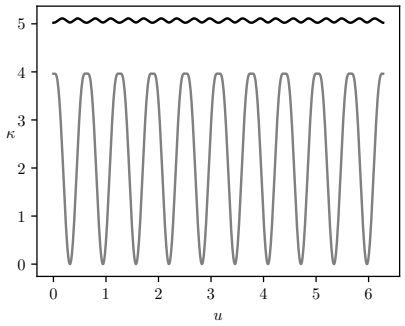

(d) $\kappa|_{t=0}$ (black) and $\kappa|_{t=\underline{t}}$ (gray).

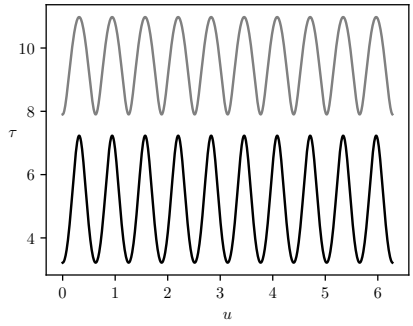

(e) $\tau|_{t=0}$ (black) and $\tau|_{t=\underline{t}}$ (gray).

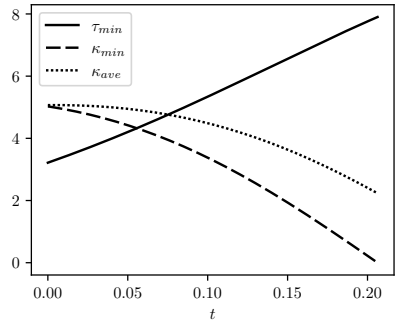

(f) Evolution of τ_{min}, κ_{min} and κ_{ave}.

Figure B.10: Numerical solution to (2.5-2.8) with the initial condition given by (B.9). The curvature κ vanishes at $\underline{t} = 0.20628$. The curves Γ_0 and $\Gamma_{\underline{t}}$ were reconstructed from κ, τ and g. The position and orientation was partially recovered using the Principal component analysis [Jol02]. However, the rotation around the z-axis was not preserved.

Index

Publication List

Publications in Impact Factor Journals

- J. Minarčík, M. Beneš: Minimal surface generating flow for space curves of non vanishing torsion. Homology, Discrete and Continuous Dynamical Systems - Series B, 27: 6605–6617, 2022,
  doi: 10.3934/dcdsb.2022011.
- J. Minarčík and M. Beneš: Nondegenerate Homotopy and Geometric Flows. Homology, Homotopy and Applications, 24: 255–264, 2022,
  doi: 10.4310/HHA.2022.v24.n2.a12.
- J. Minarčík, M. Beneš: Long-term behavior of curve shortening flow in $\mathbb{R}^3$. SIAM Journal on Mathematical Analysis, 52(2):1221–1231, 2020,
  doi: 10.1137/19M1248522.
- J. Minarčík, M. Kimura, M. Beneš: Comparing motion of curves and hypersurfaces in $\mathbb{R}^m$. Discrete & Continuous Dynamical Systems - B, 24(9):4815–4826, 2019,
  doi: 10.3934/dcdsb.2019032.

Preprints

- J. Minarčík, M. Beneš: Trajectory Surfaces of Framed Curvature Flow, 2023.

Conference Contributions

- International workshop
  BIGW: Geometric flows and related topics, Inverness, Scotland, July, 2023.
  - Lecture : *Ricci flow invariant curvature conditions*
- International workshop
  Tangled in Knot Theory, ICERM, The Institute for Computational and Experimental Research in Mathematics, Brown University, Providence, United States, May, 2023.
  - Oral presentation : *Minimal Surface Generating Flow*

- International workshop
  Workshop on scientific computing 2023, Děčín, May, 2023.
  - Oral presentation : *Trajectory Surfaces of Framed Curvature Flow*
- International seminar
  Discussion meeting on zero mean curvature surfaces in the Lorentz-Minkowski space and related areas, online, Shiv Nadar University NCR Delhi, October, 2022.
  - Oral presentation : *Minimal Surface Generating Flow*
- International seminar
  Interfaces: Modeling, Analysis, Numerics, Oberwolfach Research Institute for Mathematics, Oberwolfach, Germany, November 2022.
  - Oral presentation : *Framed Curvature Flow*
- International conference
  Topological Methods in Mathematical Physics, EMFCSC: International School of Mathematics, Ettore Majorana Foundation and Centre for Scientific Culture, Erice, Italy, September 2022.
  - Oral presentation : *Minimal Surface Generating Flow*
- International workshop
  Workshop on scientific computing 2022, Děčín, December, 2022.
  - Oral presentation : *Discrete Torsion*
- International conference
  Calculus of Variations in Probability and Geometry, UCLA, Institute for Pure & Applied Mathematics, Los Angeles, United States, February, 2022.
  - Poster presentation : *Minimal Surface Generating Flow*
- International seminar
  Combinatorial and Geometric Knot Theory, Oberwolfach Research Institute for Mathematics, Oberwolfach, Germany, November 2021.
  - Oral presentation : *Locally Convex Knots*
- International workshop
  Young Geometers Meeting, University of Copenhagen, Online, April, 2021.
  - Oral presentation : *Minimal surface generating flow for space curves of nonvanishing torsion*
- International workshop
  Winterschool on Analysis and Applied Mathematics, University of Münster, Online, February, 2021.
  - Poster : *Minimal surface generating flow for space curves of non-vanishing torsion*

- International conference
  Czech-Japanese Seminar in Applied Mathematics, Online, January, 2021.
  - Oral presentation : *Minimal surface generating flow for space curves of nonvanishing torsion*
- International workshop
  Workshop on scientific computing 2020, Online, December, 2020.
  - Oral presentation : *Minimal surface generating flow for space curves of nonvanishing torsion*
- International conference
  BJUT Conference - Knotted Fields and Applications, Beijing, China, September, 2019.
  - Oral presentation : *Minimal surface generating flow for space curves of nonvanishing torsion*
  - Poster : *Properties of codimension-two curve shortening flow*
- International workshop
  Biology, Analysis, Geometry, Energies, Links: A Program on Low-dimensional Topology, Geometry, and Applications, Minneapolis, United States, June, 2019.
  - Poster : *Properties of codimension-two curve shortening flow*
- Seminar
  Nečas Seminar on Continuum Mechanics, MFF UK, Prague, Czech Republic, February, 2019.
  - Oral presentation : *Properties of codimension-two curve shortening flow*
- International conference
  Czech-Japanese Seminar in Applied Mathematics 2018 (CJS2018), Noto, Japan, July, 2018.
  - Oral presentation : *Curvature driven flow of space curves in normal and binormal direction*
- International conference
  Czech-Japanese Seminar in Applied Mathematics 2018 (CJS2018), Noto, Japan, July, 2018.
  - Oral presentation : *Curvature driven flow of space curves in normal and binormal direction*
- International workshop
  Workshop on scientific computing 2018, Děčín, Czech Republic, June, 2018.
  - Oral presentation : *Curvature driven flow of space curves in normal and binormal direction*

- International workshop
  7th conference of the Visual Computing Competence Center, Havlíčkův Brod, Czech Republic, November, 2017.
  - Oral presentation : *Automatic identification of trains from images*
- International conference
  Future Port Prague 2017, Prague, Czech Republic, September, 2017.
  - Oral presentation : *AI in machine vision*
- International conference
  International Symposium on Computational Science 2017, Kanazawa, Japan, July, 2017.
  - Oral presentation : *Curvature driven flow of space curves in normal and binormal direction*
- International workshop
  14th Workshop on Mathematical Analysis for Nonlinear Phenomena, Kanazawa, Japan, July, 2017.
  - Oral presentation : *Curvature driven flow of space curves in normal and binormal direction*
- International workshop
  Workshop on scientific computing 2018, Děčín, Czech Republic, June, 2017.
  - Oral presentation : *Curvature driven flow of space curves in normal and binormal direction*
- International workshop
  Workshop on scientific computing 2017, Děčín, Czech Republic, June, 2017.
  - Oral presentation : *Curvature driven flow of space curves in normal and binormal direction*
- International workshop
  Workshop on scientific computing 2016, Děčín, Czech Republic, June, 2016.
  - Oral presentation : *Applications of planar and space curve evolution*
- International workshop
  Workshop on scientific computing 2015, Děčín, Czech Republic, June, 2015.
  - Oral presentation : *Numerical solution of a curvature driven flow of plane and space curves and its applications*